GRIP, GRAB, AND GROOM: THE BIOMECHANICS OF FROG AND CAT TONGUES

A Dissertation
Presented to
The Academic Faculty

by

Alexis C. Noel

In Partial Fulfillment
of the Requirements for the Degree
Doctor of Philosophy in the
School of Mechanical Engineering

Georgia Institute of Technology
August 2018

GRIP, GRAB, AND GROOM: THE BIOMECHANICS OF FROG AND CAT TONGUES

Approved by:

Professor David L. Hu, Advisor
School of Mechanical Engineering
Georgia Institute of Technology

Professor Ting Zhu
School of Mechanical Engineering
Georgia Institute of Technology

Professor Michael Varenberg
School of Mechanical Engineering
Georgia Institute of Technology

Professor Dan Goldman
School of Physics
Georgia Institute of Technology

Professor H. Jerry Qi
School of Mechanical Engineering
Georgia Institute of Technology

Date Approved: May 03, 2018

To my parents,

Joanne and Steve Noel,

whose eternal love and support
made me who I am today.

PREFACE

In the world of biomechanics, research inspiration can come from the strangest of places. For me, it was my cat Murphy. Murphy, a rambunctious kitty of 3 years, decided that the microfiber blanket he was laying on smelled tasty. In an attempt to lick the fuzzy blanket, he got his tongue stuck in the microfiber loops. As I detangled this poor, trapped cat, tongue lolling out of his mouth, I asked myself "How does a sandpaper-like tongue get trapped on a blanket?". Luckily, we had a dissected cat tongue back in the lab freezer, which I soon stuck under a microscope. Behold, the tongue was not like sandpaper, but more like a collection of tiny cat claws on the surface. Why were these spines shaped like cat claws, and why did there appear to be a tiny cavity at the tip of each spine? My exploration into the world of cat tongues provided extraordinary experiences, from holding a snow leopard tongue to handling exotic feline furs from the early 1900's in the Museum of Comparative Biology in a Harvard basement. Sticky, speedy frog tongues were equally as compelling. Studying the frog took me to places such as Zoo Atlanta, Atlanta Botanical Gardens, The Amphibian Foundation, and even a chinese supermarket. Hours were spent scraping 18 frog tongues for a tiny sample of frog saliva for testing. I was even afforded the opportunity to film the tongue of a monsterous cane toad named Princess. It is my hope that my work on animal tongues may inspire the next generation of scientists and engineers to explore unorthodox topics both critically and creatively.

Before we begin, I would like to provide a prelude to my thesis. I wrote this short comic on tongue biomechanics as a way to communicate science to the general public. It summarizes the many fascinating results and tidbits I found throughout my work on tongues.

GRIP, GRAB, AND GROOM: A SCIENCE COMIC ABOUT TONGUES

BY: ALEXIS NOEL

AS A HUMAN, GRABBING FOOD IS EASY WITH OUR OPPOSIBLE THUMBS

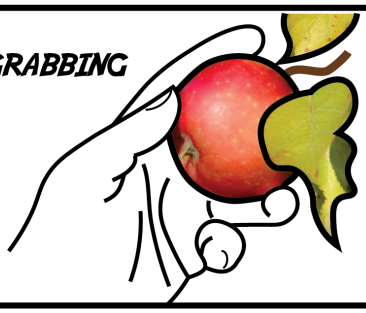

BUT HOW DO YOU GRAB FOOD WHEN YOU HAVE NO THUMBS?

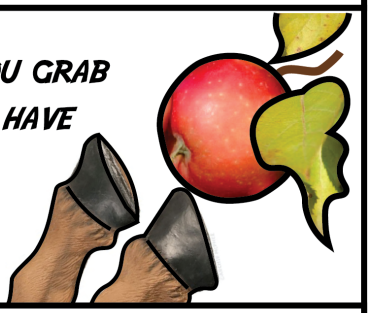

MANY ANIMALS USE THEIR TONGUE, A SOFT MUSCLE FOUND IN THE MOUTH, TO GRAB THEIR FOOD. TONGUES HAVE EVOLVED DIFFERENT FEATURES FOR GRABBING FOOD, LIKE...

THE ANTEATER WHO USES ITS STICKY, SNAKE-LIKE TONGUE TO SNATCH UP TERMITES

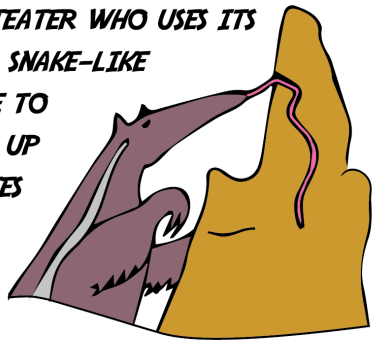

THE BAT WHO USES A MOP-LIKE TONGUE TO SUCK UP NECTAR

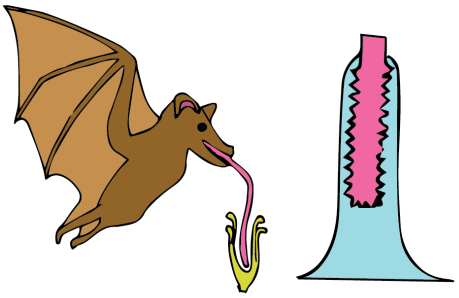

THE COW THAT USES ROUGH TONGUE SPIKES TO RIP UP PLANTS

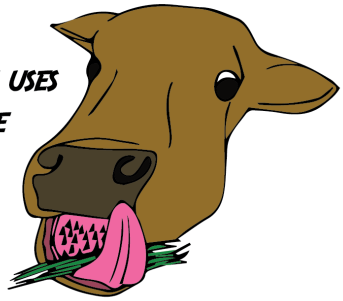

THE WOODPECKER THAT USES A LONG BARB-TIPPED TONGUE TO PIERCE INSECTS

THE WOODPECKER TONGUE IS SO LONG, IT WRAPS AROUND ITS SKULL!

FOR ALL THESE ANIMALS TO GATHER FOOD, THE TONGUE MUST

FIRST REACH

THEN GRAB

REACHING FOOD

THE PROBLEM: MUSCLE CAN ONLY CONTRACT

SO HOW CAN A TONGUE STRETCH OUT TO REACH FOOD?

FOR VERTEBRATES, THERE ARE 4 DIFFERENT TYPES OF TONGUES, EACH HAVING A DIFFERENT MECHANISM TO STRETCH AND REACH PREY

(1) THE FIRST, AND MOST COMMON TONGUE TYPE ARE MUSCULAR HYDROSTATS
THESE TONGUES STRETCH USING HYDROSTATIC ELONGATION

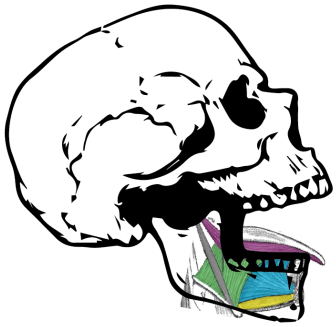

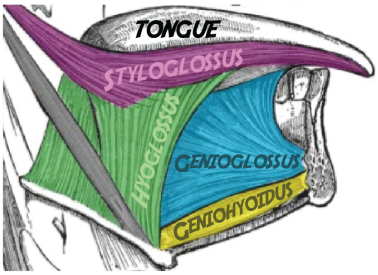

MUSCULAR HYDROSTATS, LIKE THE HUMAN TONGUE, HAVE MUSCLE BUNDLES ALIGNED IN DIFFERENT DIRECTIONS. OCTOPUS ARMS AND ELEPHANT TRUNKS ARE ALSO MUSCULAR HYDROSTATS!

MUSCLE TISSUE IS MOSTLY WATER, AND IS CONSIDERED INCOMPRESSIBLE. THIS MEANS MUSCLE VOLUME CAN'T CHANGE. SO, A DECREASE IN ONE TONGUE DIMENSION CAUSES AN INCREASE IN ANOTHER. STRETCH YOUR TONGUE OUT AND SEE HOW IT GETS NARROWER!

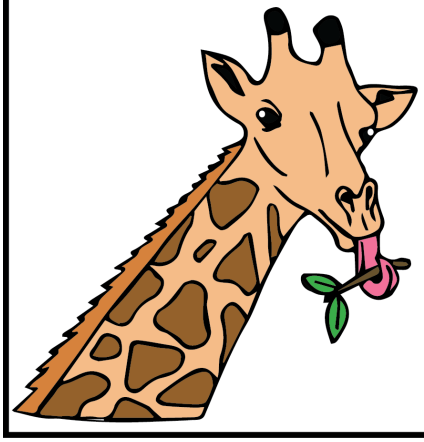

THESE DIRECTIONAL MUSCLE BUNDLES GIVE THE TONGUE EXTREME CONTROL: GIRAFFES ARE ABLE TO WRAP THEIR TONGUES AROUND BRANCHES, AND SUNBEARS CAN LICK JELLY OUT OF JARS.

THE NEXT 3 TONGUE TYPES ARE ONLY FOUND IN AMPHIBIANS AND REPTILES.
THESE ANIMALS EAT FAST-MOVING PREY, SO THEIR TONGUE MUST MOVE EVEN FASTER!

(2) MECHANICAL PROJECTOR TONGUES ARE FOUND IN FROGS AND TOADS.

MECHANICAL PROJECTOR TONGUES WORK LIKE A MOUSETRAP. THE GENIOGLOSSUS MUSCLE CONTRACTS, CAUSING THE TONGUE TO ROTATE OUT OF THE MOUTH.

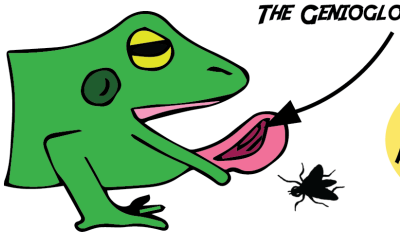

DID YOU KNOW? FROG AND TOAD TONGUES ARE ATTACHED TO THE FRONT OF THEIR LOWER JAW

UNFORTUNATELY, THESE TONGUES SHRINK AS MUCH AS 60% DURING PROJECTION, SO THE ANIMAL HAS TO LUNGE FORWARD TO COMPENSATE

(3) INERTIAL PROJECTOR TONGUES ARE ALSO FOUND IN FROGS AND TOADS.

THESE TONGUES SHOOT OUT FASTER THAN MECHANICAL PROJECTORS.

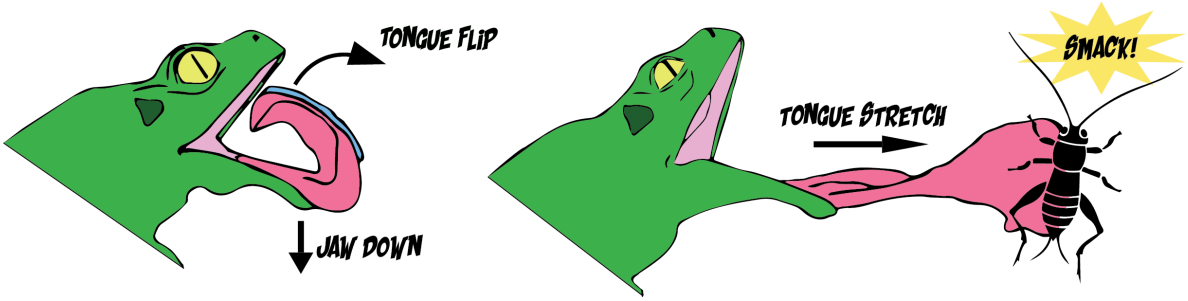

JUST LIKE MECHANICAL PROJECTORS, THE GENIOGLOSSUS CONTRACTS AND THE TONGUE ROTATES. ADDITIONALLY, THE JAW OPENS QUICKLY, CAUSING THE TONGUE TO STRETCH AND REBOUND BACK INTO THE MOUTH LIKE A BUNGEE CORD

(4) BALLISTIC PROJECTOR TONGUES ARE BY FAR THE MOST IMPRESSIVE.

THESE TONGUES ARE FOUND IN CHAMELEONS AND SOME SALAMANDERS, AND PRODUCE EXTREME ACCELERATIONS.

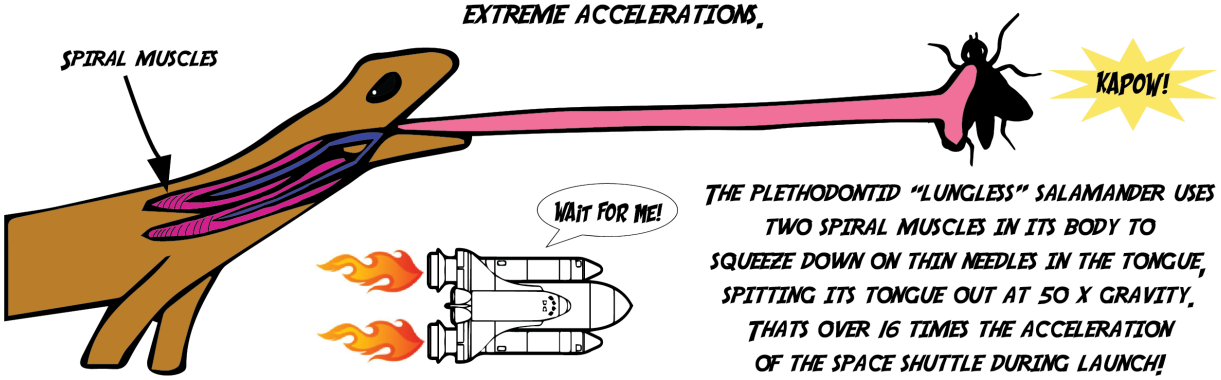

THE PLETHODONTID "LUNGLESS" SALAMANDER USES TWO SPIRAL MUSCLES IN ITS BODY TO SQUEEZE DOWN ON THIN NEEDLES IN THE TONGUE, SPITTING ITS TONGUE OUT AT 50 X GRAVITY. THATS OVER 16 TIMES THE ACCELERATION OF THE SPACE SHUTTLE DURING LAUNCH!

GRABBING FOOD

ONCE THE TONGUE REACHES THE FOOD, HOW DOES IT GRAB THE FOOD?

ONE WAY IS TO USE PAPILLAE, ANOTHER IS TO USE STICKY SALIVA

PAPILLAE

THE SKIN OF THE TONGUE IS COVERED IN TINY STRUCTURES CALLED PAPILLAE.

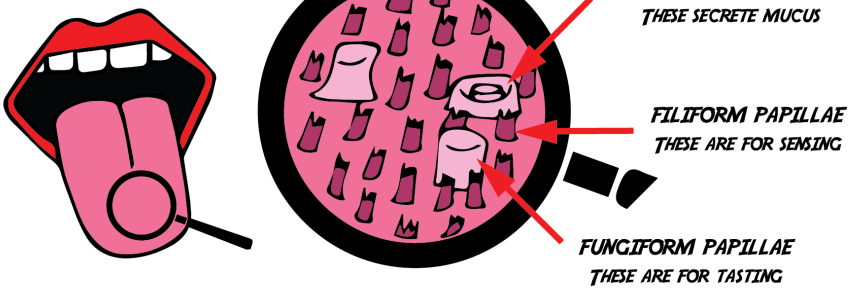

ANIMALS LIKE BIRDS, DEER, AND CATS HAVE LARGE, RIGID FILIFORM PAPILLAE THAT ANGLE DOWN THE THROAT

PENGUINS HAVE FILIFORM PAPILLAE AS LONG AS FINGERNAILS! THESE REAR-FACING SPINES WORK LIKE A ONE-WAY VALVE, PUSHING SLIPPERY FISH DOWN THE THROAT.

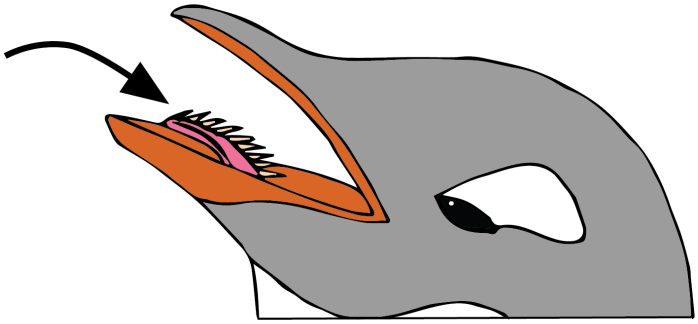

CATS HAVE A UNIQUE U-SHAPED CAVITY IN THEIR PAPILLAE. UNLIKE BIRDS, CATS USE THEIR ROUGH PAPILLAE TO TEAR MEAT OFF BONES, AND TO HELP WITH GROOMING.

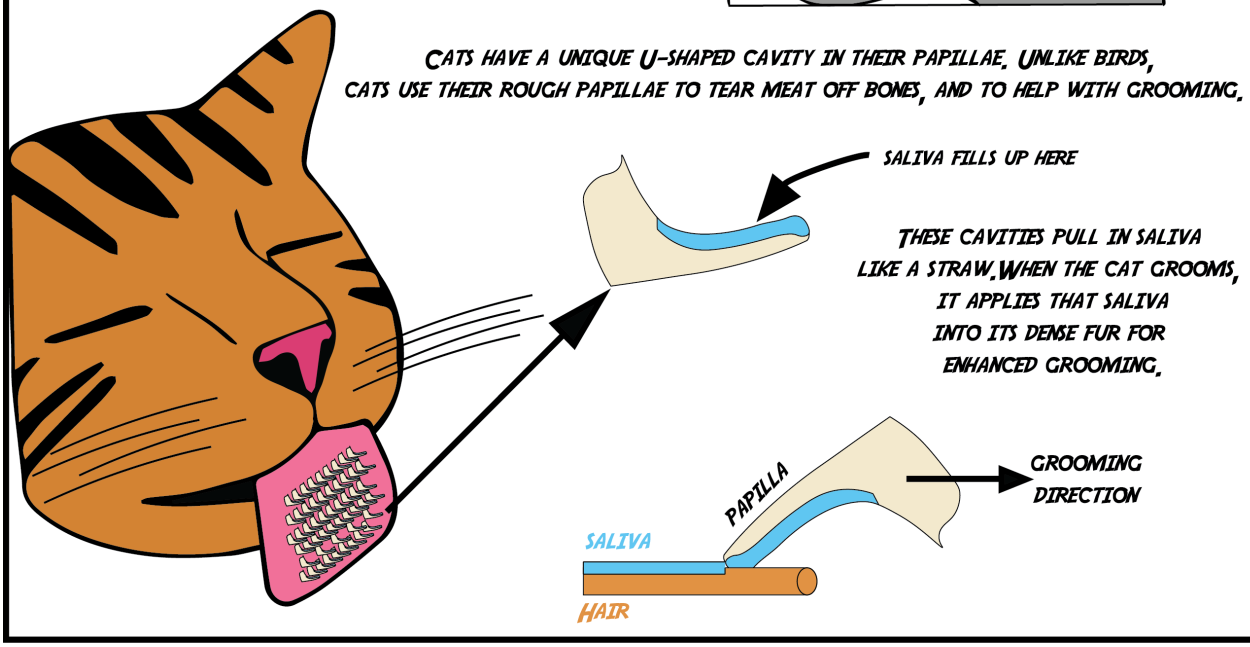

STICKY SALIVA

ANIMALS LIKE THE ANTEATER, FROG, AND CHAMELEON USE STICKY SALIVA ON THE TONGUE TO GRAB FOOD

STICKY SALIVA HELPS ADHERE TO PREY BY BEING VERY THICK, OR VISCOUS. FLUIDS THAT ARE VISCOUS RESIST MOTION.

TRY THIS AT HOME:

PUT SOME HONEY BETWEEN YOUR THUMB AND FOREFINGER. TRY TO SEPARATE YOUR FINGERS AT DIFFERENT SPEEDS. THE FASTER YOU TRY TO SEPARATE, THE HARDER IT IS! THIS IS THE DEFINING PRINCIPLE OF VISCOUS FLUIDS.

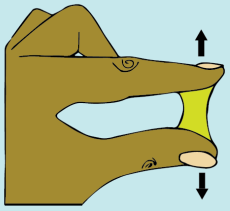

BY STUDYING THE WAY TONGUES MOVE AND GRAB, WE CAN BUILD NEW TECHNOLOGIES LIKE HAIR REMOVAL CARPET BRUSHES...

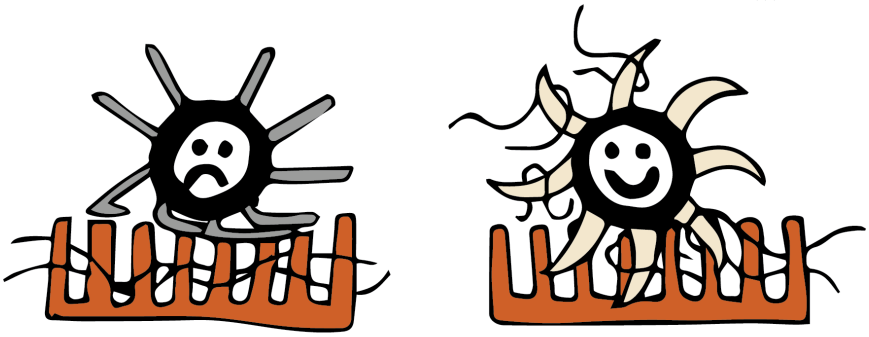

OR EVEN PERHAPS FAST GRIPPERS FOR MANUFACTURING.

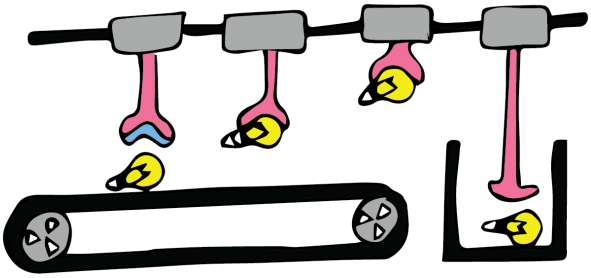

ACKNOWLEDGEMENTS

To my advisor, David L. Hu, for inspiring me to pursue a PhD in biomechanics and teaching me how to communicate science to the world.

To the National Science Foundation for their general financial support through the Graduate Research Fellowship Program. This material is based upon work supported by the National Science Foundation Graduate Research Fellowship (DGE-1650044).

To my labmates Patricia Yang, Guillermo Amador, Thomas Spencer, Marguerite Matherne, Olga Shishkov, and Alexander Bo Lee, for your company and friendship during this challenging yet rewarding PhD journey we embark on.

To Mark Mandica, for his endless support and expertise in herpetology, supply of rare frog tongues, and access to his incredible collection of amphibians at The Amphibian Foundation.

To the Atlanta Botanical Gardens for allowing us to film their exotic frog collection for many years.

To Dr. Joseph Mendelson and Zoo Atlanta for support in the frog and cat research, including filming.

To Dr. Laura O'Farrell for teaching me how to dissect deceased animals properly, and her constant assistance on our animal protocols.

To Michael Tennenbaum for training me on using the rheometer and his knowledge on rheology.

To Angela Lin, for teaching me how to use the CT scanner and microindentation machines in her laboratory.

To Candler Hobbs for his patience and expertise on taking photos of frogs catching insects, and of cats grooming (even with a cat allergy).

To Elma Kajtaz and Dr. Richard Nichols, for providing and gathering cat tongues and cat fur for my studies.

To T3 labs for providing human and porcine tongues for dissection.

To Carter Taxidermy and Feather, Fin, and Fur Taxidermy for providing tongue samples.

To Edward Ramsay and the Pathology Service of the UT College of Veterinary Medicine, and Tiger Haven for providing feline tongues.

To Hyun Choe and Jong Ha for being my first and most dedicated undergrads during my starting year of graduate school.

TABLE OF CONTENTS

LIST OF FIGURES

SUMMARY

The tongue is a soft muscle capable of grabbing different prey items through variations in tongue roughness and saliva coatings. In this thesis, I present two extremes of tongue surfaces: smooth frog tongues coated in sticky saliva, and rough feline tongues covered in rigid spiny microstructures. Frogs use a combination of their viscoelastic saliva and soft tongue tissue to adhere to and retract prey in less than 0.1 seconds. I conduct a subsequent study on 6 species of feline tongues, from lions to tigers to housecats. The hollow, rigid spines on the cat tongue aid in cleaning and detangling of fur by distributing saliva. The spines are anisotropic in direction, allowing for easy removal of fur from the tongue. Using CT scans of the cat tongue spines, I develop a flexible, 3D-printed cat tongue mimic, which is found to de-tangle fur with less force than a standard hairbrush. Lastly, an overview is provided of other biofluids, focusing on the effects of wetting.

CHAPTER I

INTRODUCTION

1.1 Motivation

The motivation behind this thesis is to understand how variations in tongue epithelial structures and fluids enhance grip functionality. The tongue may provide inspiration to the field of robotics, where gripping manipulators are often designed around a known singular object. Current robotic manipulators often use rigid components to operate with high precision and strength, such as those in car factories. However, these "hard robotic" systems are not suitable for interaction with humans or fragile objects. Within the past decade, there has been a growing interest in a new field of robotics, called soft robotics. Soft robotics looks to use compliant materials that can simultaneously sense and transport objects, with the ability to adapt to dynamic environments. The primary difficulty in soft robotics is that there are no governing equations of motion, and many systems experience high deformations if moved too quickly or during impact with targets. Additionally, gripping an object can involve numerous degrees of freedom, making controlled movement difficult[6,7]. While these restrictions may be troublesome for manmade materials, nature has evolved countless soft appendages that can move and grip, as evident in the diversity of animal tongues.

A critical challenge in soft robotics is movement. Soft systems must rely primarily on pneumatics or hydraulics, making them powerful but limited in speed and multidirectional control. As shown in **Figure 1**, a chameleon tongue can actuate at speeds nearly an order of magnitude faster than current soft robotic manipulators[8–17]. Tongue movements, in particular the inertial and ballistic projectors found in amphibians and reptiles, are capable of providing high speed, strength, and precision. Debray[18] and Hatakeyama[19] mimicked the chameleon tongue projection using a combination of a solenoid and elastic band. The recent development of additive manufacturing and silicone casting processes may make other tongue-inspired robots possible. A spiralized muscle could be replicated to simulate the radial contraction found in ballistic tongues, and could introduce a new field of high-speed soft projectors. Future tongue inspired robots may rely on technologies such as shape memory alloy to mimic muscle fibers[20], or fluidic elastomer actuators to simulate high-speed response in fish muscles[14].

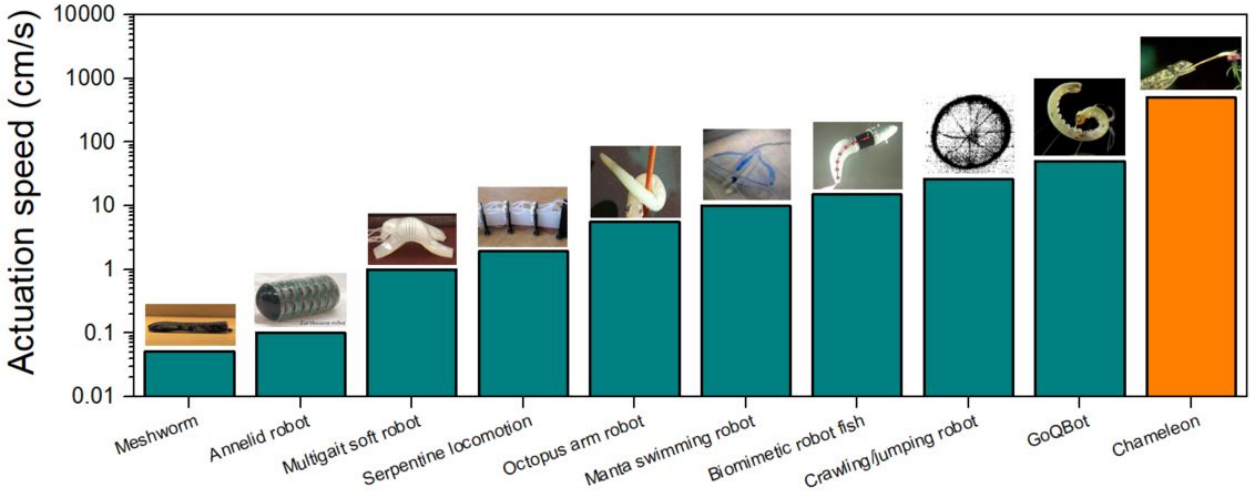

Figure 1: Actuation speeds for current soft robotic systems, which use pneumatic and hydraulic actuation methods. The chameleon tongue (as shown in orange) actuates 10 times faster than the GoQBot, the fastest recorded soft robot.

Another challenge in soft robotics is grip. Previous investigators have developed soft robotic manipulators that mimic flexible biological gripping systems such as the elephant trunk[21] and octopus arm[22]. Some grippers, such as the granular jammer[23], conform to highly textured surfaces through vacuum pressure. However, these systems rely primarily on applied frictional force, which can be difficult to control and may require knowledge on object shape and texture. Beyond friction-based grip, there has been a growing interest in bioadhesives and their applications. Adhesion to highly textured surfaces is a challenge, even for commercial tapes and glues. Vertebrate tongues have evolved many ways to grip surfaces, from using saliva adhesives to rough, sandpaper-like skin to sharp spines. While many of the biological features of tongues have been described, there lacks a theoretical framework that unifies the variety of tongues under a single goal, that of enhancing grip.

In this thesis, we ask the question: how can the contact surface of a soft robotic gripper be altered to provide grip? We turn to the vertebrate tongue for inspiration, a muscle with epithelial structures as diverse as the tongue functions themselves. We begin this investigation by exploring saliva-mediated adhesion found on the frog tongue, followed by a study on wetting and grooming enhanced by spiny microstructures on the cat tongue. We wrap up our investigation with an overview of other bioadhesives, and various tools invented during the thesis. Throughout these topics, we perform scaling analyses of morphological characteristics, kinematic observations, and theoretical modeling rooted in fluid mechanics. We close with a discussion of implications of our work and future directions.

1.2 Background

We begin with a broad background of vertebrate tongues, followed by a more detailed focus on prey capture with amphibian tongues and grooming with cat tongues.

1.2.1 The wide world of tongues

Well before the age of soft robotics, the vertebrate tongue had long intrigued anatomists. Human tongue tissue, like heart tissue, consists of bundles of muscle fibers bound by connective tissue into a three-dimensional array; it is because of this unique combination of radial and longitudinal bundles that one can peel off the fibers of a bovine steak but not the bovine tongue[24]. Doran and Baggett[25] classified mammalian tongues into two types, intra-oral and extra-oral. An intra-oral tongue is used primarily during mastication for saturating food with saliva. An extra-oral tongue is used for prey capture and food manipulation outside the oral cavity.

Extra-oral tongues accomplish a range of feats; for example, the giant palm salamander can spit out its tongue 50 times faster than the duration of a human eye blink[26], whereas the anteater navigates its sticky, 60-cm snake-like tongue into termite mounds[27]. How does the tongue differ between these two extreme scenarios? For both cases, the tongue must extend, yet herein lies the problem - the tongue comprises of biological muscle that can only contract. To solve this problem, the vertebrate tongue has evolved to convert contractive shortening into tongue elongation through four distinct mechanisms: mechanical pulling, inertial elongation, ballistic projection, and hydrostatic elongation[28,29], which I discuss in turn.

Mechanical pulling [**Figure 2A**] is employed primarily by amphibians such as frogs and toads. Such animals have a unique anatomy: in most mammals, the tongue is attached to the throat, but in frogs and toads, it is attached to the front of the lower jaw. Frogs and toads use this attachment point to propel the tongue like a mousetrap. The tongue rotates out of the mouth owing to the longitudinal shortening of the genioglossus muscle, the primary contraction muscle in the tongue. Since the tongue rotation speeds are slow and the centripetal forces minimal, the tongue unfortunately shrinks as much as 60% of its resting length. To compensate for this shortening, animals with mechanical pulling tongues will lunge their body forward to reach prey[28].

Inertial elongation [**Figure 2B**] is also used by frogs and toads. It is similar to mechanical pulling in that the genioglossus muscle contracts and causes the tongue to swing outward. In addition, the frog rapidly drops its jaw, giving the tongue an additional boost of speed[30], reaching velocities of 4 m/s. Jaw-dropping rates in inertial systems can reach 3700 deg/s, as we found in the frog *Rana pipiens*, twice the rate found in frogs that use mechanical pulling such as *Ascaphus truei*[1], which can reach 1800 deg/s. This additional speed causes the tongue to lengthen, eliminating the need for body lunging.

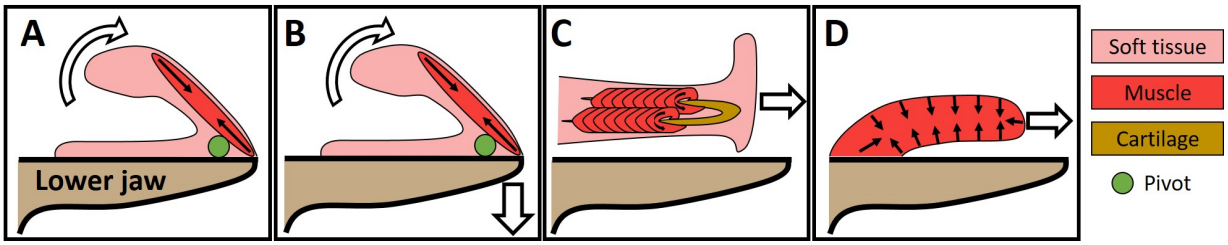

Figure 2: Tongue projection mechanisms. (A) Mechanical pulling, as seen in the Tailed Frog *Ascaphus truei*[1]. As the genioglossus muscle contracts, the tongue rotates forward. (B) Inertial elongation, as seen in the Northern Leopard Frog *Rana pipiens*. Rapid jaw opening and contraction of the genioglossus muscle causes the tongue to rotate forward and elongate. (C) Ballistic projection, as seen in the Plethodontid salamander. Muscles organized in a spiral array contract over a thin horseshoe-shaped cartilage to propel the tongue at high speeds. (D) Hydrostatic elongation, as seen in humans. Longitudinal and radial muscle fibers contract to extend the tongue.

All 160 species of chameleons and a number of species of salamanders have evolved unique ballistic projection mechanisms capable of generating tongue accelerations up to 50 times gravity[17,26,31]. The plethodontid "lungless" salamander tongue uses two spiral arrays of protractor muscles to compress the needle-like arms of a horseshoe-shaped cartilage skeleton. The skeleton folds medially as it and the surrounding soft, sticky tissue is projected out of the mouth [**Figure 2C**]. Chameleons extend their tongues using an energy storage-and-release mechanism. Cylindrical connective tissue sheaths are longitudinally loaded around a central cartilaginous bone; upon release, the loaded sheaths slide over the tip of this bone, projecting both the sheaths and the surrounding soft, sticky tissue. Mammals, to be discussed next, have a comparably more mundane technique called hydrostatic elongation.

In a review, Kier[32] described many vertebrate tongues as boneless muscular-hydrostats, composed nearly entirely of muscle that maintains an essentially constant volume. When the tongue is extended, this motion is called hydrostatic elongation. These tongues possess both longitudinal and radial muscle fibers, allowing for a high degree of motion control[33] [**Figure 2D**]. Tongues of this type share properties with octopus arms and elephant trunks. These muscles elongate by taking advantage of their incompressibility, and transmit force through internal pressure. Contraction of radial muscle causes the tongue to shrink in diameter but extend in length. For a cylindrical tongue of diameter D and length L, the volume may be written $V = \frac{\pi}{4}D^2L$. Since volume is conserved, we can write $0 = dV/dL = 2\pi DL + \pi D^2 dL/dD$, and therefore $dL/dD = -2L/D$. This constraint between tongue diameter and length makes certain tongue shapes able to extend more than others. A thin cylindrical tongue, like that of an anteater, elongates farther for a smaller decrease in diameter than a short, yet wide, tongue. Conversely, when the muscle is relaxed, the tongue is relatively short and can be conveniently stored without interfering with the upper throat.

Each of the aforementioned mechanisms is associated with tongues of different length. Tongue length is measured from tongue tip to point of attachment [**Figure 3A**]. The relationship between tongue resting length and body mass is shown in **Figure 3B** using data gathered from 12 different literature sources[1,27,34–43] as well as our own measurements, for over 70 species. Tongues of cow, coyote, Great Dane domestic dog, human, racoon, giant otter, fox, mink, rabbit, ring tail cat, hamster, rat, and squirrel are gathered from Zoo Atlanta, a local dissection lab, and a local supermarket. If tongues are received frozen, they are first defrosted before measuring resting lengths. For mechanical and inertial mechanisms, there is insufficient recorded tongue lengths to plot a trend accurately. Excluding the outliers (anteater, tube-lipped nectar bat, and pangolin), the tongue length for ballistic and hydrostatic mechanisms scales as:

$$L_{\text{ballistic}} = 73M^{0.26}(R^2 = 0.73, N = 23), \tag{1}$$

$$L_{\text{hydrostatic}} = 33M^{0.35}(R^2 = 0.81, N = 30). \tag{2}$$

As can be shown by the exponents (0.26 and 0.35), the tongues of at least hydrostatic projectors have a resting length which scales closely with body mass approximately to the 1/3 power, satisfying isometry.

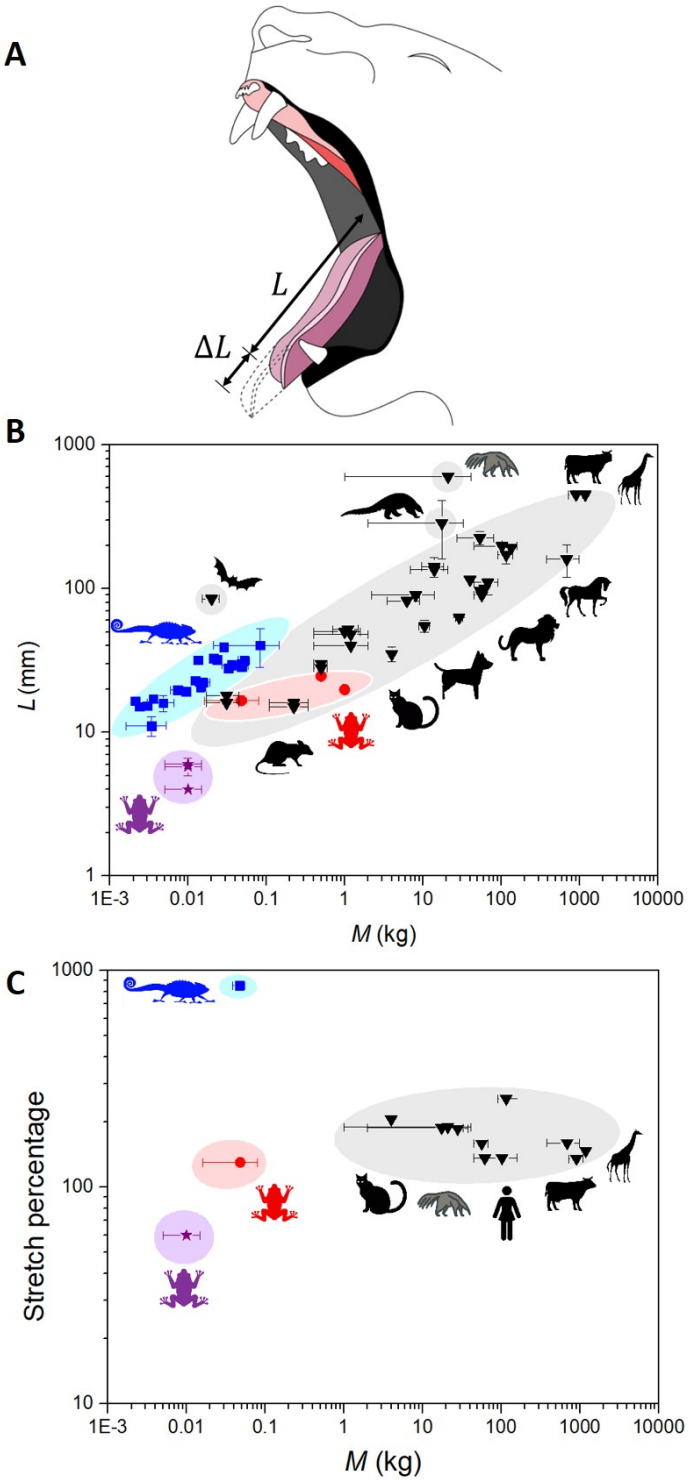

Figure 3: Feeding mechanics linked with tongue geometry. (A) Schematic diagram of a tongue. Resting length L is measured from the point of attachment to the tip of the tongue. The increase in tongue length ΔL. (B) The relationship between resting tongue length L and body mass, M. Included are the four tongue projection mechanisms defined in **Figure 2**: mechanical pulling (purple star ★), inertial projection (red circle •), hydrostatic projection (black inverted triangle ▽) and ballistic projection (blue square ■). (C) Stretch percentage across four tongue projection groups. Stretch percentage for ballistic projection (blue square) reaches well over three times that of inertial projection.

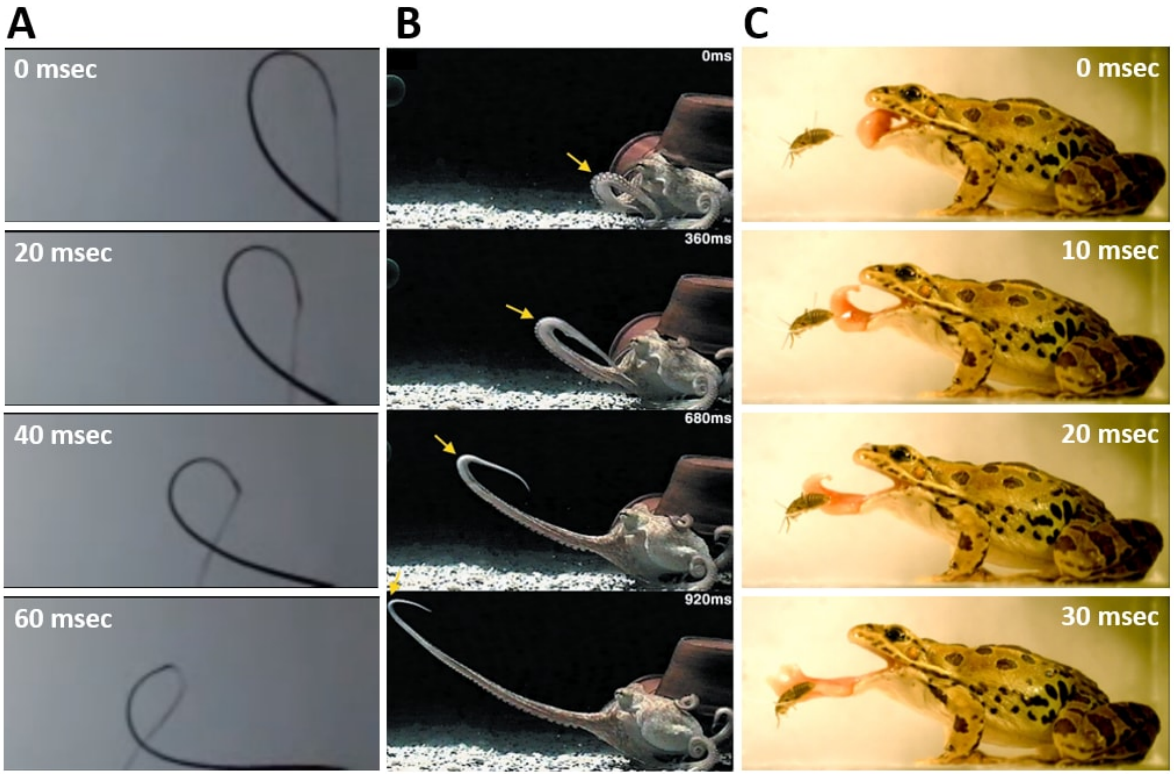

Figure 4: Whip-like motion found in hyper-redundant appendages. (A) Multiple exposures of a bullwhip exhibiting propagating waves during motion, kinematically similar to (B) an octopus arm and (C) inertial tongue projection in the frog *Rana pipiens*. Photo credit: (A) Youtube (user WorldWideWhips), and (B) Sumbre et. al 2001 [2].

Isometry, a property where body parts have constant proportions across body sizes, is shared by a variety of animals from cockroaches to humans [44]. Across a 100,000-fold change in mass, the tongue length increases nearly thirty-fold, nearly as expected by isometry. The factor of two difference in pre-factor for Eq. (1) and Eq. (2) is likely due to the different kinds of muscle tissue employed for each mechanism. For example, ballistic tongues are covered with a thick and soft epithelial tissue.

Several animals with hydrostatic tongues do not follow the same pre-factor, including the tube-lipped nectar bat *Anoura fistulata*, the pangolin *Manis javanica*, and the anteater *Myrmecophaga tridactyla*. The tube-lipped nectar bat drinks nectar from the flower *Centropogon nigricans* using a tongue that is 50% longer than its body, the longest tongue relative to body length of any mammal. The anteater and pangolin utilize snake-like tongues to gather ants and termites from insect holes. These three unique animals have specialized tongues that are detached from the hyoid bone [27,39,45], which is typically used for tongue articulation and swallowing. This adaptation allows these animals to store their extra-long tongues deep within their chest cavity. These three animals fit their own trend: $L_{\text{hydrostatic outliers}} = 177M^{0.32}(R^2 = 0.36, N = 3)$, which still follows isometry but involves tongue lengths six times longer than other hydrostatic tongues. Such adaptations demonstrate the substantial evolutionary pressures to lengthen the tongue.

A tongue that can stretch out to reach food has a higher chance of catching prey. Utilizing Kiers theory for volume conservation in muscular hydrostats [32], we write tongue "stretch percentage" as:

$$\text{Stretch percentage} = \frac{L + \Delta L}{L} * 100, \tag{3}$$

where L is the resting tongue length, and ΔL is the increase in tongue length [**Figure 3A**]. A stretch percentage of 100% means that the tongue does not change in length. Using data gathered from literature [17] and

YouTube videos to estimate ΔL, the tongue stretch percentage across vertebrates can be seen in **Figure 3C**. As shown by the black and red points in the plot, hydrostatic and inertial tongues have stretch percentages ranging from 130% to 250%. In contrast, the mechanical pulling tongue, shown by the purple point, shrinks during muscle contraction. For ballistic mechanisms, which rely on layers of sheathed tissue that extend like a telescope, the stretch percentage can reach well above 800%, as shown by the blue point representing a chameleon *Trioceros jacksonii xantholophus*.

Nishikawa first mentioned the frog tongue follows a nearly straight line from mouth to prey [28], which may help the frog to accurately target its prey. The same straight-line motion appears to be the case for the tip of a bullwhip and an octopus arm, other whip-like mechanisms that reach their targets quickly [**Figure 4**]. An octopus arm can unfurl along a single plane to snag prey with its suckers. Bullwhips exhibit a propagation of curling waves, ending in the high end-tip velocity and the well-known supersonic crack [46]. While the octopus arm and frog tongue appear similar in kinematics, the mechanisms by which they unravel are quite different. To unfurl its arm, the octopus employs a wave of muscle activation from the arms base to tip, likely to overcome the large drag forces in the water [47]. In contrast, the frog tongue stretches passively during unraveling [41], with the ability to extend in length from 36mm to 49mm, a stretch percentage of 130%. Other papers have noted stretch percentages of 180% for inertial elongators such as the *Bufo marinus* species [28,30]. This elastic stretching of the tongue also aids in tongue withdrawal, with the tissue springing back like a bungee cord, requiring less effort from the hyoglossus retractor muscle. Despite the differences in tissue extensibility, the bullwhip, octopus arm, and frog tongue are all able to project along a straight line with speed and precision; the comparable shape in which these different systems unravel deserves future investigation.

How does a frog tongues stretch relate to its material properties? During inertial tongue projection, rotational kinetic energy U_k from rapid jaw opening is transferred into elastic potential energy U_e. When the tongue is fully extended, there likely remains some kinetic energy in the form of waves along the tongue. We assume a bounding case of complete transfer to elastic energy, $U_\mathrm{k} = U_\mathrm{e}$ The elastic potential energy in the tongue tissue may be written as $U_\mathrm{e} = \frac{EA_0\Delta L^2}{2L}$, where E is the Youngs modulus and A_0 is the tongue cross-sectional area. Rotational kinetic energy (U_k) can be calculated from high-speed videos. To maximize the tongue reach, ΔL, for a fixed amount of kinetic energy, the Youngs modulus (E) should be as low as possible. In other words, to stretch far, the tongue should be soft.

Softness of materials is characterized by the materials stiffness or Youngs modulus: the lower the Youngs modulus, the easier it is to stretch the tissue. The Young's modulus is defined as the ratio of stress over strain to deform a material, and is valid for small deformations, where force necessarily changes linearly with displacement. Beyond this linear regime, the Youngs modulus must be used with care because biological tissue is often anisotropic and viscoelastic in nature. As detailed by McKee [48], tissue stiffness can span several orders of magnitude based on the direction and location that it is measured. In addition, the Youngs modulus of a tissue can vary between vivo or ex vivo, due to muscle activation by the animal.

The two most common ways to measure Young's modulus are by tensile stretching and indentation. Tensile stretching involves measuring the bulk muscle stiffness in a singular direction, while whereas indentation involves measuring the surface stiffness of skin (known as the epithelial tissue stiffness). For example, within the elastic regime at low deformations, the human tongue has an estimated bulk Youngs modulus of 294 kPa [49] and an epithelial Youngs modulus of 15.2 $\pm$ 3.9 kPa, which we measured using flat-plate indentation ex vivo. Thus, the tongue epithelial tissue is nearly 20 times softer than the bulk tissue. It is this notably different epithelial tissue that we explore in further sections.

Food can often be slippery, furry, or just plain hard to reach. To propel food into the mouth, animals are often aided by teeth, hands, paws, or lips. The tongue also has a dazzling array of prehensile functions. More notable work on tongue functionality includes studies on cat lapping by Reis et al. [43], dog lapping by Crompton and Musinsky [50], and tongue sensing through papillae deformation [51]. Historically, the tongue has received little attention as a manipulator, and instead has been regarded as an organ of taste or mastication. However, the skin of the tongue, known as the epithelial tissue, can be altered to help adhere to foods and fluids [52]. The epithelial surface of the tongue is covered in microstructures called papillae, as shown in **Figure 5A-F**. The two dominant types of papillae are fungiform and filiform. Fungiform papillae often take the shape of discs or mushrooms, and contain high concentrations of nerve endings and taste buds; due to the low density of fungiform papillae on the tongue, they are not considered to aid in grip. In this thesis, we focus primarily on the filiform papillae, which hereon will be referred to simply as papillae. Using data

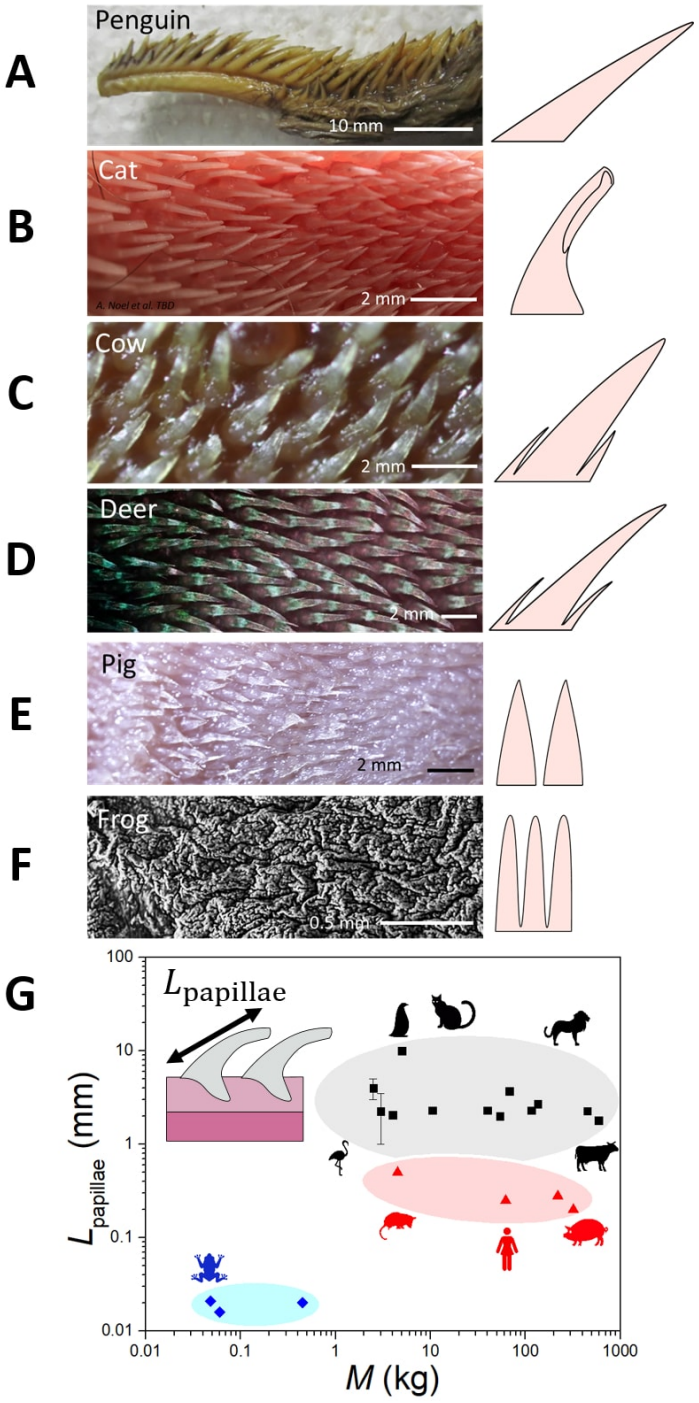

Figure 5: A tongue's surface projections, or papillae, range over 3 orders of magnitude in length. Papillae photographs (left) and schematics (right) of (A) nestling penguin *Aptenodytes fosteri*, (B) domestic cat *Felis catus*, (C) cow *Bos taurus*, (D) deer *Odocoileus virginianus*, (E) pig *Sus domesticus*, and (F) frog *Lithobates catesbeianus*, arranged from the longest to shortest papillae. Rigid papillae (A-D) tilt towards the throat, whereas soft papillae (E-F) do not. (G) Papillae length linked with grip technique. Large, rigid papillae (black square ■) greater than 1 mm are used for grip and tissue penetration. Soft papillae smaller than 1 mm are used for holding saliva on the tongue to enhance food saturation (red triangle △) and adhesion (blue diamond ⋄). (G, inset) Papillae length L_{papillae} measured from tongue surface to papilla tip. Photo credit: (A) Pablo Tubaro and Yolie Davies, Bernardino Rivadavia Natural Sciences Argentine Museum.

from literature[51,53–61] along with our own measurements, we find that papillae sizes range over three orders of magnitude [**Figure 5G**] and can have varying levels of keratinization, with some as rigid as fingernails. Large, rigid papillae are more than 1 mm long and help improve grip, like the claws on a cat. In contrast, papillae from 10 to 500 micron lengths are softer and are primarily used to hold saliva on the surface of the tongue, enhancing saturation and lubrication of food. Small papillae can also grip onto viscous saliva, which in turn helps the tongues of insectivores to adhere to prey.

1.2.2 Adhesion from small, soft papillae and viscous saliva

Although tongues of human, pig, and frog appear smooth, microscopy reveals that these tongues are covered in tiny, flexible papilla of lengths much less than 1 mm. The primary purpose of such short papillae is to hold saliva on the tongue. Saliva has a number of functions, including lubricating and protecting oral tissue, aiding in taste, and providing enzymes to enhance food breakdown and digestion[62]. Without saliva, food would be difficult to swallow and oral tissue would dry out, a risk for animals far from a water source. Short papillae are not keratinized and act instead like a soft toothbrush, utilizing surface tension of saliva to keep the tongue surface wet. The papillae may counteract the effects of evaporation and gravity that would otherwise drain the tongue of its saliva.

The most widely used evaporation equation is one proposed by Carrier[63], where the rate of evaporation e from a pool of water scales as $e \sim \frac{A_s V_b \Delta P}{Y}$. Intuitively, evaporation increases with the tongues exposed surface area A_s and breathing velocity V_b, and decreases with the latent heat of evaporation of saliva Y, which has units of kJ/kg. To retain humidity, animals from frogs to mammals close their mouths. Opening the mouth and letting the tongue hang out like dogs can help animals regulate heat. It is an open question as to how papillae regulate evaporation. Papillae can increase evaporation if they extend beyond the height of the saliva, increasing surface area, but these heights have yet to be measured in vivo.

At what point does gravity overcome surface tension and cause fluid to drain? The dimensionless Bond number Bo measures the relative importance between gravitational forces which scale as $\rho g h_0$ and surface tension forces which scale[64] as σ/a where ρ and σ are the density and surface tension of the water (which we assume to be near to saliva), g is gravitational acceleration, h_0 is the height of the saliva within the array, and a is the spacing between papillae. Surface tension can prevent drainage of the saliva if the Bond number is less than 1:

$$Bo = \frac{\rho g h_0 a}{\sigma} = \frac{\text{gravity}}{\text{surface tension}} < 1. \tag{4}$$

If we assume the saliva reaches the tips of the papillae, and papillae height and spacing is recorded at 0.25 mm and 0.1 mm respectively[51], then the Bond number for saliva in human papillae is 0.003, meaning that the papillae do an excellent job of keeping the saliva in place.

Although eating dry foods can absorb saliva, the tongue can easily wet itself again. The spreading of saliva is driven by a process called imbibition, or rough wetting. It is defined as the motion of liquid through a rough surface, such as fluid spreading in a paper towel. Imbibition is driven by a balance between capillary pressure and viscous dissipation. Bico and Quere[65] analyzed rough wetting, and developed the diffusion law to determine how the fluid front z moves in time:

$$z = \left(\frac{2}{3\beta} \frac{\cos(\theta_\mathrm{f}) - \cos(\theta_\mathrm{c})}{\cos(\theta_\mathrm{c})} \frac{\sigma L_\mathrm{papillae}}{\nu} t \right)^{1/2} \tag{5}$$

where θ_f is the contact angle on a flat surface, θ_c is the critical contact angle of imbibition, ν is the saliva viscosity, and β is a numerical factor to adjust for the presence of texture. We will use Eq. (5) in Chapter 5 to model the spreading rates of saliva across the tongue surface. To ensure that the tongue does not dry out during mastication, the saliva secretion rate must be greater than or equal to the saliva wicked into food. Virot and Jung[66] found that measured chewing frequency is greater than a limit set by saliva secretion rate and food bolus size, suggesting that additional saliva may be secreted to ensure tongue desiccation does not occur.

The function of saliva ranges from lubrication[67] to adhesion, depending on the saliva viscosity. Saliva is composed of many different ingredients, including electrolytes, proteins, enzymes, and mucins. It is the

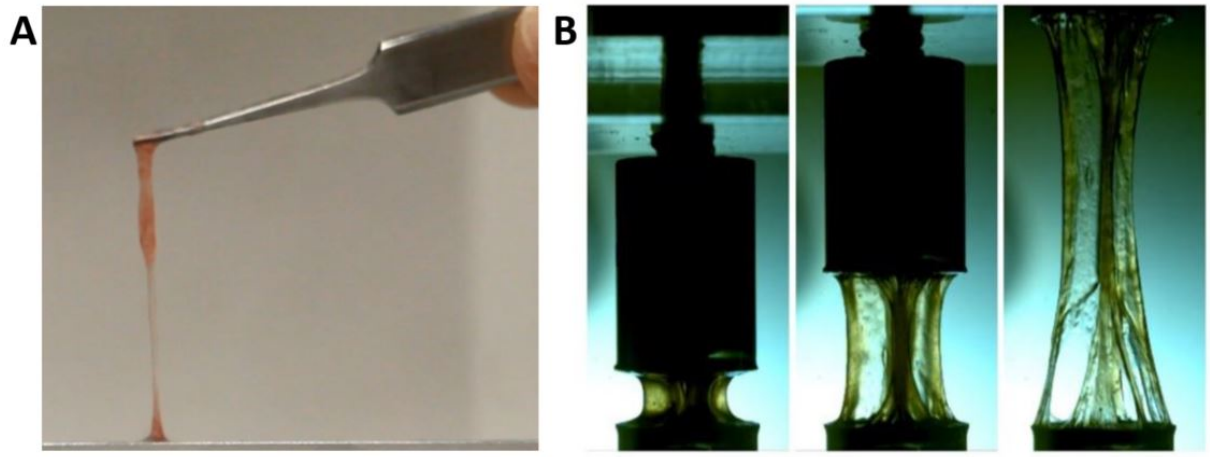

Figure 6: Saliva exhibits viscoelastic, shear-thinning properties. (A) Frog saliva from *Rana pipiens*, pulled using forceps stretched between two plates, shows high fibrosity in the form of fluid threads. (B) Frog saliva from *Rana pipiens*, stretch between two plates using the elongational rheomter Elo-Rheo. Fluid ribs indicate high elasticity.

mucins that have the greatest effect on viscosity[68]. Mucins are high-molecular-weight long-chain glycoproteins - it is these proteins that also give saliva the stringy effect, or fibrosity, allowing long threads of saliva to be stretched like hot cheese[69], a characteristic of certain non-Newtonian fluids [**Figure 6**]. Such long threads can commonly be seen in baby's drool or when handling a frog tongue. Mucin also gives saliva properties similar to those of paint, which is watery when spread with a brush, but solid-like when left on walls. This property is called shear-thinning, where viscosity decreases with shear rate.

In this thesis, we focus our attention on the unique saliva and epithelial tissue of the frog tongue, both which work together to act as a powerful adhesive. There are over 4,000 species of frog and toad that use a sticky, whip-like tongue to grab prey faster than a human can blink[70]. There is no known commercial mechanism that can match the grabbing speed of the frog tongue, let alone adhere to a highly textured surface like a fly. One may think that the frog tongue succeeds in capturing only lightweight prey; however, the frog tongue can pull up to 1.4 times the frogs body weight[71]. The tongue can adhere to surfaces that are hairy, feathery, furry, and slippery prey, such as tarantulas, birds, mice, and even other frogs. Little is known about the underlying physics that makes the tongue so sticky.

Frogs studies date back to the 1800's, when Augustus Waller published a paper on the frog tongue nerves and papillae[3]. Even then, Waller was fascinated with the soft, sticky nature of the frog tongue: "The attention of physiologists was first directed by me to the peculiar advantages possessed by the tongue of the living frog...the extreme elasticity and transparency of this organ induced me to submit it to the microscope" [**Figure 7**]. Kleinteich and Gorb were the first to measure the frog tongue retraction force in the Horned Frog *Ceratophrys cranwelli*; the average adhesive strength was 3.01 $\pm$ 2.53 kPa with a maximum recorded adhesive strength of 17.7 kPa. In the animal kingdom, these values are not the highest: the leaf beetle and Tokay gecko have adhesive strengths of 16.5 kPa and 100 kPa, respectively[72,73]. However, adhesive strength alone is not the most accurate indicator of stickiness. In our investigation, we also make clear the tongue's mechanism of adhesion. Kleintech postulated that the tongue acts like sticky tape or pressure sensitive adhesive (PSA), a permanently tacky surface that adheres to substrates under light pressure[55,71]. We show that the frog tongue acts more like a car's shock absorber than a PSA; its viscoelastic nature enables rapidly applied forces to be dissipated in the tongue tissue. The adhesivity of the tissue is due to the unique saliva, which is able to flow into textured surfaces and grip firmly during tongue retraction.

The most challenging part of catching prey is keeping the prey on the tongue. In this phase, the tongue accelerates back into the mouth using strong retraction muscles[74]. How does the prey remain stuck to the tongue? Previous models of adhesion have considered soft surfaces (e.g., Sneddon[75], Johnson-Kendall-Roberts[76] and Maugis[77]). These models consider adhesion in the context of surface energy and cannot be applied here since our soft substrate is coated in a layer of viscous fluid. In this thesis, we model adhesion

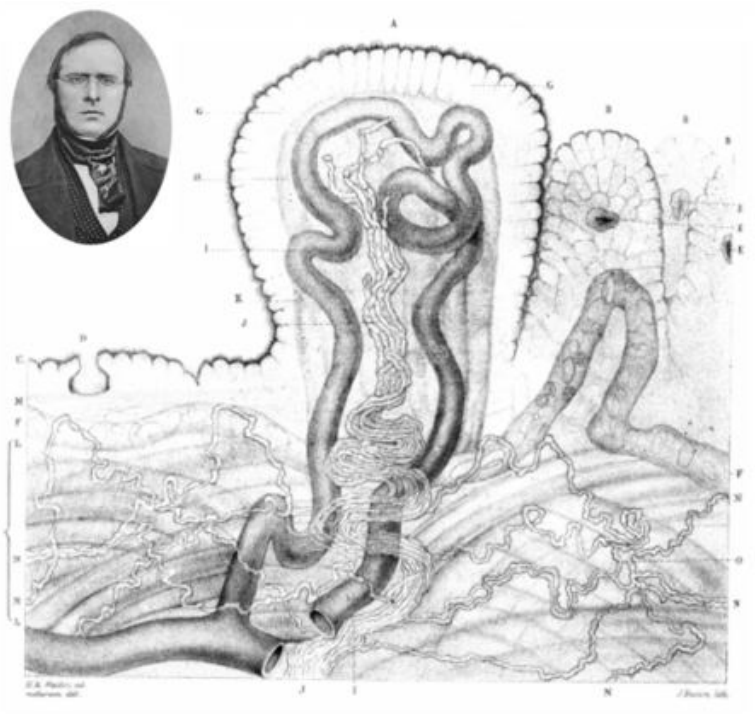

Figure 7: Augustus Waller and his study on frog papillae[3]. One of the earliest known papers to depict a hand-drawing of a frog papillae.

using the Stefan adhesion equation, a thin film separation theory for viscous fluids, for both frog tongue studies and fingertip sweat studies. This type of adhesion is also known as tack, and has been used to analyze biological adhesives such as limpet pedal mucus[78]. Stefan[79] performed the earliest work on tack, where he measured the time required to separate two flat discs immersed in a viscous fluid at a constant force. However, for the case of adhesives, we must consider the separation of two flat discs with a limited element of fluid in between (rather than immersed in fluid). Dienes and Klemm[80] re-derived the Stefan equation for the case of a viscous fluid between two flat plates, where the radius of the specimen changes with time due to the motion of plate separation (i.e. fluid volume is constant). This alternative Stefan equation describes the relationship between applied force F_{adh} and displacement h between the plates as:

$$F_{\text{adh}} = -\frac{3\mu\pi^2 R_0^4 h_0^2}{2\pi h^5}\frac{dh}{dt}, \tag{6}$$

where μ is the fluid viscosity, R_0 is the plate radius, h_0 is the initial plate spacing, and h is the plate spacing over time. As seen by Eq. (6), peak force occurs during initial separation. Additionally, force to separate plates is directly dependent on the viscosity of the fluid: the more viscous the fluid, the harder it is to separate the plates. It is important to note that Stefan adhesion is rooted in three assumptions: that both plates are rigid, the fluid is Newtonian, and the initial fluid thickness is much less than plate radius $h_0 << R_0$. For the case of the frog tongue, a soft surface coated in a non-Newtonian saliva, two of these assumptions are broken; however, this alternative Stefan equation can still be used in certain regimes. In this thesis, we present a series of adhesive models of increasing sophistication, incorporating saliva rheology in combination with tongue viscoelasticity.

1.2.3 Gripping and grooming with rigid papillae

Large papillae arise in cats, hoofed animals, and birds. Some penguins, geese, and flamingos have 1-cm long backwards-slanted spines to help push slippery plants and prey down the throat. Hoofed animals such as

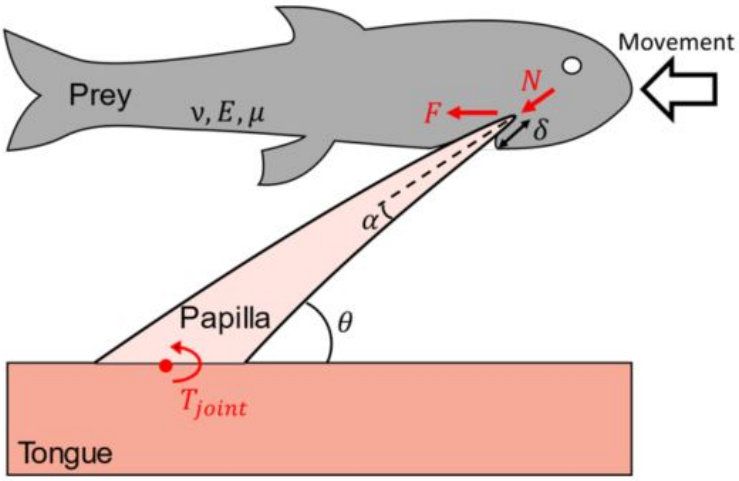

Figure 8: Sharp, rigid papillae enhance soft tissue grip through angled indentation. A schematic of a fish resting on a penguin papilla (n.b. not to scale) showing applied normal force N, applied force from movement F, tissue Poissons ratio ν, Youngs modulus E, papilla cone half-angle α and tongue surface angle θ, and papillatongue joint resistive torque T_{joint}.

deer use conical papillae to tear plant matter. Cows do not have upper front teeth, necessitating an even rougher grip than deer. This grip is accomplished by the cows trident-shaped papillae. We can model how papillae grip the surface by using microindentation theory[48]. For a conical indenter pressing into a soft tissue, the relationship between depression distance δ and applied normal force N is:

$$\delta = \sqrt{\frac{\pi}{2}\frac{N\sin(\theta)}{\tan(\alpha)}\frac{1-\nu^2}{E}}, \tag{7}$$

where α is the half angle opening of the cone, θ is the angle between cone and tissue surface (if the indenter is not perpendicular), and ν and E are the Poissons ratio and Youngs modulus of the tissue, respectively. Eq. (7) is also used to measure the Young's modulus of ex vivo biological tissues, where the tissue is assumed to be linearly elastic and homogeneous at small deformations. For grip, we use the example of the tongue of the penguin *Aptenodytes fosteri* (Emperor penguin), as shown in **Figure 8**, interacting with a fish to investigate how papillae may interact with a soft object.

Consider a fish resting on the penguin papillae, approximated as a cone [**Figure 5A**], as it slides into the throat to the right. The fish applies a normal force N onto the sharp tip of a single papilla, causing deformation of the fishs skin. Clearly, penetration depth increases with sharper papillae and increased applied force. Papillae are indeed quite sharp: we find that a domestic cat papilla[81] has a cone angle of 7° and a deer papilla of 9°. A cow has trident-shaped papilla, with the central spike having a cone angle of 15° and the adjoining spikes reaching 9°. By comparison, a cat claw has a cone angle of 8°. While the cat papilla and cat claw have similar cone angles, it is important to note that the conical tip radius of the cat claw is 0.09 mm, much sharper than the cat papillae of radius 0.14 mm. The smaller tip radius makes the claw more likely to puncture tissue.

The backwards-slanted papillae work like a one-way valve, allowing food to slide into but not out the mouth. If the fish in **Figure 8** slides to the right, the papilla rotates clockwise and slides out of its insertion point. Conversely, if the fish slides to the left, the papilla rotates counter-clockwise and its tip digs deeper, resisting the motion. The rotation of the papillae is further resisted by connective tissue at the papillaes base, which apply a resistive torque T_{joint}. While many animal tongues contain rigid papillae for grip, none are as unique as the feline papillae. In this thesis, we will be focusing on the filiform papillae found on the feline tongue, and how it aids in grooming and wetting of fur.

Cats are the world's most popular pet, with over 74 million household cats in the United States alone. These small, furry, carnivorous mammals are known to excel in stealth, balance and sensing. Cats have paws that are optimally damped for quiet movement[82], aerial righting reflexes to recover from large height drops[83], tactile whiskers for sensing contours[84], large omnidirectional ears that can hear two octaves higher than humans[85] and a lapping mechanism to minimize splash during drinking[43].

Cats can spend up to 24% of their awake time grooming their fur coat[86], removing loose hairs, fleas, and regulating body temperature[87–89]. If left ungroomed, loose hair, dirt, and feces can form matted fur, causing infection or painful tugging of the skin. Grooming cat fur is no easy task, due to its two layers: an exposed topcoat used for environmental protection, and a hidden undercoat of down hairs used for thermoregulation[90]. It is well known that long-haired breeds of domestic cat run a high risk of fur matting, requiring additional grooming. Why do long-haired breeds of domestic cat require attentive grooming, while long-haired cats such as the snow leopard do not? To answer this question, we look to the original and still most effective cat grooming tool, the tongue.

The cat tongue is most recognized for the sharp, backward-facing keratin spines called filiform papillae. The first study on cat papillae concluded that these keratin structures are conically shaped[91]; in later studies, this observation was never contradicted[92,93]. In my combined experimental and theoretical study, I examine the tongues of six cat species and show that the papillae are not conically shaped, but rather scoop-shaped. These cavo papillae wick up saliva, which is then distributed to the fur for enhanced grooming. Many organisms utilize surface tension to drink, walk, climb, and jump[94–96]. During lapping, felines have been shown to use their smooth tongue tip to pull up water[43], while dogs create a cuplike shape with their tongue to scoop up water[97]. A smooth cat tongue, while ideal for drinking, would only wet the exposed topcoat during grooming. The cavo papillae on the cat tongue can penetrate past the topcoat and wet the undercoat.

In this investigation, we hypothesize that these microcavities in the papillae allow the cat to coat more hairs during grooming. Understanding how these papillae distribute fluid is beneficial for both cleaning technologies and pet medicinal applications, where novel fluid applicators for dense arrays of fibers is in demand.

1.3 Thesis outline

In this thesis, we investigate several mechanisms employed by animal tongues to grip, grab, and groom. For all studies, we develop novel experimental and theoretical techniques to visualize and understand the biomechanics driving the gripping or wetting mechanism. Most of this thesis is drawn from recent papers and preprints[41,81,98], while the remainder details smaller investigations into the sticky nature of biofluids. Chapter 2 summarizes the experimental methodologies used in the thesis.

We begin at Chapter 3, where we investigate the adhesivity of the frog tongue. Through high speed videography, we find that the frog tongue can capture prey in under 0.07s, and can reach accelerations of 120 m/s^2, 12 times the acceleration of gravity. The insect is able to stick to the tongue under these extreme accelerations due to a combined effort of soft tongue tissue and viscoelastic saliva. Through microindentation techniques, we find that the frog tongue is 10 times softer than the human tongue, and contains both elastic and damping properties to help reduce pulling force on the insect. We find that tongue softness is comparable across 7 other species. Through rheological testing, we find that frog saliva is a non-Newtonian, shear-thinning fluid, capable of rapidly transitioning from high viscosity to low viscosity. These two viscosity scenarios aid in either prey capture or prey removal. We then apply our theoretical model for adhesion through a tack test, incorporating both the elastic tongue tissue and viscoelastic saliva.

In Chapter 4, we investigate how the sharp, hollow cavo papillae on the cat tongue aid in grooming. We begin this investigation with high speed videography, where we record grooming kinematics. We then present tongue and cavo papillae characteristics for a variety of cats, using tongues collected from 6 different cat species. We present mathematical models that detail the relationship between papillae and fur for both long and short-haired species of cat. We develop a grooming mimic, using a real cat tongue and cat fur, which simulates a wet cat tongue moving through fur at measured grooming velocity. We find that the saliva penetrates the fur through porous wicking; we use Darcy's capillary model for wicking in porous media to model saliva penetration depth into fur. Lastly, we discuss how the papillae aid in thermoregulation by distributing saliva through the hairs.

Chapter 5 discusses how other biofluids aid in wetting and adhesion. We start by investigating the

mechanics behind wetting on microtextured tongue tissue for pig and deer. We then discuss how earwax fluid properties and air circulation within the inner ear aids in dust collection.

In Chapter 6, we present the various tools and mimics invented during the thesis. We first detail Elo-Rheo, a portable elongational rheometer built to test non-Newtonian fluids, from frog to anteater saliva. This elongational rheometer is able to pull two circular plates apart at both linear and exponential rates, up to 1 m/s. Elo-Rheo was then retrofitted into a grooming mimic, to replicate cat grooming kinematics and forces. For the cat grooming study, we develop a hairbrush, inspired by the hollow papillae on the cat tongue. The hairbrush mimics the anisotropic nature of the papillae, which can rotate in a flexible substrate and distribute fluids into dense arrays of fibers. We conclude this thesis in Chapter 7, where we discuss implications of our work and future directions.

CHAPTER II

EXPERIMENTAL TECHNIQUES

2.1 General Techniques

2.1.1 Tongue sample collection

Mammalian and amphibian tongues for the entirety of this thesis were gathered from a variety of locations. Tongue samples were collected from the following amphibians: *Rana pipiens* (Ranidae) *Lithobates catebeianus* (Ranidae), *Ceratophrys cranwelli* (Ceratophyridae), *Rhinella marina* (Bufonidae), *Kaloula pulchra* (Microhylidae), *Lepidobatrachus laevis* (Ceratophryidae), *Scaphiopus holbrookii* (Scaphiopodidae) and *Phyllomedusa trinitatis* (Phyllomedusinae; Hylidae). Tongues were collected from the following mammals: cow, coyote, white-tailed deer, Great Dane domestic dog, human, racoon, giant otter, fox, mink, rabbit, ring tail cat, hamster, rat, squirrel, pig, domestic cat, bobcat, cougar, snow leopard, tiger, lion, and human. Between measurements, the tongue samples were kept frozen, and defrosted no more than 5 times. Tongues were gathered from Zoo Atlanta, T3 Labs, Feather, Fin, and Fur Taxidermy, Great Wall Chinese Supermarket, University of Tennessee Veterinary Department, and Atlanta Botanical Gardens.

2.1.2 Measuring tongue length L

Tongue resting length L for ex vivo tissue was measured from the frontmost tip of the tongue to the point of attachment in the throat or mouth cavity. Data was gathered from 12 different literature sources [1,27,34–43] as well as our own measurements, for over 70 species. All measurements were taken for soft, defrosted tissue.

2.1.3 Measuring change in tongue length ΔL

Change in tongue length ΔL was measured as the difference between resting tongue length and fully extended tongue length. Data was gathered from literature [17], from a previous study [41], and from the following YouTube videos: "Longest dog tongue ever?!" by Finchesca, "Tongue Stretch" by British Arabian College of Equine Studies, "Pulling a cat tongue out" by Funny videos without sound, "Inside the tigers mouth" by Brians Art for Animals, "Funny sheep sticks tongue out" by Warbinator, "How long is this pangolin's tongue!" by Africa Geographic, and "Having some cow tongue" by OrangeCabinet.

2.1.4 Measuring papillae length $L_{\mathbf{papillae}}$

For tongues of penguin, cow, deer, pig, domestic cat, bobcat, cougar, snow leopard, tiger, and lion, filiform papillae lengths L_{papillae} were measured from tip to base attachment for largest papillae. Measurements were taken using a USB microscope.

2.2 Techniques used in Chapter 3: The adhesive frog tongue

2.2.1 High speed videography and kinematics of frog tongue projection

Five leopard frogs *Rana pipiens* (Sullivan Company) were used for high speed videography of tongue projection. The frog was placed into a clear acrylic container and a 0.5 gram cricket was suspended with fishing twine. Tongue projection was filmed from the side using a Phantom Miro M110 high-speed camera at 1,400 fps. The video was analyzed using Tracker to determine tongue kinematics. A sinusoidal fit is applied to the insect capture kinematics data (black □) from **Figure 10B**, and the applied tongue force (black line in **Figure 15A**) is determined to be $F_{\text{tongue}} = (m_{\text{t}} + m_{\text{p}})B\omega_{\text{b}}^2 cos(\omega_{\text{b}} t)$, where $m_{\text{t}} = 0.5$ grams is the average mass of the frog tongue, $m_{\text{p}} = 0.5$ grams is the average mass of the prey, $B = 0.0205$ meters is the amplitude of the tongue tip during prey capture and $\omega_{\text{b}} = 105 s^{-1}$ is the tongue base frequency.

2.2.2 Tissue softness measurement

A Bose ElectroForce 3100 was used to perform quasi-static probe indentation tests on all frog tongue tissue samples. A leopard frog tongue was collected and tested within 1 hour of death; tongues from all other frog and toad species were frozen post-mortem, then defrosted and tested. Each species was tested 3 times except for *Phyllomedusa trinitatis* which was tested once. Each tongue was tested in the elastic solid regime, where stress is linear with strain. A rigid, flat-ended cylindrical indenter of diameter 2 mm was used to probe the tissue at a rate of 0.02 mm/s. The force-displacement model for a cylindrical indenter is:

$$F = \frac{2E_{\text{tongue}} r \delta}{1 - \nu^2} \tag{8}$$

where E_{tongue} is the tongue's Young's modulus, r is the indenter radius, δ is displacement, and ν is the Poisson's ratio. Poisson's ratio is assumed to be 0.5 for a perfectly elastic material[48]. The Young's modulus was calculated from the force and displacement measured from the indenter.

2.2.3 Dynamic indentation

Using the same setup from the quasi-static indentation test, the cylindrical indenter was sinusoidally pressed into the tongue tissue at various frequencies with an amplitude of 1 mm, and the force was recorded. The Kelvin-Voight model is used to represent the tissue as an elastic spring and purely viscous damper in parallel. The system is described by the linear differential equation: $m\ddot{u}(t) + C(\omega)\dot{u}(t) + K(\omega)u(t) = f_0 \sin(\omega t)$, where m is the indenter mass, $C(\omega)$ is the damping coefficient, $K(\omega)$ is the stiffness coefficient and ω is the frequency. The sinusoidal resistive force is given by $F(t) = f_0 \sin(\omega t)$, and the applied indenter displacement is given by $u(t) = u_0 \sin(\omega t - \phi)$, with a phase shift ϕ. The stiffness and damping coefficients for each frequency can be determined by measuring ϕ, f_0 and u_0, and are given by the following solutions to the differential equation[99].

$$K(\omega) = \left|\frac{f_0}{u_0}\right| \cos(\phi) + m\omega^2 \tag{9}$$

$$C(\omega) = \left|\frac{f_0}{u_0}\right| \frac{\sin(\phi)}{\omega} \tag{10}$$

The Young's modulus can be determined by using Eq. (9), with $K(\omega) = \frac{2E_{tongue}r}{1-\nu^2}$.

2.2.4 Saliva shear viscosity tests

Saliva was collected by opening the mouth of a recently euthanized frog and rubbing its tongue on a plastic sheet. The thin layer of saliva was then swirled using tweezers until a saliva globule was formed. The globule was immediately placed in a sealed container. For one frog, this process took less than 30 seconds. We were able to collect saliva with minimal evaporation due to the unique seal of the frog mouth, which protects from water leakage. This process was repeated for all frog specimens. Care was taken to use an intact tongue so that blood did not contaminate the sample. The 0.3 mL saliva sample was placed in a cone-plate rheometer (Anton Parr MCR 501) and a frequency sweep test was performed from 0.01 s^{-1} to 10 s^{-1} to determine the shear viscosity. During the test, the sample was surrounded by a ring of water to reduce saliva evaporation rate. Following the hour-long experiment, the saliva was intact, with only slight evaporation found at an edge.

2.2.5 Saliva Stefan adhesion

A Bose ElectroForce 3100 was used to perform Stefan adhesion tests on a leopard frog saliva sample. A rigid, flat-ended cylindrical indenter of radius 5.5 mm was brought into contact with a saliva sample of height 0.5mm, then retracted at a speed of 0.02 mm/s to a total displacement of 1.5mm. The force from three trials was recorded. The force sensor had a reading offset of 0.02 N. Between each trial, the saliva was scraped off the indenter and reapplied to the base platform to reduce air pockets in the sample. The duration of each trial was 75 seconds, with approximately 60 seconds between each trial. The third trial exhibited exhibited slight evaporation of the saliva sample, as evident in the data discrepancy.

2.2.6 Quasi-static adhesion

Using a Bose ElectroForce 3100, a 5.5 mm radius aluminum indenter was brought into contact with a freshly severed leopard frog tongue then retracted at a rate of 0.02 mm/s. The force from 11 trials was recorded, then averaged for **Figure 14C**. To reduce sliding of the frog tongue and the base plate, the bottom of the tongue was wiped dry prior to experimentation.

2.2.7 Peeling visualization

A transparent acrylic indenter of radius 5.5 mm was used to visualize peeling during quasi-static adhesion. The indenter was created on a lathe, and the base sanded with high grit to ensure optical clarity. A Canon EOS 1D camera was used to film the progression of full contact to separation. The video was then analyzed using MATLAB to find total contact area between tongue and indenter over time.

2.2.8 Dynamic simulation

The frog tongue and prey is modeled as a mass-spring-damper system [**Figure 10C**]. Using the principle of superposition, the applied tongue force ($m_p\ddot{y}(t)$) can be modeled as a summation of unit impulses over time. Using the convolution integral, we can combine the applied tongue force curve with the response for a unit impulse for our single degree-of-freedom system[100]. The convolution integral provides the spring stretch δ over time.

2.3 Techniques used in Chapter 4: Cat tongue papillae aid in grooming

2.3.1 High speed videography, kinematics, and forces during grooming

To measure grooming kinematics of a domestic cat, a wet washcloth is wiped on the upper back of the cat to entice the cat to groom. Grooming was filmed from the side using a Phantom Miro M110 high-speed camera at 500 fps. The video was analyzed using Tracker to determine tongue kinematics. Additional kinematic data for large cats is gathered through YouTube videos. As shown in **Figure 9** below, measured lick length L_{lick} is 3 times longer than tongue length L_{tongue} for domestic cats. Next, to measure tongue grooming forces, a piece of fake nylon fur (of hair length 8 cm) is secured to an AMTI HE6x6 force plate. The fur is sprayed with an attractant, to entice the cats to lick the fur. As lick data is collected, a camcorder at 30 fps is used to sync grooming patterns to force measurements.

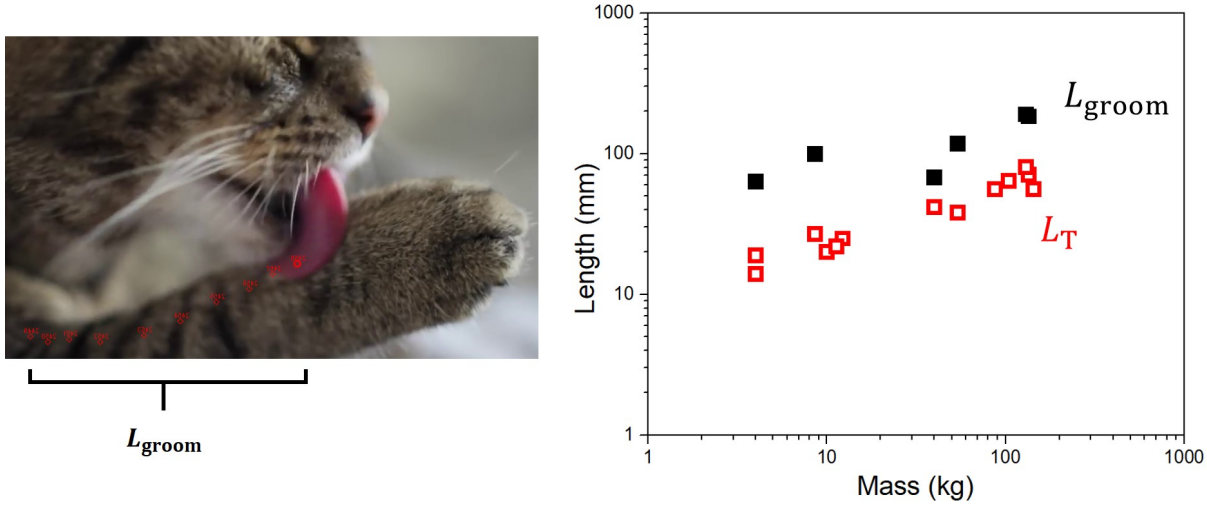

Figure 9: Grooming lick length. (left) Tracking the tongue during grooming using Tracker software. (right) Lick length is 3 times longer than tongue length.

2.3.2 Papilla μCT visualization

The tongue samples are donated from the following groups: six Felis catus from the Applied Physiology department at Georgia Tech, one Panthera tigris from Zoo Atlanta, three Lynx rufus and one Puma concolor from Carter Taxidermy, and three Panthera tigris, one Panthera uncia, one Panthera leo from the Department of Small Animal Clinical Services at University of Tennessee and Tiger Haven. While frozen, the largest grooming papilla from each tongue is removed using a scalpel and tweezers. Care is taken to avoid compressing the papillae. Each cat papilla is individually scanned using a Scanco μCT50 x-ray micro-computed tomography machine using a 3.5mm diameter tube, at highest resolution. Cavity width, height, and volume are measured from the scan using Blender software.

2.3.3 Fur properties

Fur specimens for cat species *Acinonyx jubatus*, *Caracal caracal*, *Felis sylvestris*, *Panthera pardus*, *Panthera leo*, *Panthera uncia*, and *Panthera tigris* are measured at the Museum of Comparative Zoology at Harvard University. Additionally, samples of bobcat *Lynx rufus*, mountain lion *Puma concolor*, and lynx *Lynx lynx* fur are purchased from Promise Land Tannery. Using a portable USB microscope, we measure down hair radius and length. Additional fur density and length values are gathered from literature[101–103].

2.3.4 Young's modulus of tissue and papilla

We measure the softness of the domestic cat tongue in the perpendicular direction using microindentation. A Bose ElectroForce 3100 was used to perform probe indentation tests *ex vivo* on a cat tongue tissue sample. The cat tongue was collected and tested within 10 hours of death. A rigid, flat-ended cylindrical indenter of diameter 2 mm was used to probe the soft tissue on the underside of the tongue (no spines). Within the linear elastic solid regime, the Young's modulus was determined using Eq. (8). The average Young's modulus of the cat tongue is 9.1 $\pm$ 3.7 kPa (N = 5 trials). The softness value correlates well to the Young's modulus of muscle at 7 kPa[104]. Next, we remove a single papillae from the cat tongue tissue and test the Young's modulus in a Hysitron TriboIndenter nanoindenter. The Young's modulus of the papillae is 1.66-1.94 $\pm$ 3% GPa, similar to human fingernails[105].

2.3.5 Resistive torque of a papilla in tissue

We measure the torque vs. angular deflection of an embedded papilla in the soft tissue through tensile testing with a Bose ElectroForce 3100. A loop of diameter 0.4 mm was created using copper wire. The tongue tissue was secured vertically to a plate and the wire loop was placed around the tip of a single papillae. The wire loop was then pulled vertically at a constant rate of 0.02 mm/s, and the corresponding force was measured. The wire loop was not observed to slip during trials. The tongue tissue surface was coated in an oil-based UV dye for visualization. The force vs. displacement data of the spine tip is shown in **Figure 20**, and follows an exponential trend as shown in the solid red line. This deflection characteristic is similar to a progressive spring, often used to limit displacement.

2.4 Techniques used in Chapter 5: Biofluids in wetting and adhesion

2.4.1 Visualizing earwax motion in human ear canal

A USB microscope with an endoscopic attachment is inserted into a human ear canal to visualize motion of earwax. The human subject is asked to move their jaw up and down during filming.

2.4.2 Measuring earwax viscosity

A 0.5 mL earwax sample was collected by swabbing the ear canal of a rabbit, pig, sheep and dog using a metal scoop tool. Each sample was immediately placed in a sealed container. Each sample was then placed in a cone-plate rheometer (Anton Parr MCR 501) and a frequency sweep test was performed from 0.001 s^{-1} to 1 s^{-1} at a temperature of 39 C to determine the shear viscosity. During the test, the sample was surrounded by an evaporation blocker to reduce environmental influence.

CHAPTER III

THE ADHESIVE FROG TONGUE

In this combined theoretical and experimental study, we investigate the mechanism by which frog tongues stick to insects. We present measurements of the tongue kinematics during prey capture, the rheological properties of the saliva, and mechanical properties of tongue tissue. We then apply these measured properties in a mathematical model for the work of adhesion of the frog tongue. We show that the tongue's unique stickiness results from a combination of a soft, viscoelastic tongue coupled with non-Newtonian saliva. The shear-thinning saliva spreads over the insect during impact, grips it firmly during tongue retraction, and slides off during swallowing. This combination of properties gives the tongue 50 times greater work of adhesion than known synthetic polymer materials such as the sticky-hand toy.

3.1 Mechanical properties of the frog tongue

3.1.1 Kinematics of prey capture

We perform high speed videography of the common leopard frog *Rana pipiens* capturing crickets attached to a string, as shown in **Figure 10(A)**. The frog's tongue stretches by 60% over the course of 0.03 seconds, ten times faster than a human eye blink. **Figure 10(B)** shows the corresponding tongue displacement δ during both successful and unsuccessful capture. For simplicity, only the vertical direction is shown. A sinusoidal fit (shown as solid lines) is applied to the tongue displacement data (black □), and the applied tongue force is determined. Acceleration on the insect can reach 120 m/s^2, 12 times the acceleration of gravity. These high forces necessitate a high adhesion force to the tongue, which we investigate in a series of tests. We will use a floating spring-mass-damper system to model prey capture [**Figure 10(C)**].

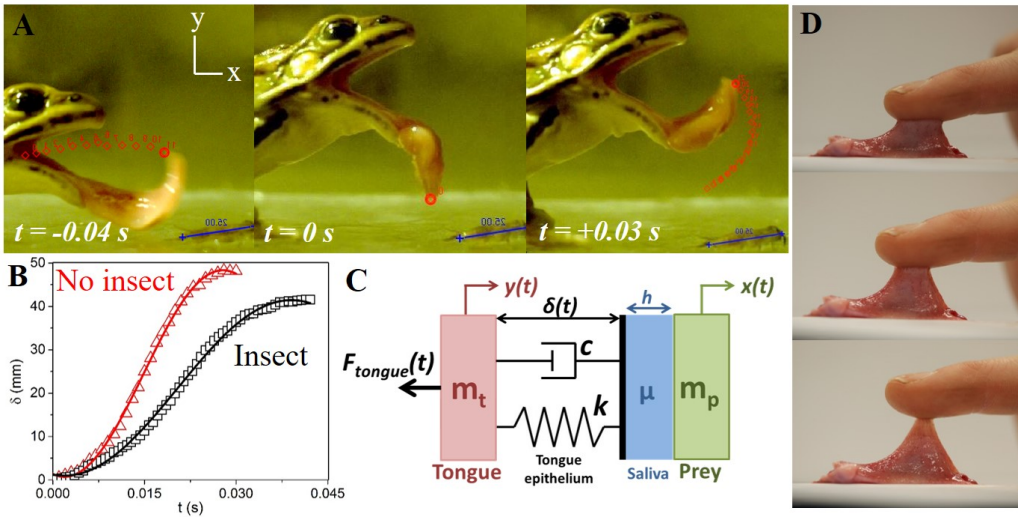

Figure 10: Frog tongue projection. (A) Attempted prey capture in *Rana pipiens*. Red dots indicate tracking of tongue tip. (B) Tongue displacement during insect retraction, measured from tongue tip, for failed insect capture (red △) and successful insect capture (black □). Solid lines represent sinusoidal fit. (C) Model of tongue using mass-spring-damper system. (D) Finger retracted from tongue surface showing its strong adhesion.

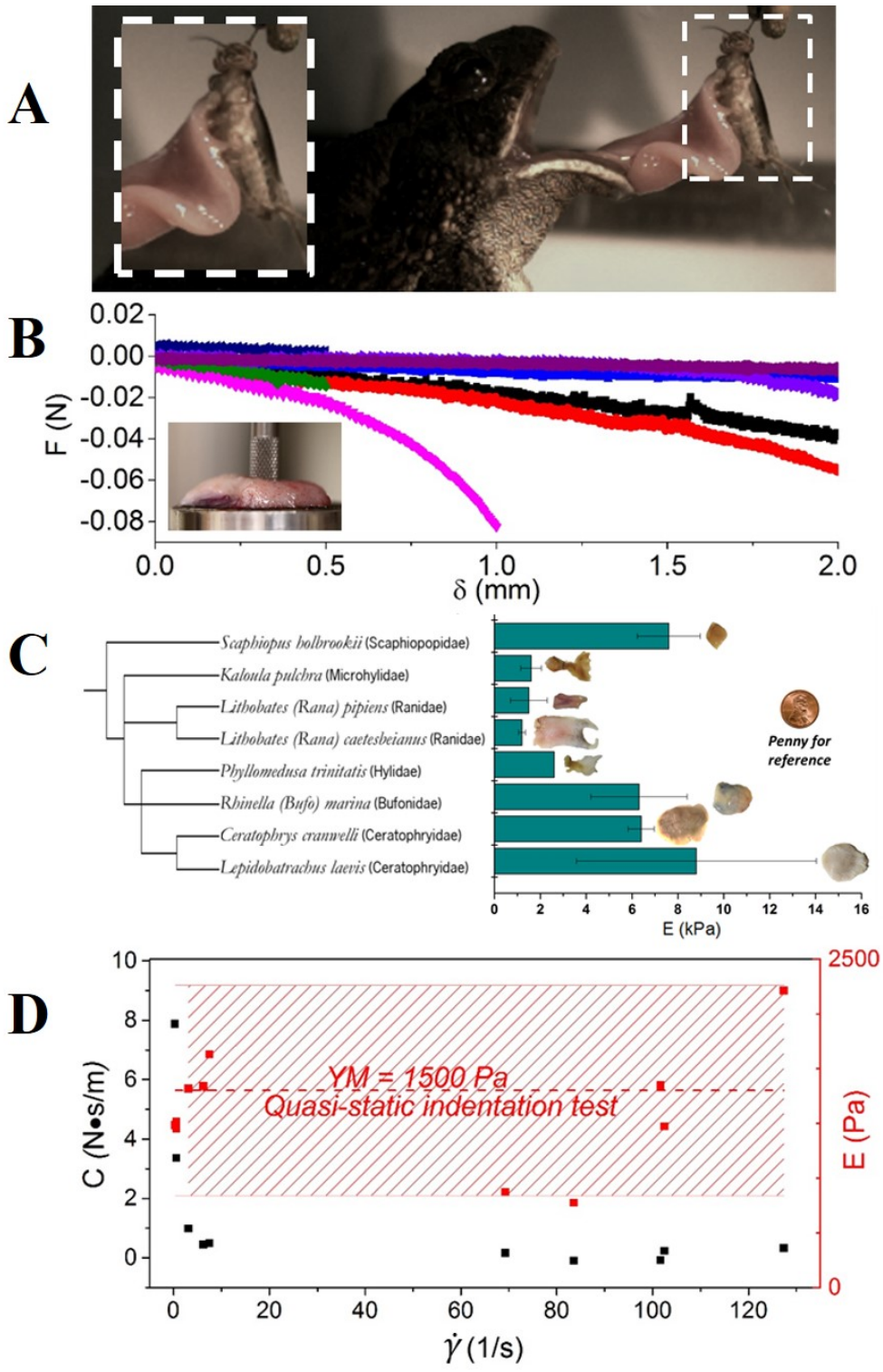

Figure 11: Tongue material properties. (A) Stretching of tongue epithelium during prey capture. (B) Relation between force and displacement for indentation tests shown in the inset. (C) The phylogenetic tree of amphibian species in this study. Young's modulus for 8 species, measured by quasi-static test. (D) Damping coefficients (black □) and Young's modulus (red □) for the frog tongue, measured in a dynamic tensile test. The average Young's modulus and error bars from part (C) is shown as red dotted line.

3.1.2 Tongue tissue properties

We collect the tongues of 6 frogs and 2 toads, which have been frozen for over a year at the Atlanta Botanical Garden. A phylogenetic analysis shows that the frog and toad species tested are distantly related [**Figure 11(C)**]. When the frog retracts its tongue, the insect's inertia pulls it in the opposite direction, as shown in **Figure 11(A)**. We measure the Young's modulus of the tongue epithelium in the perpendicular direction using microindentation with a flat-end cylindrical indenter[106] [**Figure 11(B)**]. Our model species for this study, the leopard frog *Rana pipiens*, has a tongue softness E_{tongue} of 1.5 ± 0.8 kPa which is 1/3 the average softness across the species tested. When utilizing indentation techniques, materials with similar Young's modulii include: muscle at 7 kPa[104], rat spinal cord at 3 kPa[107] and rat brain, which we tested, at 3.0 ± 2.1 kPa. Human tongue, which we tested, had an epithelium stiffness of 15 kPa, 10 times greater than the leopard frog.

Our previous test can only describe the low-speed behavior of the tongue. To understand high-speed behavior, we perform a dynamic indentation test[99] [**Figure 11(D)**]. We model the tongue epithelium using the Kelvin-Voight model, as a linear spring of stiffness k and purely viscous damper in parallel, with the underlying assumption of tissue homogeneity. At frequencies above 1 Hz, the damping coefficient is $c = 0.23$ N · s/m. The Young's modulus, calculated from the corresponding stiffness, matches the results of our quasi-static indentation test.

3.1.3 Saliva properties

Saliva is known for being viscoelastic, having properties of both a fluid and a solid [**Figure 12(A)**]. Saliva is secreted from mucus glands on the tongue papillae, saturating the epithelial tissue like a hydrogel. We measure the maximum possible thickness of the saliva layer by measuring the change in weight induced by wiping a tongue clean of saliva. The average layer height h_0 is 0.5 mm ± 0.2 mm, nearly 7 times thicker than human saliva[108]. To validate, we dip a freshly severed frog tongue in liquid nitrogen then view the tissue cross-section. The saliva is visualized as a semi-opaque layer, while the tissue is pink and opaque [**Figure 12(B)**]. The saliva layer ranges from 0.2mm to 0.7mm.

To measure saliva shear viscosity, a 0.3 mL sample is placed inside a cone-plate rheometer and viscosity measured across several orders of magnitude of shear rate. The results closely match the Carreau-Yasuda model[109] for shear-thinning fluid (solid lines in **Figure 12C**), where the viscosity μ is given by

$$\mu = \mu_\infty + (\mu_0 - \mu_\infty)(1 + (\lambda\dot{\gamma})^a)^{\frac{n-1}{a}}, \tag{11}$$

where μ_0 and μ_∞ are the asymptotic viscosities at zero and infinite shear rate, $\frac{1}{\lambda}$ is the critical shear rate when viscosity decreases, a is the width of transition, and $(n-1)$ is the power law slope fitting the transition region. Our two trials with separate samples show the results are repeatable. At low shear rates, frog saliva viscosity μ_0 plateaus at 70 Pa · s, whereas, at high shear rates, frog saliva viscosity drops to 1.2 Pa · s. The critical shear rate $\dot{\gamma}_{cr} = \frac{1}{\lambda}$ ranges from 1.4 to 2 s^{-1}.

While the low shear rate of μ_0=70 Pa · s may seem high, other shear-thinning biological muci have similar values at low shear rates such as human lung mucus μ=50 Pa · s[110] and sundew plants μ = 122 Pa · s[5]. Human saliva[4] and sundew plant mucus[5] both exhibit shear-thinning properties, and also follow the Carreau-Yasuda model, as shown in **Figure 12(E)**. However, frog saliva experiences a shift in steady-state viscosity over a shorter transition range than other shear-thinning biofluids.

While many animals secrete saliva through glands in their oral cavity, amphibians secrete saliva through glands on their tongue. Frog tongues have saliva glands located in-between papillae[111], allowing the tongue to become saturated with thick, viscous saliva. Based on these measurements, we can understand the necessity of saliva glands on the frog tongue by comparing Eq. (5) for wetting across a tongue, for human and frog saliva. In a low shear-rate scenario, frog saliva is 175 times the viscosity of human saliva and human papillae are 12 times taller than frog papillae. If we assume the surface tension of both saliva's is close to water, and the pre-factor $\frac{2}{3\beta}\frac{\cos(\theta_f)-\cos(\theta_c)}{\cos(\theta_c)}$ of human and frog saliva is comparable, then we find frog saliva would spread only 2% of the distance that human saliva moves in the same amount of time. Thus, glands in frogs must deliver the saliva directly to the location they are needed.

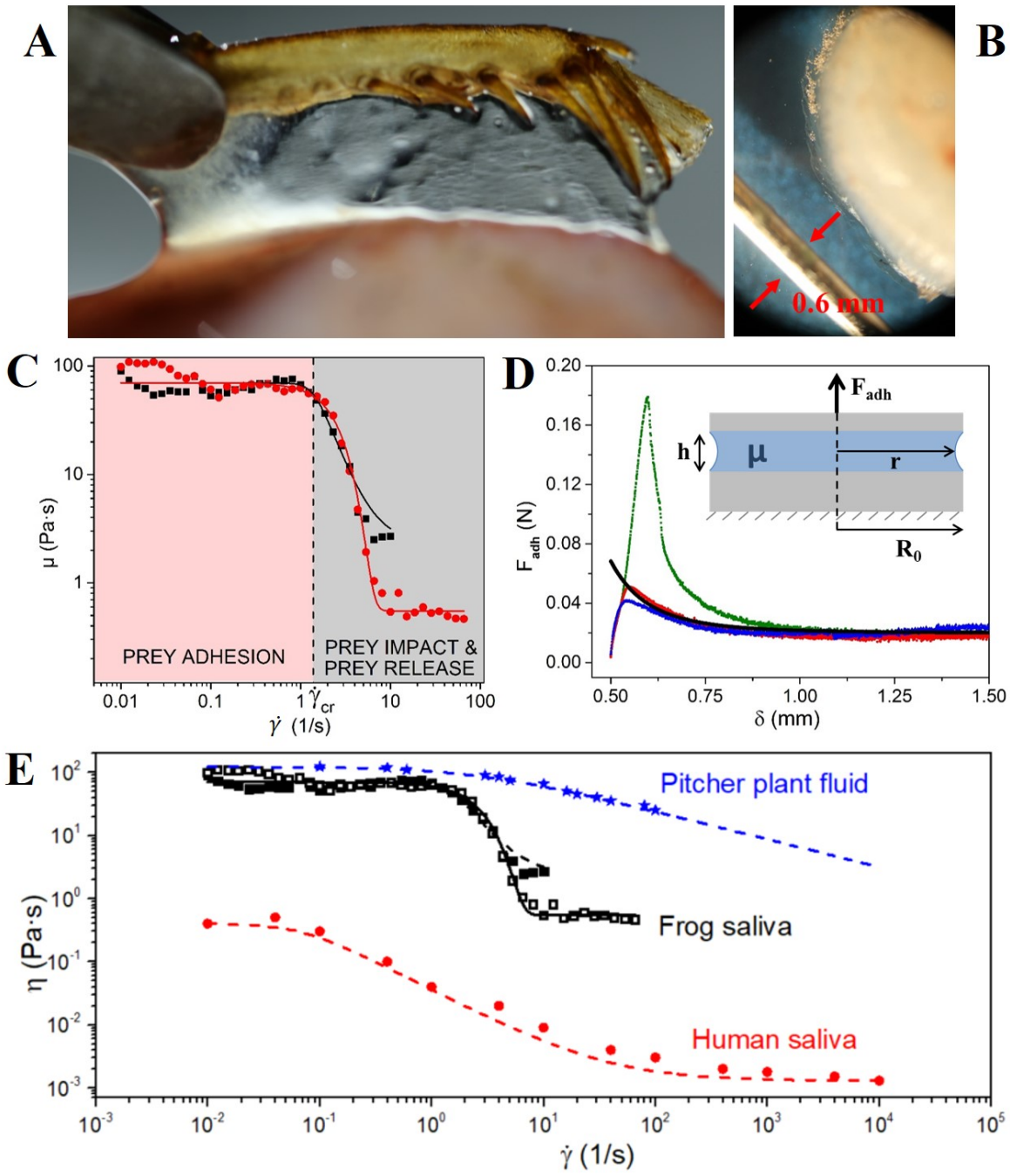

Figure 12: Saliva properties. (A) A cricket leg is retracted from the frog tongue. (B) Flash-frozen frog tongue with liquid nitrogen. Saliva thickness ranges from 0.2mm to 0.7mm (C) Frequency sweep test of frog saliva. Black and red symbols denote experiments, solid lines the Carreau-Yasuda theoretical model. (C) Separation forces for frog saliva sandwiched between two parallel plates as shown in inset. Blue (□), red (□) and green (□) symbols denote 3 experimental trials. The black line denotes the Stefan theory, which matches well with experimental results, validating that Stefan adhesion can be used for low shear rate regimes. (D) Shear viscosity μ of human saliva (red circle ○), frog saliva (solid and hollow black square □), and pitcher plant fluid (blue star ⋆). All biofluids decrease in shear viscosity μ with increasing shear rate $\dot{\gamma}$. The Carreau-Yasuda model for shear-thinning fluids (dashed line) is used to fit experimental data. Data has been replotted from the following sources: human saliva[4], sundew plant fluid[5].

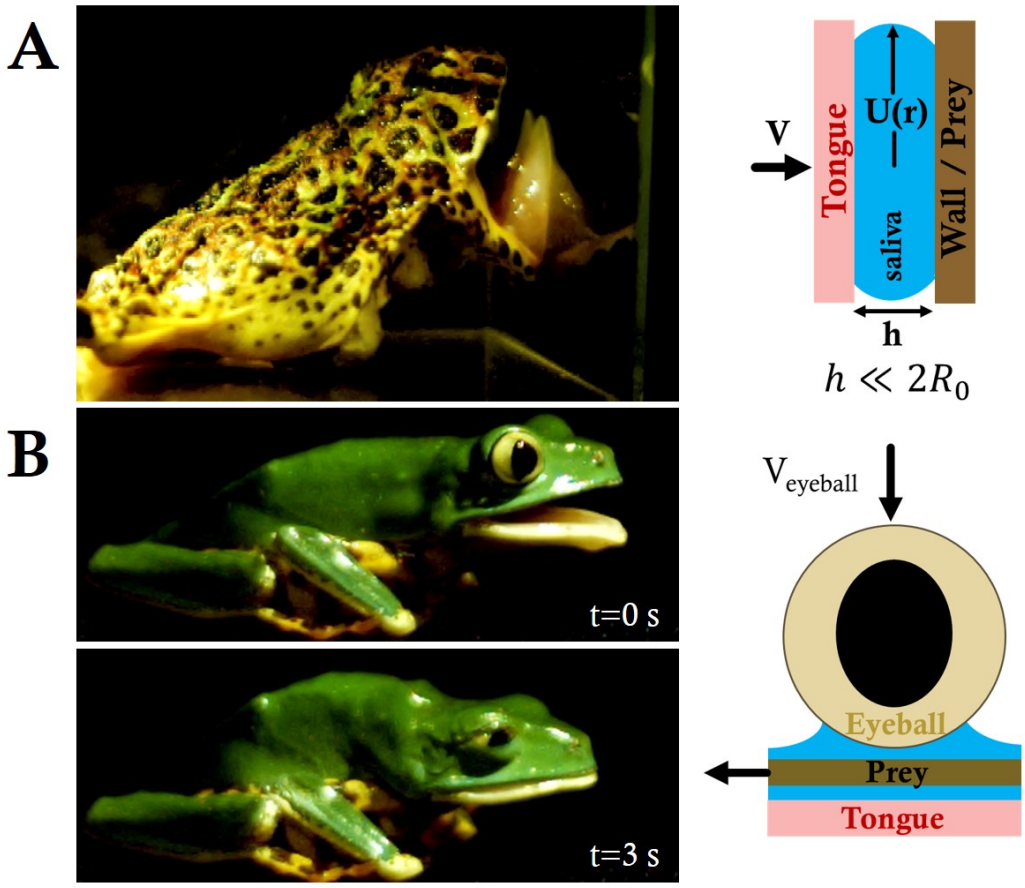

Figure 13: Duality of saliva viscosity during prey capture. (A) Horned frog *Ceratophrys ornata* impacting tongue on a glass wall. Upon tongue impact, saliva evacuates laterally, causing high shear rates in the fluid layer and a subsequent drop in viscosity. This low viscosity regime allows the saliva to penetrate cracks of prey and maximize surface contact. (B) Monkey frog *Phyllomedusa* dropping eyeballs into mouth cavity during swallowing of prey. Theoretical pressure from eyeball on prey causes high shear rates in saliva layer, allowing the insect to slide into the throat.

For frogs, a saliva with variable viscosity increases functionality in all phases of prey capture, as labeled in **Figure 12(C)**. The duality of this saliva viscosity makes catching and releasing prey a simple matter for the frog: viscous saliva adheres the tongue to prey, and watery saliva allows the insect to slide off the tongue.

3.1.4 The importance of saliva in prey impact and release

During prey impact, a low viscosity saliva is better at penetrating rough surfaces and increasing contact area, much like paint on a wall. **Figure 13(A)** shows the tongue and insect modeled by two circular flat plates, identical to the Stefan adhesion experiment in **Figure 12D, inset**. During impact, the plates are compressed at velocity V. If the layer is thin ($h \ll 2R_0$), the corresponding shear rate is $\dot{\gamma} \sim \frac{U(r)}{h}$, based on thin layer Couette flow, where $U(r)$ is the fluid velocity in the radial direction. Since the saliva is incompressible, we may use conservation of volume to write the velocity $U(r) = \frac{Vr}{2h}$ and the radius of the saliva as $r = R_0\sqrt{\frac{h_0}{h}}$. Together, the relationship between shear rate $\dot{\gamma}$ and plate velocity V may be written as:

$$\dot{\gamma} \sim \frac{VR_0\sqrt{h_0}}{2h^{5/2}}. \tag{12}$$

The leopard frog tongue can reach impact speeds up to V=4,000 mm/s. If we assume instantaneous impact, or fixed surface contact, the resulting in saliva shear rates of $\dot{\gamma} = 40{,}000\ s^{-1}$, well above $\dot{\gamma}_{\rm cr} = 2\ s^{-1}$, the limit at which frog saliva viscosity drops by two orders of magnitude. High speed impact takes advantage of the saliva's rheological properties to increase tongue adhesivity while simultaneously overcoming the insect reaction time.

This change in saliva viscosity is also useful for removing insects once inside the mouth. As shown in **Figure 13B**, when insects enter the mouth, the frogs eyeballs retract into the mouth cavity, pressing down on the insect and saliva layer between tongue and prey. Using Eq. (12) for an measured eyeball retraction speed of $V_{\rm eyeball}$=100 mm/s across 3 species (*Phyllomedusa*, *Ceratophrys ornata*, and *Lepidobatrachus laevis*), we find resulting saliva shear rate to be $\dot{\gamma} = 200\ s^{-1}$, well above $\dot{\gamma}_{\rm cr} = 2\ s^{-1}$. This high shear, low viscosity regime allows the insect to slide off the tongue and into the throat.

3.2 Adhesive theory

3.2.1 Prey adhesion

During retraction, adhesion force $F_{\rm adh}$ consists of a surface tension force $F_{\rm s}$ and viscous force $F_{\rm v}$: $F_{\rm adh} = F_{\rm s} + F_{\rm v}$. We consider normal separation of only frog saliva sandwiched between circular, rigid, flat plates. The surface tension force[112] scales with the product of the Laplace pressure $\frac{\gamma}{h_0}$ and contact area R_0^2, yielding $F_{\rm s} \sim \frac{\gamma R_0^2}{h_0}$, where R_0 is the plate radius, γ is the surface tension, and h_0 is the initial saliva layer thickness. Using $R_0 = 5.5$ mm, $\gamma_{\rm water} = 0.072$ N/m and $h_0 = 0.5$ mm, the surface tension force contributes less than 10% to the overall force required for insect adhesion, and is neglected from consideration hereon.

The adhesive force $F_{\rm adh}$ is now equal to the viscous force $F_{\rm v}$. The viscous force holding the plates together is given by the Stefan equationi in Eq. (6), shown in **Figure 12D**. The separation rate of the plates $\frac{dh}{dt}$ will be labelled as separation velocity V. The Stefan equation is valid if the saliva layer is thin, the fluid is an incompressible Newtonian fluid and the flat plates are rigid. Is it possible to use the Stefan equation to model adhesion on a soft, deformable frog tongue coated in a thin layer of viscoelastic saliva? We test the validity of the force law in Eq. (6) by separating frog saliva of zero shear viscosity μ_0= 70 Pa·s trapped between two flat aluminum plates of radius $R_0 = 5.5$ mm [**Figure 12(D)**]. Since 2 of 3 trials closely match the Stefan theory trend, we will use the force law from Eq. (6), hereon.

Previous studies[71–73] have measured adhesion force $F_{\rm adh}$, which only partially describes adhesive strength. A whole picture of the adhesion process is given by work of adhesion W, the energy expended to remove an adhesive from a solid surface. This measurement encompasses all sources of energy storage and dissipation during the full time of contact. For this study, the work of adhesion is defined as the area under the force-displacement curve, from initial displacement till adhesive failure. In tribology, the work of adhesion is defined as the work to separate two adjacent phases of a liquid-liquid or liquid-solid phase boundary from each other, or the energy released in the process of wetting. While we use an identical term, we are not referring to the tribological phenomenon. The resultant value of work of adhesion is then divided by the initial contact area, $W_{\rm adh} = \frac{1}{A}\int F_{\rm adh} d\delta$. The average work of adhesion for the separation of frog saliva between two rigid plates is $W = 0.09$ N/m.

We now consider the effect of tongue softness. We perform a quasi-static separation test of a frog tongue and a rigid, flat aluminum indenter [**Figure 14(A,B)**]. We conduct 5 tests with retraction velocity (V) ranging from 0.1 mm/s to 4 mm/s. The relationship between force and displacement are shown as the scatter data in **Figure 14(C)**. The tongue can be stretched by 8 mm, more than twice the thickness of the tongue, without breaking contact. We observe from **Figure 14(A)** a negligible change in saliva layer height during indenter retraction. Therefore, we can relax the rigid plate assumption by assuming the saliva does not stretch during adhesion ($h \approx h_0$).

Theoretical predictions for force-displacement are shown as solid lines in **Figure 14(C)**. We can relate adhesion force to shear rate of the saliva at the fluid-air interface by combining Eq. (11), Eq. (12) and Eq. (6) with the assumption that $h = h_0$,

$$F_{\rm adh} = \frac{3\pi R_0^3 \dot{\gamma}[\mu_\infty + (\mu_0 - \mu_\infty)(1 + (\lambda\dot{\gamma})^a)^{\frac{n-1}{a}}]}{h_0}. \tag{13}$$

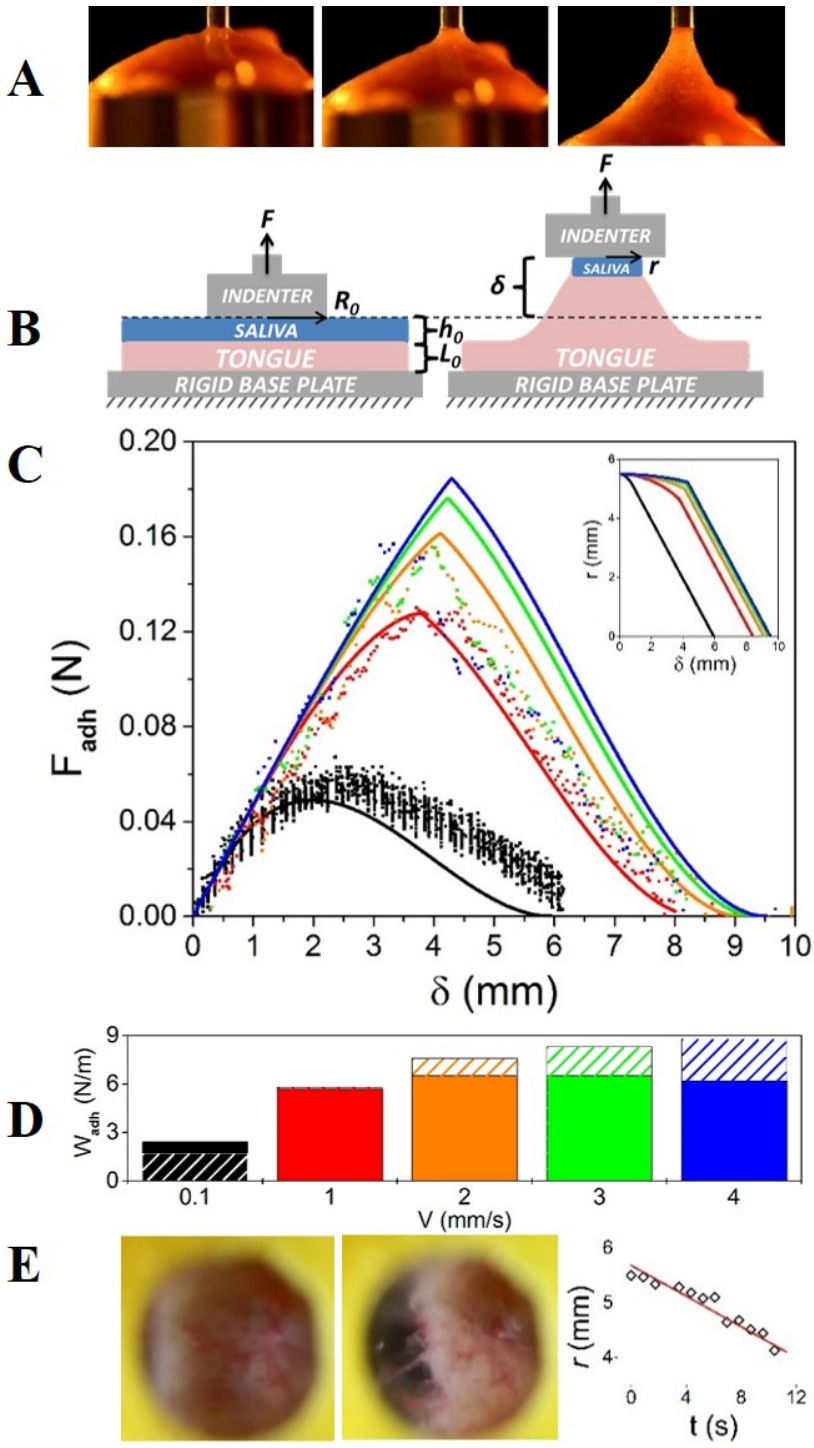

Figure 14: Quasi-static tests. (A) Time sequence of an indenter pulling away from the frog tongue. (B) Schematic of quasi-static test. (C) Relation between force and displacement. Mathematical model denoted by solid lines. Various retraction speeds are shown including 0.1 mm/s (black), 1 mm/s (red), 2 mm/s (orange), 3 mm/s (green) and 4 mm/s (blue). Inset shows model predictions of average contact radius. (D) Work of adhesion W_{adh} for each retraction rate. Experiments are solid colors, with theory overlaid in hatched color. (E) The tongue peeling is visualized through a transparent acrylic indenter. Graph shows average contact radius decreases linearly with displacement.

We present a solution for the adhesive force F_{adh} which combines saliva rheology, elastic force of the tongue, and viscous resistance by Stefan adhesion. The solution is found by iteration. As the indenter retracts, the tongue stretches, applying an elastic force on the saliva layer $F_{\text{elastic}} = \frac{E_{\text{tongue}}\pi r^2}{L_0}\delta$ where r is the contact radius, L_0 is the thickness of the tongue sample and δ is the indenter displacement. In steady-state, the elastic force of the tongue equals the adhesive force of the saliva $F_{\text{elastic}} = F_{\text{adh}}$. The internal damping of the tissue is disregarded for this quasi-static test. The variables that change as a function of displacement are the adhesion force $F_{\text{adh}}(\delta)$, strain rate $\dot{\gamma}(\delta)$, and contact radius $r(\delta)$. Initial conditions are $F_{\text{adh}} = 0$ N, $\dot{\gamma} = 0s^{-1}$ and $r = 5.5$ mm. For each incremental change in δ, $F_{elastic}$ is calculated then substituted into Eq. (13) to find the corresponding shear rate $\dot{\gamma}$. An increase in shear rate drives a shrinking of the contact radius. The incremental change in contact radius dr may be written as $dr = -U(r)dt$ where $U(r) = \dot{\gamma}h_0$, assuming a Couette flow profile in the saliva. Throughout the simulation, we assume the saliva thickness remains constant, in accordance with our observations.

When we ran the above version of the solution, we found that the strain rate diverged, and the tongue broke contact prematurely. As an ansatz, we cap the strain rate from above based on our experimental observations. A transparent acrylic indenter is retracted at a fixed rate from the frog tongue surface, and the peeling area over time is measured [**Figure 14E**]. Specifically, we observe the average contact radius varies linearly with displacement, suggesting that strain rate has a maximum finite value. Based on conservation of mass, the largest strain rate that can be attained is $\dot{\gamma}_{\max} = \frac{V}{h_0}$, since the maximum velocity within the saliva is the indenter velocity, $U(r) = V$. This cap is used in our computations, and results in the contact radius r are shown in the inset of **Figure 14(C)**.

Our iterative technique captures the experimental force values well, across a range of applied indenter speeds. Physically, the peak force represents the point at which the saliva begins to flow, when the shear rate exceeds the critical shear rate. Our model also also predicts the change in contact radius in **Figure 14(C)** inset. The linear change in contact radius is qualitatively similar to our experiments. We note the radius decreases quickly once the saliva drops in viscosity. Physically, the model demonstrates two phases in the adhesion. In the first phase, the tongue is stretched progressively, which increases the force applied to the saliva. The saliva remains unchanged in both height and viscosity because it is below its critical shear rate. In the second phase, the elastic force from the tongue is sufficiently high that the saliva begins to flow, breaking off contact with the tongue. The contact area decreases and the adhesion force decreases accordingly. In both phases, the adhesion force arises from the stretching of the tongue. The maximum force obtained arises from the rheological properties of saliva which drive the onset and rate of peeling of the saliva layer.

The work of adhesion for each experiment (solid color) is approximately 5.5 N/m is shown in **Figure 14(D)**. Our mathematical model (patterned color) matches closely, within 25% of the experiments. The work of adhesion with the tongue is 60 times greater than for saliva between rigid plates. Thus, the softness of the tongue is an important factor in increasing the work of adhesion, or the perceived stickiness. The rheology of the saliva also plays a role in this high work of adhesion. In comparison to items of comparable softness, work of adhesion of the tongue is 40 times greater than known soft, sticky materials such as tree frog toe pads (0.15 N/m)[113] and sticky hand toys (0.13 N/m), which do not have a viscoelastic coating.

3.2.2 Dynamic simulation

We use a dynamic simulation to investigate the importance of tongue damping in a real prey capture scenario using the floating spring-mass-damper system in **Figure 10(C)**. The tongue epithelial tissue represents a spring-damper in parallel. The damping coefficient is given by the measured value $c = 0.23$ N $\cdot$ s/m. The spring stiffness (k) can be extrapolated from the measured Young's modulus $E_{\text{tongue}} = 1500$ Pa and the contact radius of a cricket, $r = 4$ mm. The applied force F_{tongue} is extrapolated from the high-speed video data in **Figure 10B**. The saliva layer sits between the spring-damper and the prey; by examining the force exerted by the spring and damper, we can determine the force exerted on the saliva F_{saliva}. Our equation of motion is:

$$-m_p\ddot{y}(t) = m_p\ddot{\delta}(t) + \dot{\delta}(t) + k\delta(t), \tag{14}$$

where $y(t)$ is the acceleration of the tongue based on experimental data, spring constant $k = \frac{E_{\text{tongue}}A}{L_0}$ and $\delta(t)$ is the epithelial displacement between tongue muscle and prey. We write the force exerted on the saliva

as $F_{\text{saliva}}(t) = k\delta(t) + c\dot{\delta}(t)$.

As shown from the quasi-static iterative model in Eq. (13), a larger applied force on saliva will generate higher shear rates, which can cause separation. For clarity, we will refer to F_{adh} as F_{saliva} for the dynamic simulation. The applied force F_{saliva} should be minimized to keep the insect attached. Tongue elasticity stores energy in the tissue and damping absorbs the stored energy. If the tongue had no damping coefficient, the stored energy would be exerted back onto the insect, resulting in higher peak forces. **Figure 15(A)** shows how the applied force changes with the addition of a damping coefficient. Peak force on the saliva can decrease as much as 30% from the addition of a damping coefficient.

Damping not only alters the peak force applied but the work that is done on the saliva. **Figure 15(C)** shows how epithelium displacement $\delta(t)$ changes with damping. The predicted value of $\delta = 1.5$ mm for the measured damping is close to the displacement observed in experimental footage in **Figure 15(B)**, top. Without damping, the tongue epithelium would stretch up to 4 mm, likely resulting in fracture. The total work for each case is summarized in the bar chart in **Figure 15(D)**. The work performed on the saliva for the damped tongue is 2 N/m, which is about a third of the work required to separate the saliva. However, without damping, the work is 4.5 N/m and may result in the tongue separating from the insect. The damping of the tongue acts like the shock absorber of a car. Damping allows higher forces to be exerted on the prey before peeling occurs. The use of shocks has been shown to be an important feature to reduce force and oscillation, such as in mammalian paws[82] and soft soles in running shoes[114].

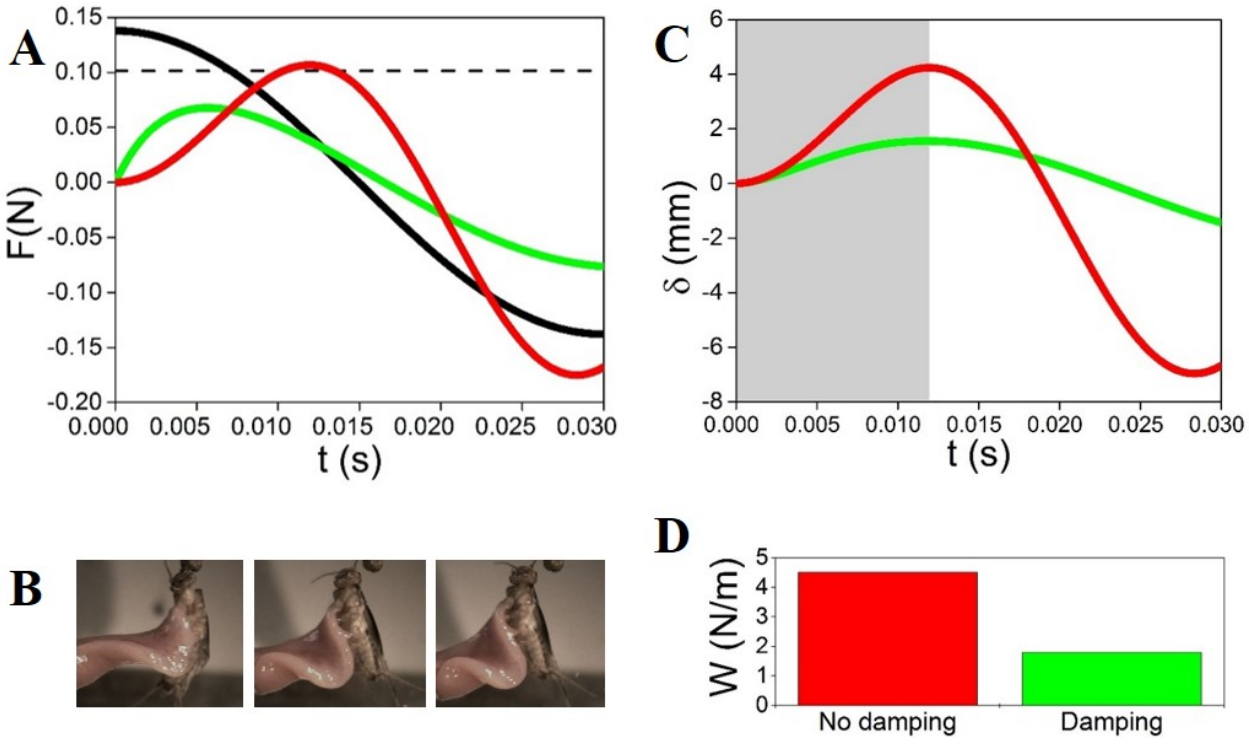

Figure 15: Dynamic simulation of frog tongue. (A) Time course of the applied force on tongue F_{tongue} (solid black line). The separation force on the saliva F_{saliva} is shown for two damping coefficients. Zero damping is in red, and realistic damping ($c = 0.23$ N*s/m) is in green. The dashed black line represents the force at which saliva flows and prey is released. (B) Time course of the stretch of the tongue tongue epithelial tissue. Experimental video footage illustrates the stretch. (C) Work of adhesion for the two damping coefficients tested.

3.3 Discussion

The study of adhesives has long been inspired by amphibians, reptiles and invertebrates. The gecko is the champion of dry adhesion, using van der Waals forces derived from its thousands of setae. The limpet *Patella vulgata L.* excretes thick mucus to adhere to wet, rough surfaces, using the viscous forces associated with Stefan adhesion[73,78]. Comparatively less work has been done on frog tongues, a wet bioadhesive. Previous investigators have speculated that the sticky saliva acts like a pressure sensitive adhesive such as scotch tape. In our study, we find the tongue's adhesion is more subtle than that. The tongue's stickiness is a result of both material properties of the tongue and rheological properties of its coating. In comparison, modern sticky tapes are often made of stiff materials. Forces applied to the tape directly cause separation in the adhesive. In the frog, applied forces are either dissipated in the tongue's internal damping or stored in its stretchy tissue. A stiff tongue would result in reduced contact area during prey impact, and in turn reduced adhesion force during retraction. The shear-thinning properties of saliva emulate paint, a well known shear-thinning fluid. Paint is thrown onto a wall with a brush, flowing at high speeds to create an even coating. At low speeds, it clings to the wall. In the same way, the saliva coats the insect on impact, but sticks to the prey in retraction.

Our study shows that an even and thin coating of the saliva is critical to prey capture. This study points to the importance of the saliva in prey adhesion. During our adhesion testing, areas of the frog tongue would dry out and cause nearly instantaneous fracture from the indenter. Any non-uniformities in the layer will cause stress concentrations and areas where fracture can occur during prey retraction. The frog likely has several biological adaptations to protect its saliva. We observe that the frog prevents its tongue from desiccation by keeping its mouth shut. In addition, the densely packed papillae create a composite-like surface structure which may aid in continuous adhesion of saliva to tissue, much like a hydrogel[55].

3.4 Chapter Summary

Frog tongues have a number of properties that enable successful high-speed prey capture. First their tongue is one of the softest biological materials known, enabling the tongue to wrap around the prey during impact, facilitating a large contact area. Second, the tongue is highly damped like a car's shock absorber. As an insect is yanked in at high speed, the insect's inertia induces large separation forces. These forces are reduced by the internal damping in the tongue. We use mathematical modeling to show that without the tongue's damping, the insect is in danger of breaking contact with the insect. Lastly, the tongue is coated with a thin layer of saliva with non-Newtonian properties like paint. The saliva flows upon impact with prey, grips when the prey is retracted, and then flows again when the frog swallows. The combination of these favorable traits may be useful in designing reversible adhesives that stick at high speed.

CHAPTER IV

CAT TONGUE PAPILLAE AID IN GROOMING

The cat tongue is covered in sharp, rear-facing spines called papillae. These papillae are commonly thought to be used in grooming, although their precise function is a mystery. In this combined experimental and theoretical study, we examine the tongues of six cats: domestic cat, bobcat, snow leopard, cougar, tiger, and lion, to elucidate the mechanism by which cat tongues groom fur. Using micro-CT technology, we show that the papillae contain a hollow cavity at the tip, contrary to previous literature. These cavo papillae hold and distribute saliva deep into the fur layers. A constant papilla height across cat species corresponds to the height of compressed fur, suggesting papillae evolved to extend deep into the fur. Using Darcy's capillary model for wicking in porous media, we find that saliva on the tongue surface can only wet the top-half of the fur layer, further suggesting that papillae are needed to penetrate into the undercoat. We design and build a 3D-printed cat tongue mimic, incorporating 3D printed versions of a cat's papillae into a silicone substrate. The mimic exhibits lower grooming forces than a normal hairbrush, and is easier to clean. The unique shape and function of the papillae may inspire new ways to clean ubiquitous surfaces like carpets and furs.

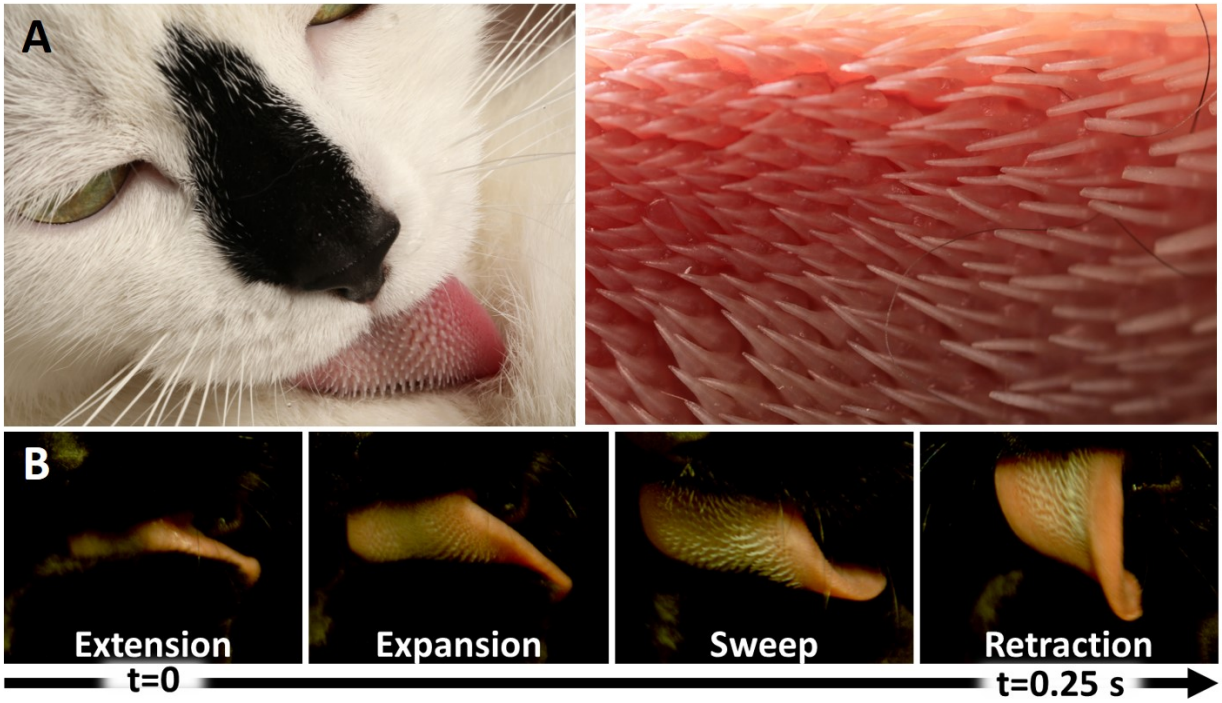

Figure 16: Grooming mechanics. (A, left) A domestic cat grooming its fur. (A, right) A domestic cat tongue. Anisotropic papillae point towards the throat. (B) The four phases of cat grooming: tongue extension, tongue lateral expansion, sweeping of the tongue through fur and lastly retraction of the tongue in a U-shape curl.

4.1 Grooming and the tongue

4.1.1 Grooming kinematics and forces

Our study begins with grooming observations of the domestic cat *Felis catus* using high-speed videography [**Figure 16A**]. A single grooming sweep has four phases, including extension of the tongue, lateral expansion and stiffening of the tongue tissue, a full sweep of the tongue through the fur, and finally retraction of the tongue in a U-shape curl [**Figure 16B**]. During stiffening of the tongue tissue, the spines can rotate until they are perpendicular to the tongue. The domestic cat grooms at speeds of $v_{\text{groom}} = 220 \pm 9$ mm/s, at a frequency of 3.2 ± 0.6 licks/s (N=5), with a grooming lick length of $L_{\text{groom}} = 63 \pm 20$ mm. We gather grooming velocity data for 7 additional species of cats using online YouTube videos (Table 1, Appendix A), and observe that these cat tongues also contain sharp papillae. The grooming speeds and lick length will be input parameters in our mathematical model that predicts the volume of saliva deposited.

We attach a fake nylon fur sample to the surface of a force plate, and entice the cat to groom the fake fur using catnip. We measure the forces applied by the tongue along the length of the lick, as well as into the plate [**Figure 17A**]. The domestic cat presses down with 0.1 N of force, which we will replicate in our tongue grooming mimic later in the study. For the fake fur, applied force along the direction of the lick reached peaks of 0.05 N; however, lick force will vary based on surface texture.

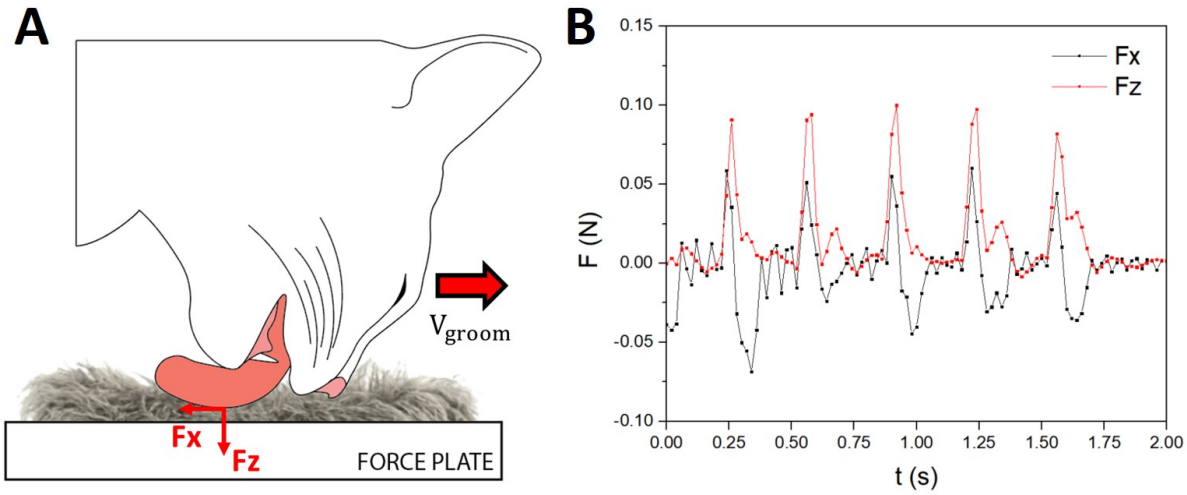

Figure 17: Measuring grooming force. (A) Schematic of experimental setup for cat grooming across a force plate. (B) Grooming forces for a domestic cat. Normal forces reached a peak of 0.1 N.

4.1.2 Hollow papillae hold saliva

We collect the tongues of six cats post-mortem in the Felidae family: domestic cat *Felis catus*, bobcat *Lynx rufus*, cougar *Puma concolor*, snow leopard *Panthera uncia*, tiger *Panthera tigris*, and lion *Panthera leo* [**Figure 18A**]. A phylogenetic analysis using phyloT software shows that the cat species tested are distantly related [**Figure 18A,inset**]. We perform a full scan of a domestic cat tongue using a Scanco μCT50 x-ray micro-computed tomography machine, and find two distinct regions of papillae in the distal and proximal end of the tongue [**Figure 18D**]. The distal region, highlighted in the dotted box in the figure, contains large papillae in sparse density, while the proximal region contains small papillae in high density. Our high speed footage of grooming shows that only the distal region interacts with the fur during grooming. From hereon, all references to tongue length and width will refer not to the entire tongue, but to the length and width of this distal region. Moreover, references to the papillae will refer to papillae in this distal region. These measurements are given in Tables 2 and 3 of Supplement A.

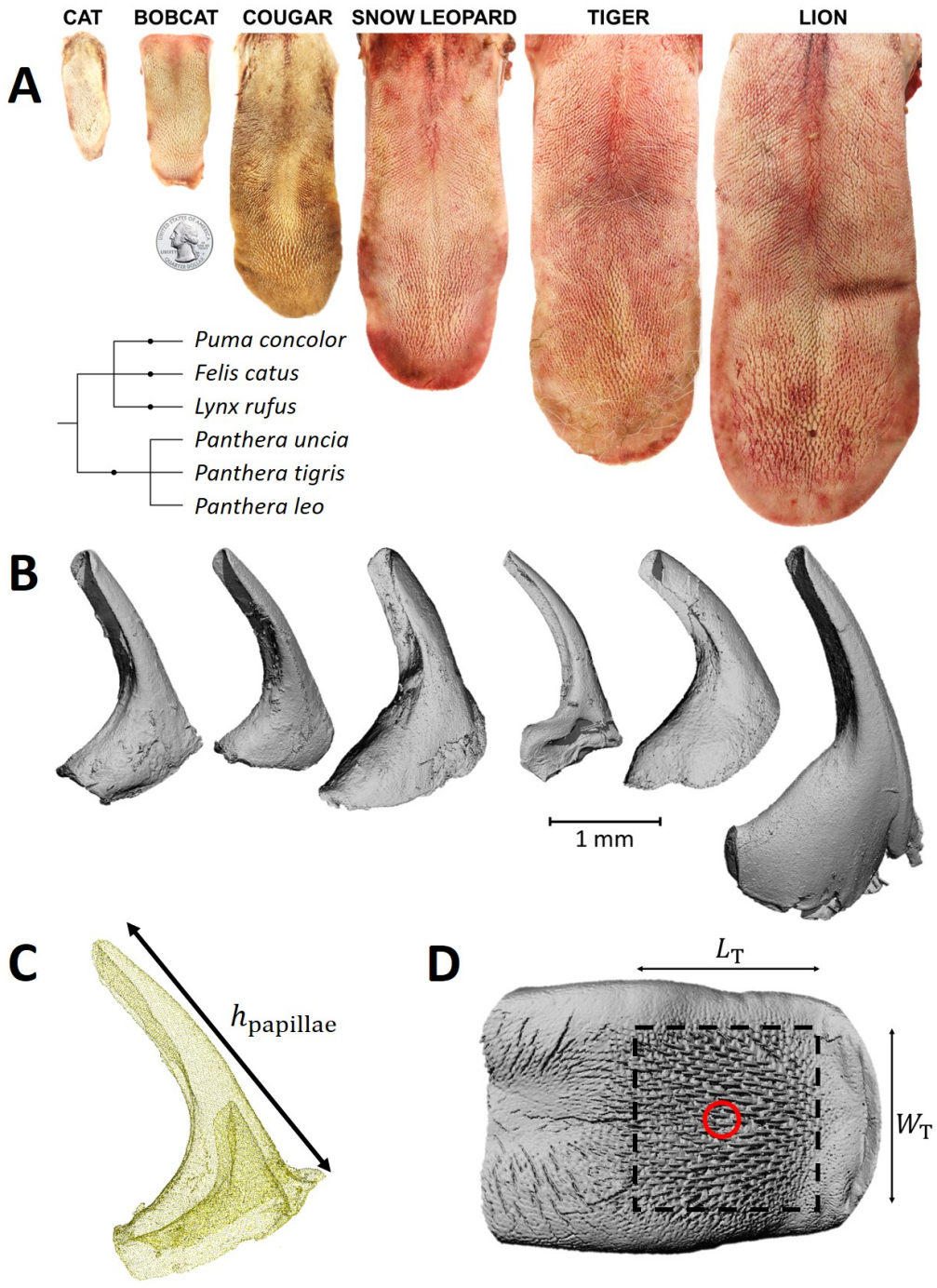

Figure 18: The cat tongue and papillae. (A) Tongues from domestic cat *Felis catus* (C), bobcat *Lynx rufus* (B), cougar *Puma concolor* (CO), snow leopard *Panthera uncia* (SL), tiger *Panthera tigris* (T), and lion *Panthera leo* (LI). (A, inset) The phylogenetic tree of cat species in this study. (B) μCT scans of largest cavo papillae, all to scale. Cavo papillae cavity height is h_{papillae}=1.4 $\pm$ 0.2 mm across species ($h_{\text{papillae}} \sim M^{0.04}$). (C) A transparent model of a domestic cat cavo papillae, illustrating cavities present. Base cavity attaches to tissue, while tip cavity holds fluid. (D) μCT scan of a domestic cat tongue. Front region of the tongue contains large, rigid cavo papillae, and rear region contains small, soft papillae. Tongue length, width measured for grooming surface, and scale with cat mass as L_{T},$W_{\text{T}} \sim M^{0.41}$, respectively.

Having identified the relevant region of the tongue for grooming, we use tweezers and a scalpel to remove the largest cavo papilla from the center of each distal region of the cat tongue, as shown by the red circle in **Figure 18D**. We clean the papillae, and generate a 3D model using the μCT50 scanner [**Figure 18B**]. A papilla has several unique features, including a hollow cavity at the base for tissue attachment, a smooth claw-like curvature, and a unique U-shaped cavity at the tip [**Figure 18C**]. Prior to papilla removal, papillae length h_{papillae} is measured from the tissue surface to papilla tip; h_{papillae} reflects maximum penetration depth of papillae during grooming. Despite cats varying over 30-fold in weight, papillae length remains at a constant h_{papillae}=2.3 $\pm$ 0.2 mm (N=6) across cat species, suggesting that papillae length may be important to functionality during grooming.

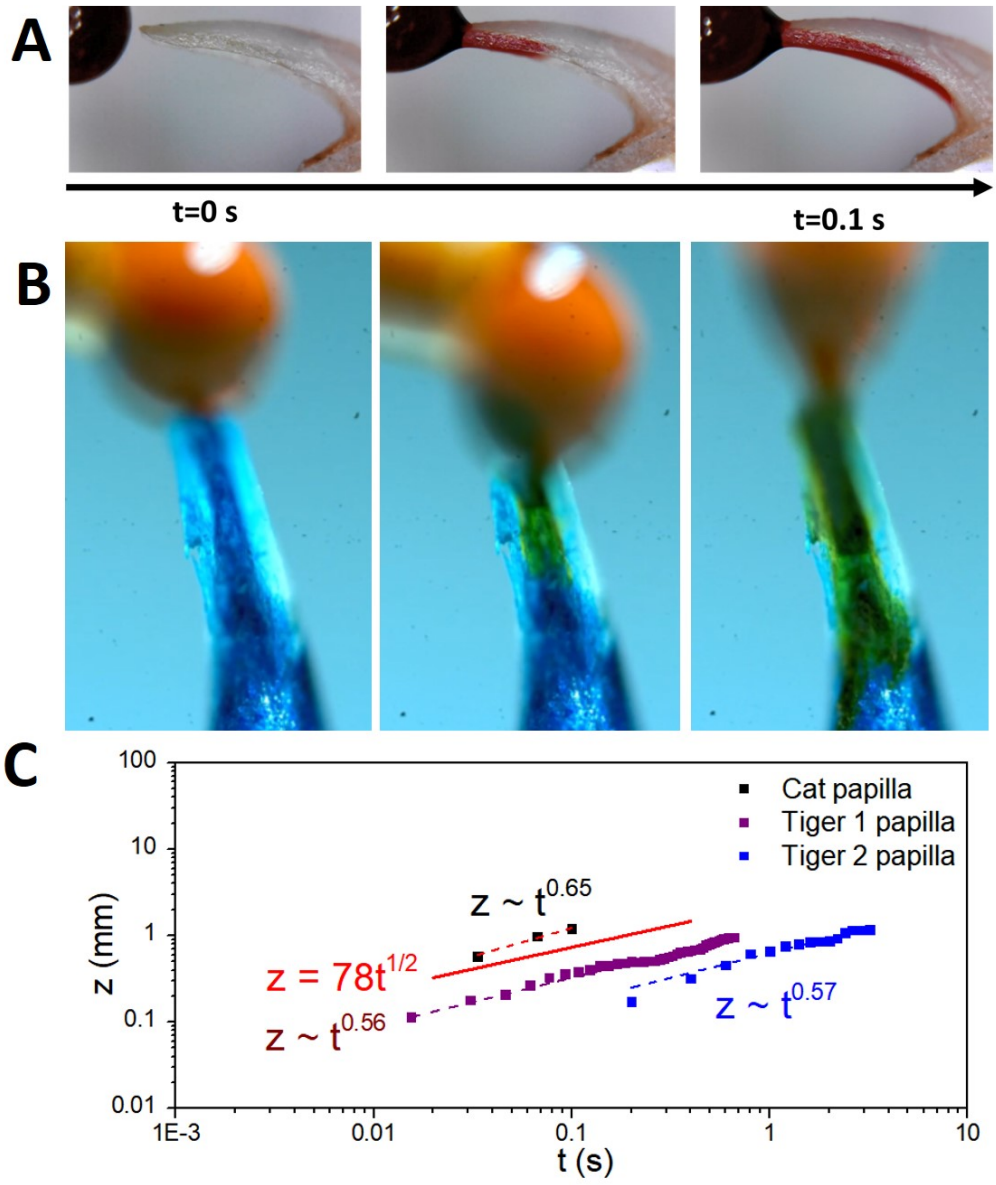

Figure 19: Dye wicking up papilla. (A) Domestic cat papilla wicking red food dye in under 0.1 s. (B) Tiger papilla wicking orange food dye. A precursor film can be seen advancing before the bulk fluid motion. (C) Washburn's law fitting to dye wicking up cat and tiger papilla. The theoretical fluid contact angle is 89.9° $\pm$ 0.15°.

We explore the functionality of these papillae, and report two findings: first, the hollow cavity wicks up and holds fluids. The U-shaped cavity is shown to wick up water in under 0.1 s [**Figure 19A**]. Using the Bond number[64], we show that gravitational forces are negligible compared to surface tension, $Bo = \frac{\rho g {w_{\text{cavity}}}^2}{\sigma} = 0.012 \ll 1$, where w_{cavity} is the papilla cavity width, g is gravitational acceleration, and ρ, σ are the density and surface tension of water, respectively. Thus, once fluid is wicked into a papilla, it can only be removed by contact with fur. A drop of food coloring wicks up a cat papilla cavity according to a power law of $t^{0.65}$ (R^2=0.97), and up a tiger papilla cavity with a power law of $t^{0.56}$ (R^2=0.98), where t is time. This exponent, close to 1/2, is similar to Washburn's Law for capillary flow in a halfpipe of radius r (identical to a capillary tube), where flow is resisted only by viscous dissipation. Washburn's Law[115] states that the fluid front z follows as $z = (\frac{\sigma r \cos(\theta)}{2\mu})^{1/2} t^{1/2}$, where θ is the fluid contact angle, and μ is the fluid viscosity. By fitting Washburns law to the data [**Figure 19C**], we find that the theoretical fluid contact angle is close to 90 degrees (89.9° ± 0.15°, N=3). A precursor film can be seen spreading ahead of the fluid front [**Figure 19B**], likely caused by micropatterns in the keratinized surface of the papilla. For the domestic cat, each papilla can hold a maximum of 0.014 μL of saliva, for a total of 4.1 μL across 290 papillae, around a tenth of an eyedropper drop. We dip a severed cat tongue in water, allowing excess fluid to drip off, and find that the fluid in the papillae cavities accounts for 5% of total fluid on the top of the tongue. While it's not a large volume, we will show that papillae penetration into fur allows saliva to reach areas that the tongue surface cannot.

Our second finding is that cats can change the angle of their papillae by contracting their tongue. This allows the papillae to stand erect for grooming, or to lay flat to the tongue to push loose hairs towards the throat. For eating, this papillae directionality prevents food from falling out of the mouth. From the high speed video, the papillae are seen to reach a maximum angle of 90° from the tissue to papillae tip. It is known that the papillae are attached to the tongue epithelium by a soft keratinized tissue[92], which is lodged into the cavity at the base of the papillae. The Young's modulus of the papillae is measured at 1.66 - 1.94 ± 3% GPa, similar to human fingernails[105] and five orders of magnitude stiffer than the cat tongue tissue, of 9.1 ± 3.7 kPa (N = 5 trials). We measure the resistive torque of a cat papilla in tongue tissue ex vivo. **Figure 20** shows that the relationship between angle θ and torque T_{joint} is highly nonlinear; in particular, the torque increases exponentially as the papillae are rotated counter-clockwise. Stiffening of the tongues muscular tissue would further increase joint torque.

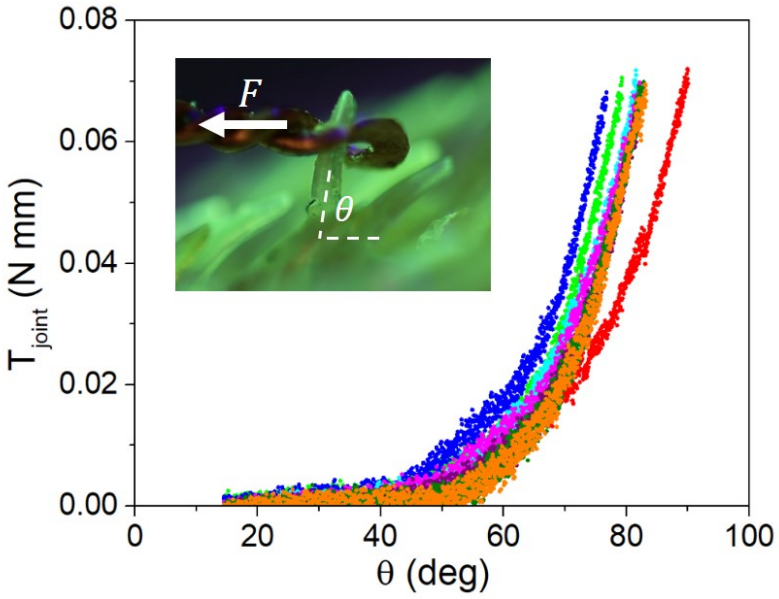

Figure 20: Papilla resistance to rotation in tongue tissue. As the angle θ between papilla and tongue tissue increases, the papilla resistance to rotation (or resistive joint torque T_{joint}) increases exponentially. Each color is a different trial using the same papilla.

4.1.3 Cats compress fur during grooming

We present a mathematical model for the height of cat's fur, which is compressed by the tongue during grooming. The cat fur coat has two layers, the topcoat and the undercoat. The topcoat consists of thick guard hairs, which are used to protect the undercoat from the environment. Although they are hidden from sight, the undercoat primarily consists of thin down hairs, which can outnumber guard hairs 24:1, and are used for thermoregulation[90]. Given their predominance in giving fur its shape, we only consider down hairs in our analysis. Just like in a sponge, the compression height of fur is most dictated by its porosity ϵ, the fraction of air in a given volume,

$$\epsilon = \frac{V_{\text{air}}}{V_{\text{total}}} = \frac{V_{\text{total}} - V_{\text{hairs}}}{V_{\text{total}}}. \tag{15}$$

Uncompressed cat fur, just like a bird's down feathers, is mostly air, with porosity values approaching one (0.97 for domestic cat, 0.98 for tiger, 0.99 for snow leopard). This large fraction of air provides the cat excellent insulation from the elements. As the tongue presses down on the fur during grooming [**Figure 21A**], air evacuates, decreasing fur porosity as shown in **Figure 21B**. We calculate the ensuing value of porosity by considering the geometry of the hairs.

In Eq. (15), we consider a rectangular prism of fur, with fur height h_{fur}, and width and length of the tongue W_{T}, and L_{T} as shown in **Figure 21A,B**. The air volume V_{air} can be written as the total volume V_{total} minus the volume V_{hairs} of all hairs in this region. Each down hair is cylindrical with a radius r_{hair} and length L_{hair}. The total hair volume is the product of the volume of each hair $\pi r_{\text{hair}}^2 L_{\text{hair}}$, and the number of hairs, which can be written as the hair density per unit area, ρ_{fur}, multiplied by the area $W_{\text{T}} L_{\text{T}}$. Thus, Eq. (15) simplifies to:

$$\epsilon = \frac{h_{\text{fur}} W_{\text{T}} L_{\text{T}} - \rho_{\text{fur}} W_{\text{T}} L_{\text{T}} \pi r_{\text{hair}}^2 L_{\text{hair}}}{h_{\text{fur}} W_{\text{T}} L_{\text{T}}}. \tag{16}$$

Simplifying and rearranging Eq. (16) gives us the relationship between fur depth h_{fur}, the distance between the skin and tongue, and porosity ϵ as:

$$h_{\text{fur}} = \frac{\rho_{\text{fur}} \pi r_{\text{hair}}^2 L_{\text{hair}}}{1 - \epsilon}. \tag{17}$$

Eq. (17) makes sense: the more the hair layer is compressed, the lower the porosity. We can take Eq. (17) to its very limits by considering the maximum compression of fur. The closest the cylindrical hairs can pack together is in a hexagonal packing arrangement[116], resulting in the lowest attainable porosity of

$$\epsilon_{min} = 1 - \frac{\pi\sqrt{3}}{6} = 0.093. \tag{18}$$

We use this value of the minimum porosity to determine the minimum compressed height of fur. In addition, we measure fur density, hair radius, and hair length by hand at the Museum of Comparative Zoology at Harvard University for species *Acinonyx jubatus*, *Caracal caracal*, *Felis sylvestris*, *Panthera pardus*, *Panthera leo*, *Panthera uncia*, and *Panthera tigris*; additional fur density and length values are gathered from literature[101–103] and purchased fur samples. These values of ρ_{fur}, r_{hair}, and L_{hair} are given in Table 4 in Appendix A, and are inputted into Eq. (17) to estimate the minimum compressed fur height for different cats. For example, we find that the domestic cat can compress its fur from 37 mm to 1.2 mm, a tiger from 30 mm to 0.6 mm, and a persian cat from 81 mm to 2.6 mm.

Figure 21C shows the relationship between minimum compressed fur height and papillae height for different cats. We use the average cat papillae length of h_{papillae}=2.3 ± 0.2 mm for cats without a tongue sample. We see that the data separates into two distinct regimes, depending on the height of the compressed fur. If the papillae can reach the skin during fur compression ($h_{\text{papillae}} \geq h_{\text{fur}}$), we categorize these cats as "groomable". The caracal, cheetah, and leopard are the most "groomable" cats, due to their short, sparse fur. These cats should have no difficulty grooming themselves. The snow leopard has a fur height of 0.6 mm and a papillae height of 2.3 mm, but even it can still groom.

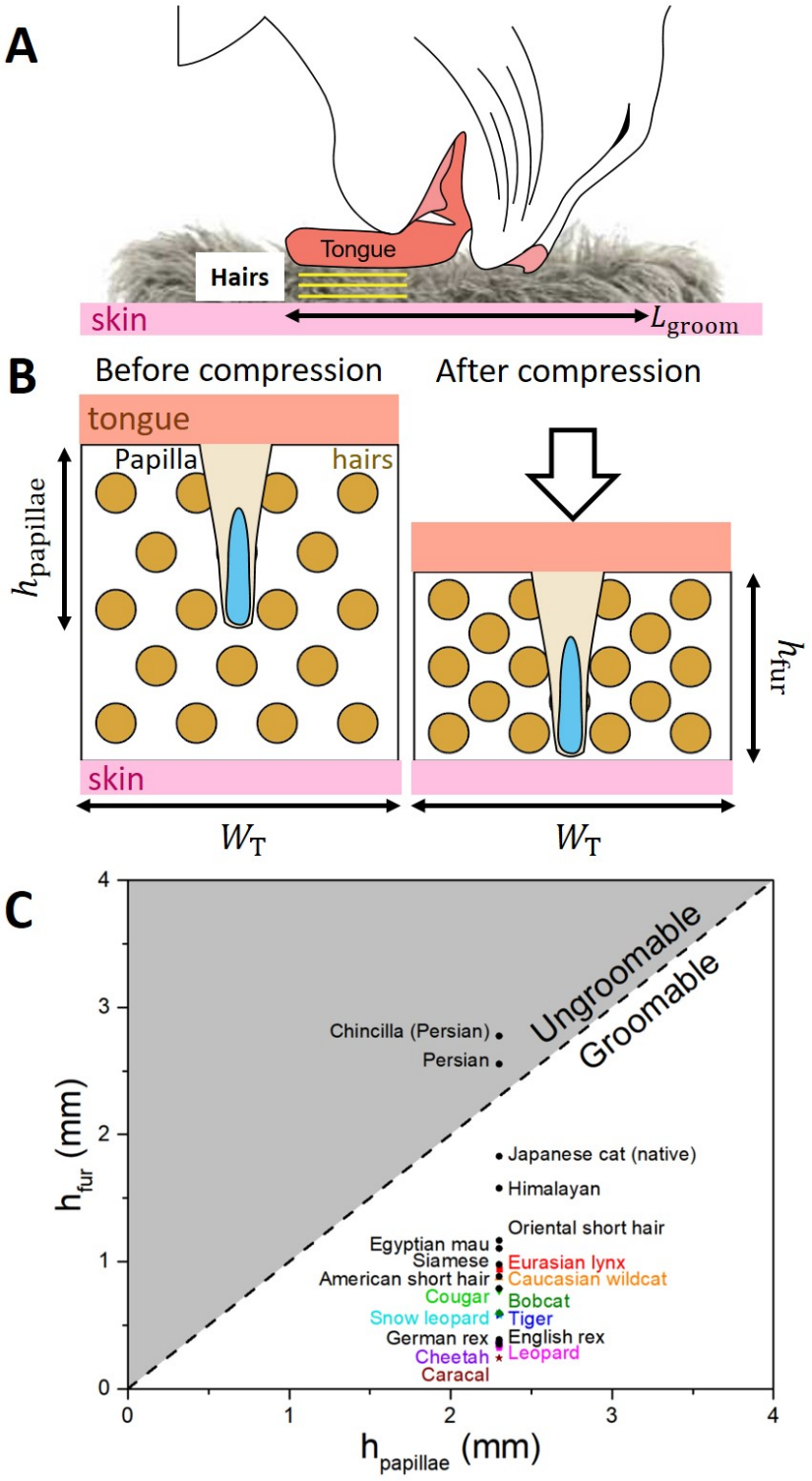

Figure 21: Fur compression during grooming. (A) Grooming schematic. (B) Fur compression schematic. As the tongue presses down on the fur, air is evacuated, reducing porosity. (C) Theoretical compressed fur height h_{fur} and measured papillae height h_{papillae}, with dashed line indicating $h_{\text{papillae}} = h_{\text{fur}}$. Ungroomable cats lie above the line ($h_{\text{papillae}} < h_{\text{fur}}$), and groomable cats lie below the line ($h_{\text{papillae}} \geq h_{\text{fur}}$).

Conversely, if the papillae cannot reach the skin ($h_{\text{papillae}} < h_{\text{fur}}$), fur matting and tangles may occur, making the cat "ungroomable". Long-haired domestic breeds, such as Persian cats, are notoriously known for matted fur; our results validate this observation, as these Persian breeds fall into the "ungroomable" region. While the papillae and the fur are on different parts on the body, we show that there is a morphological connection to enable grooming. In the next section, we measure the amount of fluid wicked into fur during grooming by both tongue and papillae, and provide supporting theory based on fur porosity.

4.2 Fur wetting

During grooming, the fur acts like a sponge to absorb saliva. We apply Darcy's model for wicking in porous media[117] to determine the depth of saliva penetration. The tongue is idealized as an infinite reservoir of fluid. In reality, the dorsal side of the tongue can only hold a maximum of 0.12 μL of water, and therefore our analysis is only valid for volumes wicked below this amount. The depth that the saliva penetrates may be written

$$h_{\text{saliva}} = \left(\frac{4K\sigma\cos(\theta)}{\epsilon\mu R_{\text{p}}}\right)^{1/2} t^{1/2}, \tag{19}$$

where K is permeability, R_{p} is the mean pore radius of the fur, and t is the time in which the fluid reservoir is in contact with the porous media. We assume that saliva is penetrating an array of cylinders, the hairs, in the transverse direction. Cat saliva is assumed to have the same surface tension and viscosity as water. The mean pore radius across a bank of constant-radius fibers may be written[118]:

$$R_{\text{p}} = 2r_{\text{hair}}\frac{\epsilon}{1-\epsilon}. \tag{20}$$

The permeability K of the porous media is determined using the Carman-Kozeny equation for transverse flow through cylindrical fibers[119]:

$$K = \frac{{r_{\text{hair}}}^2}{4k}\frac{\epsilon^3}{(1-\epsilon)^2}, \tag{21}$$

where k is the Kozeny constant, equal to 10 for transverse flow. Fur has a unique exception to being a porous media, in that the mean pore radius will change as fluid is introduced. This is due to the fact that hairs are flexible, and will bend when surface tension forces are applied. As analyzed by Py and Boudaoud[120], wet fibers aggregate into bundles, where the porosity of these bundles is considered to be close-packed hexagonal packing. Therefore, hairs will form bundles when wetted, decreasing porosity to its lowest attainable value [**Figure 22A,B**]. Thus, in our analysis, we use $\epsilon = \epsilon_{\text{min}} = 0.093$.

Just like a sponge, the saliva can penetrates deeper the longer it is in contact with fur. For grooming, the contact time $t \sim \frac{L_{\text{T}}}{v_{\text{groom}}}$ scales as the ratio of tongue length and grooming velocity v_{groom}. We substitute this contact time into Eq. (19) to estimate the depth the fluid has seeped. Fluid will fill the air pockets between hairs; therefore, the theoretical volume of fluid wicked into the fur V_{fluid} is:

$$V_{\text{fluid}} = \epsilon h_{\text{saliva}} W_{\text{T}} L_{\text{groom}}, \tag{22}$$

where L_{groom} is the lick length during the grooming scenario. By substituting h_{saliva} from Eq. (19) into Eq. (22), the volume of saliva wicked may be written:

$$V_{\text{fluid}} = \left(\frac{\sigma\cos(\theta)}{\mu}\right)^{1/2} \left(r_{\text{hair}} L_{\text{T}} W_{\text{T}}^2\right)^{1/2} \left(\frac{L_{\text{groom}}^2}{v_{\text{groom}}}\right)^{1/2} \left(\frac{\epsilon^3}{20\,(1-\epsilon)}\right)^{1/2}. \tag{23}$$

Eq. (23) consists of four components: saliva properties, fur and tongue properties, grooming kinematics, and porosity, respectively. Values for these components are given in Appendix A. Intuitively, Eq. (23) tells us that the higher the porosity ϵ, the more fluid will wick into fur.

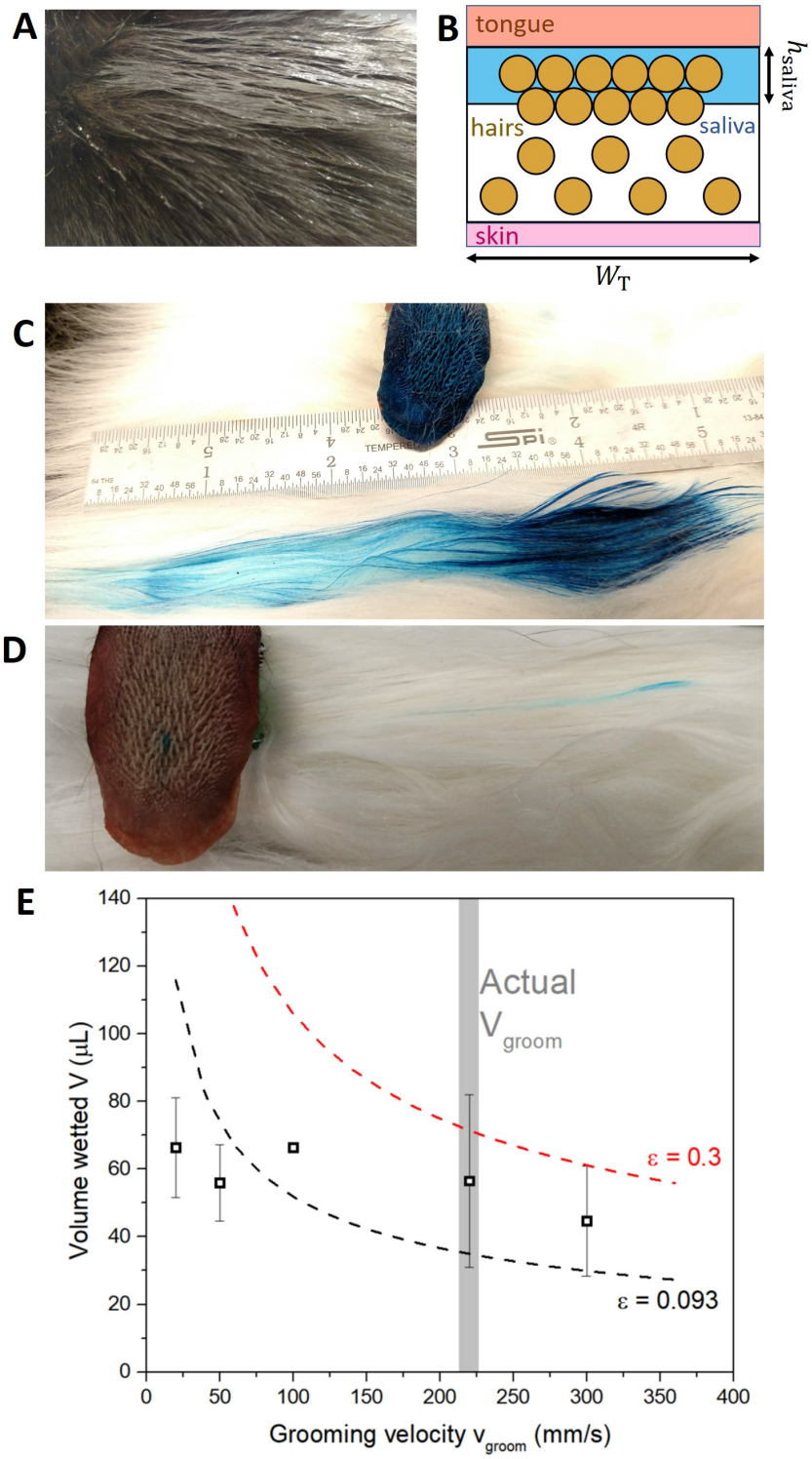

Figure 22: Saliva on tongue wets fur. (A) Wetted cat fur. (B) Schematic of wetted hairs clumping, reducing porosity. (C) Dye released from a saturated cat tongue, for a full grooming lick. (D) Dye released from a single filled papilla, for a full grooming lick. (E) Saliva deposited onto fur across grooming velocities using a grooming mimic. Fluid volume deposited onto fur for domestic grooming velocity of $v_{\text{groom}} = 220$ mm/s falls within a porosity range of 0.093 to 0.3, confirming that hairs clump when wetted.

We test our prediction for volume of saliva wicked by performing an automated grooming experiment. In the methods section, we describe the design and construction of a a "grooming machine" that pulls a cats severed tongue through its own fur. The machine drives the tongue at a fixed normal force and constant velocity. An image of the path created by a dyed cat tongue is shown in **Figure 22C**. In our experiments, we dip a dry tongue in water, let excess fluid drip off, then weigh the wetted tongue. After the tongue is moved through the fur, we re-weigh the tongue to determine amount of fluid removed during grooming.

Figure 22E shows the water volume released during each subsequent lick of our grooming machine. We conduct tests using grooming velocities from 20 mm/s to 300 mm/s, with cat grooming velocity equal to 220 mm/s. We measure the maximum water that can be held on a cat tongue, and find that the cat can deposit 50% of its total fluid capacity in a single grooming lick. It is thus critical that the cat retrieve its tongue between licks to rewet the tongue surface. For domestic cat grooming velocity, 56.6 ± 25.6 μL^3 of water is released in one lick, approximately the volume of an eyedropper drop. This volume falls within range of our predictions of saliva released, shown by the dashed red and black lines, corresponding to clumped porosity values from 0.093 to 0.3, indicating that our model has captured the essence of saliva release.

Cat papillae are able to penetrate past the wetted, clumped hairs on the top surface of fur to wet the dry hairs. Given the time of tongue contact, our prediction for saliva depth is $h_{\text{saliva}} = 0.54$ mm, assuming wetted hair clumping always results in $\epsilon_{min} = 0.093$. Based on tongue compression, the dry fur underneath will have a porosity range of $\epsilon = 0.23$ - 0.66. By subtracting $h_{\text{saliva}} = 0.54$ mm from h_{fur}, we find that the saliva on the tongue can only ever wet up to half the fur layer, necessitating other ways of wetting. To wet the dry fur close to the skin, the papillae penetrate into the dry fur layer to distribute saliva from the cavities.

For the domestic cat, each papilla can hold a maximum of 0.014 μL of saliva, for a total of 4.1 μL across 290 spines, around a tenth of a eyedropper drop. The fluid in the spines accounts for 5% of total fluid on the top of the tongue. As the fluid-filled papillae move through the fur, the fluid wicks into the hairs. The lick length at which fluid will be emptied L_{empty} from the papillae can be found by equating the volume in the spine to the volume wicked out:

$$V_{\text{cavity}} = \epsilon h_{\text{saliva}} w_{\text{cavity}} L_{\text{empty}} \tag{24}$$

where h_{saliva} is porous penetration depth from Eq. (19), and w_{cavity} is the papilla cavity width. For an ideal scenario, where a cavity is full at 0.014 μL, and using a wetted porosity value of $\epsilon = 0.093$, we find the papillae to empty at $L_{\text{empty}} \approx 6$ mm in a single lick, 10% of a grooming lick length $L_{\text{groom}} = 63$ mm. Although the saliva in the papillae is at maximum 5% of the tongue saliva, this saliva can be inserted quite deeply into the fur, as shown by the blue dye released from a single cat papilla in **Figure 22D**.

4.3 Thermoregulation

Unlike humans, primates, and horses, cats do not have sweat glands on their skin to keep cool[121], with exception of paws. It has long been hypothesized that grooming helps cats thermoregulate. Indeed, it has been shown that wetted fur aids in evaporative cooling in cows[122]. The cooling effect of sweat or saliva is due to the high heat of vaporization of water, pulling large amounts of heat from its surroundings during evaporation. It has been estimated that around 1/3 of the cat's evaporative water loss is due to saliva evaporation in fur[123].

For endotherms, the basal metabolic rate (BMR) reflects the amount of energy expended per unit time at rest, and can be used to estimate the total amount of heat produced by that animal. For domestic cats, the BMR conforms to an intraspecies allometric scaling[124,125] of BMR=$293M^{2/3}$, where M is body mass in kg and BMR is in kJ/d. Based on this scaling, a domestic housecat of mass 2.2 kg must expel heat at a rate of 5.7 watts to not overheat.

From our study, cats distribute saliva throughout their fur using U-shaped papillae. In an ideal scenario, all saliva held within the papillae would be deposited each lick. If all deposited saliva evaporates, the evaporative cooling rate is calculated as:

$$\frac{Q}{t} = \frac{m}{t} L_{\text{v}}, \tag{25}$$

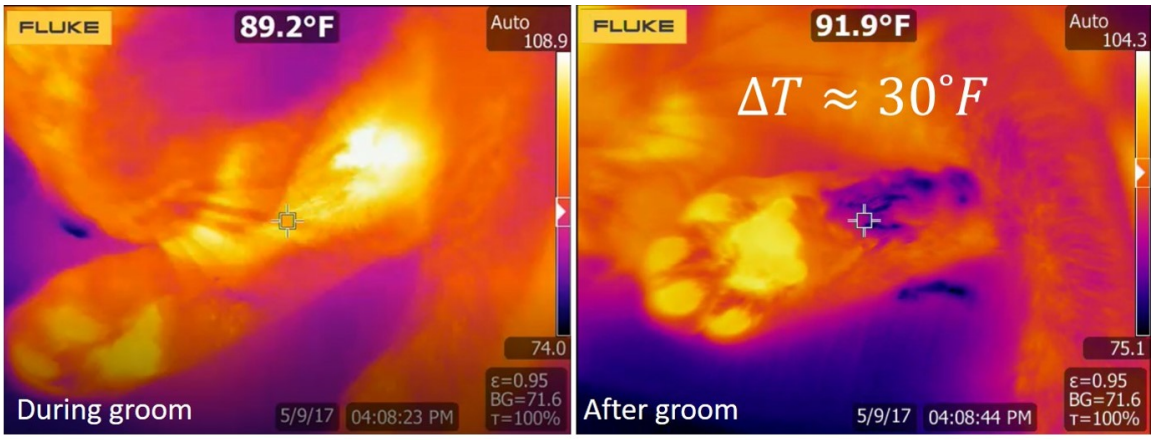

Figure 23: Thermal images of a cat grooming its leg. During the groom (left), heat from the tongue can be seen warming the fur. After the groom (right), evaporation causes a temperature drop of 30°F between paw pad and exposed fur.

where Q/t is the cooling rate, m/t is the amount of saliva deposited per unit time, and L_v is the latent heat of vaporization of water at a body temperature. For the average cat body temperature of 39°C, the latent heat of vaporization measures 575 cal/gm. Domestic cats sleep on average 14 hours per day and groom during 24% of its awake time[126]; therefore, a cat grooms 2.4 hours per day. Based on the measured lick frequency and maximum papillae cavity volume, the cat can deposit 73 grams of saliva per day with only the papillae, assuming papillae are refilled after every lick. We consider only papillae due to proximity to the skin. We find that cooling rate Q/t can reach a maximum of 2 watts, nearly 40% of the needed heat release. However, the latent heat is taken not just from the skin (like sweat evaporation), but from the sensible heat transferred across hairs and trapped air within the fur. The remainder of excess body heat is expelled through conduction, convection, and radiation across the fur, paws, and ears. This estimation does not consider the saliva deposited from the tongue tissue, which can generate a temperature difference of up to 30°F between skin and topcoat and increase the cooling rate [**Figure 23**].

What if cats did have sweat glands on their skin? If we assume a sweat gland density (1.2 mil glands/m^2) and perspiration rate (350 gm/day per m^2) similar to humans[127], sweat cooling rate would be 1.6 watts, accounting for 30% of the needed heat release. It is unknown why many mammals do not possess sweat glands; we can speculate that sweat released at the skin would find difficulty in evaporating within dense fur, due to the reduced convective flow in the trapped air causing an increase in humidity and consequent decrease in evaporation rate. As shown by Kimmel et al.[122], water further away from the skin increases the total dissipated heat.

4.4 Discussion

Cats have existed for nearly 11 million years, with the first domestic cat Felis catus appearing around 10,000 years ago in Southwest Asia[128]. Since then, there has been significant breed variation in terms of hair length. Feline hair length is determined by a gene designated as the L locus, where long hair is the recessive trait[129]. Long hair is typically associated with thermoregulation; cats in cold regions need to insulate body heat, but also need to cool their body during warm seasons. It is well known that saliva spreading aids in evaporative cooling[89], from rats[130] to kangaroos[131]. However, cats do not have sweat glands on their body, only on their paws[121]. By spreading saliva along hairs and to the skin, cats are able to pull additional heat from the body.

A potential problem with saliva distribution in fur is in regards to the cat allergen Fel d 1. It is estimated that around six million Americans are allergic to cats[132], or more specifically the protein Fel d 1. This protein is highly concentrated within cat saliva, dermis oils, and anal glands. Previous research has shown high concentrations of Fel d 1 in the fur[133,134]. Our study on saliva-filled papillae may shed light on how the

protein is spread via grooming. The current solutions to reduce the allergy are either immunotherapy [135], or to shampoo the cat, which reduces concentration of Fel d 1 in the fur for around a week [132]. It is our hope that this research may inspire new grooming tools for felines that both aid in hair grooming and potential removal of the Fel d 1 protein.

4.5 Chapter Summary

The cat tongue is a multifunctional tool, capable of distributing saliva to clean and cool the fur layer. In our study, we found that this unique cavo papillae exists on cats both large and small, and is long enough to penetrate through most all fur layers to the skin. This penetration allows the cavo papilla to distribute saliva to the root of the hairs. The saliva in the papillae and on the tongue is pulled onto the hairs through wicking, which we model using Darcy's capillary model for wicking in porous media. We mimic this grooming mechanic using a grooming machine, and a real cat tongue and cat fur sample. We find that with our theory, we expect a compressed fur porosity between 0.1 and 0.2, similar to what is measured when wetted hairs clump together. With the addition of the wetted tongue, close to 50% of the saliva is distributed to the fur during a single lick, however is only able to penetrate up to 50% of the fur depth.

CHAPTER V

BIOFLUIDS IN WETTING AND ADHESION

An additional aspect of this thesis is in regard to biofluids for wetting and grip. In this chapter, we explore how fluids wet the surfaces of textured tongues, and how non-Newtonian earwax aids in dust collection. These topics reveal interesting findings, and warrant further attention in future research.

5.1 Wetting of tongues

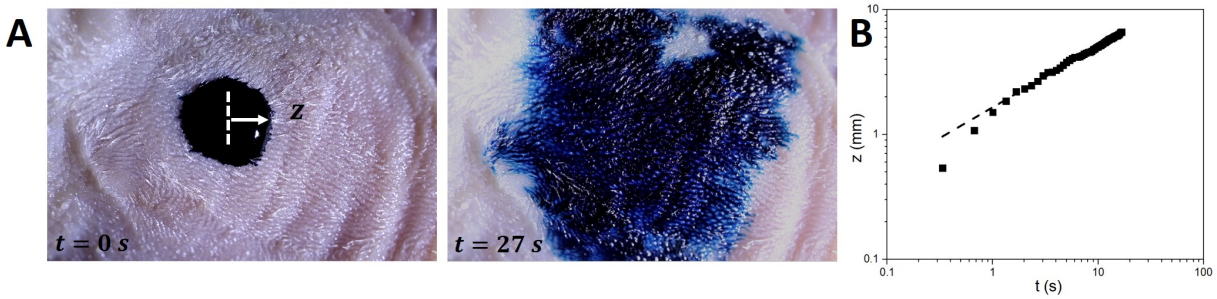

Figure 24: Drop spreading on a pig tongue ex vivo. (A) Multiple exposures of a drop of blue dye spreading. The fluid front z was measured from drop center to the drop edge. (B) Time-course of position of fluid front z. Fluid imbibes through the papillae with a front that moves with $t^{1/2}$, following a balance between capillary pressure and viscous dissipation.

Saliva plays a key role in maintaining oral health as well as aiding in digestion, speech and sensation. How does saliva flow on a dry tongue versus a wet tongue, and how does papillae size change flow rate? We first consider a dyed water drop impacting a dry tongue of the pig *Sus scrofa* **Figure 24**. The pig tongue has soft filiform papillae of measured length 0.2 mm. Tracking of drop shows that it spreads with a time course $z = 1.6t^{0.5}$ mm ($R^2 = 0.99$). This scaling exponent (0.5) from our pig tongue experiment in **Figure 24** matches well with the 1/2 exponent predicted by Eq. (5). The front moves at a peak velocity of 1.6 mm/s, and with decaying speed as the drop spreads. According to the measured scaling, if a dry pig tongue were exposed to only a single drop of fluid with no forced flow, it would take nearly an hour of wicking for the tongue, of measured length 192 mm, to become fully wet. To increase the spreading rate of saliva, animals compress their tongue with food and the roof of the mouth.

We now consider a deer tongue, which has rigid filiform papillae of length 3.7 mm. We dip a dry deer tongue [**Figure 25A, left**] and a wet deer tongue [**Figure 25A, right**] into a vat of food dye, then film the rate of fluid progression up the tongue using time-lapse videography. In a vertical wicking scenario for a dry deer tongue, capillary force is resisted by both viscous force and gravitational force. To simplify this problem, we assume flow between N number of parallel plates with a known velocity profile. For two plates with spacing $2w$=0.37 mm and height h=0.5 mm, the flow is characterized by:

$$\frac{(2h+2w)\rho\cos(\theta)}{2\rho hw} - gz - \frac{3(2h+2w)\mu z\dot{z}}{2\rho hw^2} = 0, \tag{26}$$

where θ, ρ, and μ are the contact angle, density, and viscosity of water, respectively. Using MATLAB, we solve Eq. (26) for z, and compare to the wicked area [**Figure 25B**]. While spacing and heights are approximate, the time rate of change of area matches well with the experimental data. Next, we soak a fresh deer tongue in water, then immediately dip the tongue into the vat of food dye. The motion of the fluid can

be characterized by diffusion, which is also plotted in **Figure 25B**. Fluid is found to wick faster in a dry tongue than in a wet tongue due to the large capillary forces.

5.2 Eaxwax as a dust collector

We now consider the role of earwax in dust collection within the inner ear canal of mammals. The ear is subject to invaders such as dust, insects, mud and even feces. Earwax is composed of keratin, cholesterol and long chain fatty acids[136]. The secretion of earwax has long been though to protect the ear and remove intruders[137]. However, the function of earwax is not fully understood. Earwax is known to gather on epithelial cells in the outer third of the ear canal, and migrates to the canal opening over the course of 11 weeks[138].

We first photograph earwax within the human ear canal in-vivo using a USB microscope with an endoscopic attachment. As shown in **Figure 26A,B**, the earwax is observed to create web-like surfaces between hairs in the ear canal, in addition to earwax drops generating the "beads-on-a-string" effect found only in viscoelastic fluids[139]. Next, we perform a 2D CFD analysis on air circulation within the ear canal [**Figure 26C**]. Assuming a human running pace of 1.5 m/s, with human ear canal dimensions, we find that circulation happens within the outer third of the ear canal. Surprisingly, earwax production occurs only in the outer third of the ear canal[136]. Lastly, we collect samples of earwax from rabbit, pig, sheep, and dog as shown in **Figure 27A** and perform a frequency sweep test in a cone-plate rheometer. From the rheological data, we show that earwax is a shear-thinning fluid, where viscosity drops with increasing shear rate [**Figure 27(B)**]. At least 2 trials were performed for each earwax sample. The viscosity for all tested animals follow the same curve given by:

$$\eta = -0.97\dot{\gamma} + 3.1 \tag{27}$$

where η is the shear viscosity and $\dot{\gamma}$ is the shear rate. From literature, we compare the ear canal diameter and length for a variety of species[140–146] and show that ear canal length L and diameter D scale with mammalian mass as $L, D \sim M^{1/3}$ [**Figure 27C**]. From this study, we show that all mammalian earwax is non-Newtonian, following the same shear-thinning curve regardless of species.

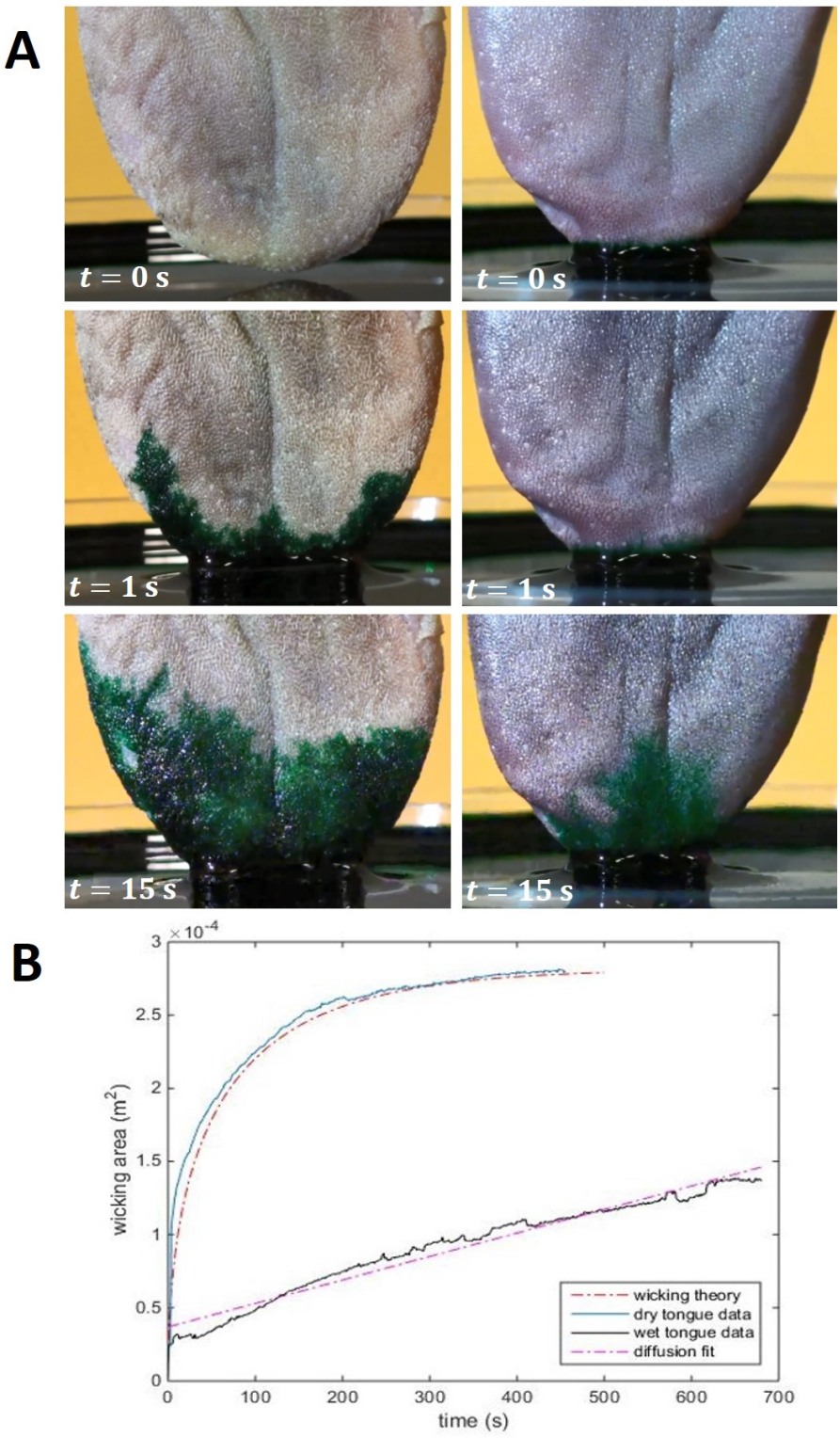

Figure 25: Fluid wicking up a deer tongue ex vivo. (A, left) A dry deer tongue immersed in a vat of green food coloring. Flow is driven by surface tension forces, and restricted by gravity and viscosity. (A, right) A wet deer tongue immersed in a vat of green food coloring. Dye travels up the fluid layer on the tongue via diffusion. (B) Experimental data matches well with theory for both a dry and a wet deer tongue. A wet tongue is able to pull fluid faster than a pre-wetted tongue.

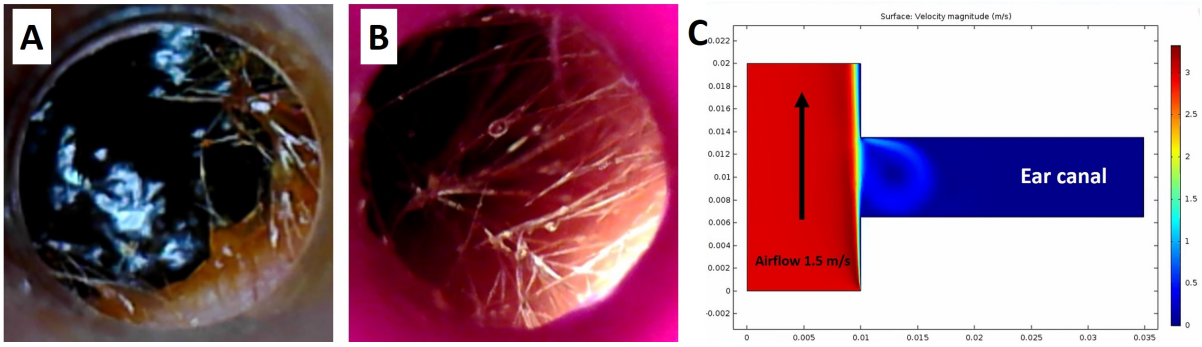

Figure 26: Earwax coating hairs within the human ear canal. (A) Two separate images of earwax within human subject 1. The earwax is shown to create web-like surfaces between hairs, increase total surface area in contact with the air. (B) Two separate images of earwax within human subject 2. The earwax is shown to coat individual hairs, producing "beads-on-a-string" structures.

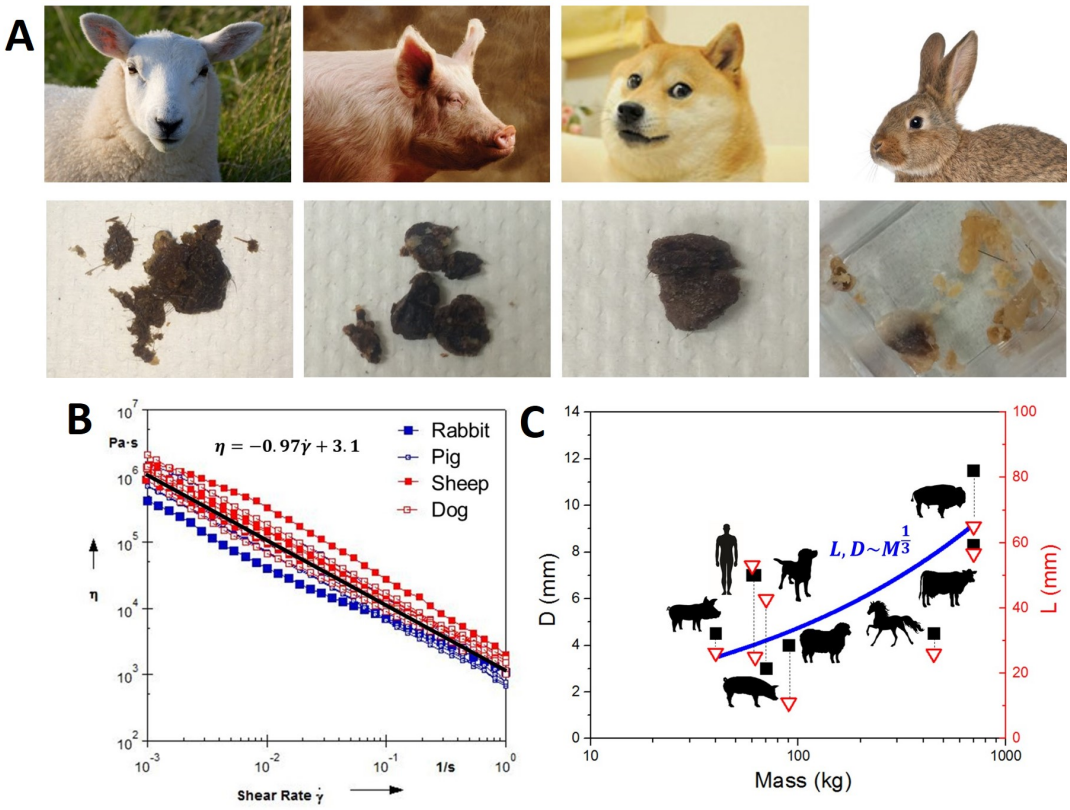

Figure 27: Earwax and ear canal properties. (A) Earwax samples collected from sheep, pig, dog, and rabbit. (B) Viscosity of earwax. We find that earwax is a shear-thinning fluid, and the viscosity of all tested animals follow the same relationship regardless of species. (C) Ear canal dimensions versus animal mass. We find that the ear canal scales as $M^{1/3}$.

CHAPTER VI

INVENTIONS

In the world of research, it is common that a new tool or technique be invented for progress to occur. In this chapter, we present the two inventions developed during the thesis, and the potential applications beyond the intended study.

6.1 Elo-Rheo

When testing biofluids, it can often be important to characterize both the shear and extensional properties, which can vary drastically. Fluids such as pitcher plant mucus[147], sundew plants[5], and spider silk[148] are composed of long-chain glycoprotein networks, which give the fluids unique adhesive properties through viscoelasticity. The highly adhesive nature of these fluids categorizes them as bio-adhesives, which exhibit unique strain hardening properties during normal separation; extensional viscosity increases by orders of magnitude as strain rate increases. The extensional rheometer was developed to measure the extensional properties of fluids by stretching samples to large strains, then measuring forces or rate of change in fluid thread diameters. During the study of the frog tongue, we wished to test elongational viscosity of several mammalian and amphibian salivas, a property rarely recorded. The elongational viscosity provides insight on adhesive grip, as there is no way to compare how well these fluids would function as adhesives in live prey capture scenarios.

In the field, portable methods to compare biological fluids are both inaccurate and expensive. While professional extensional rheometers, such as the CaBER or FiSER, provide accurate measurements, they are expensive and not portable. Many biological samples (such as saliva) degrade within hours; once the sample reaches the machine, the fluid properties may have changed dramatically. There is a need for quickly measuring fluid samples directly in the field; lab settings may affect animal saliva response or the saliva sample. On-site data analysis machines are being made possible by technology; for example, SCUVA (self-contained underwater velocimetry apparatus) is helping to provide in-situ field measurements of animal-fluid interactions[149].

We developed a lightweight, portable extensional rheometer, titled Elo-Rheo, for under $1,000 **Figure 28**. The machine works by pulling a single plate vertically using a rack-pinion system, driven by an encoded brushed motor. Elo-Rheo is capable of separating plates at rates up to 1 m/s. To measure fluid-thinning behavior, the plates can be pulled apart exponentially, while a separate high-speed camera can observe the change in diameter of the fluid thread. A Futek miniature S-Beam load cell can be attached to the base plate, measuring the associated forces during fluid separation.

At a later point in the thesis, Elo-Rheo retrofitted into a grooming machine, to aid in the cat tongue study **Figure 29**. The machine was turned on its side, allowing a feline tongue to be attached to the top plate and dragged through various fur samples. The fur samples were attached to a AMTI HE6x6 force plate, which measured the simulated grooming forces in the X, Y, and Z directions.

6.2 The cat tongue brush

How well does a cat tongue detangle fur as compared to a hairbrush? We looked to answer this question during the thesis by developing a cat tongue mimic at 4 times the size of a real tongue. Using the μCT scan of a domestic cat papilla, we 3D printed a simplified papilla without the cavity using a Formlab stereolithography machine (a resin-based 3D printer). We then embedded an array of 3D-printed papillae in a silicone substrate [**Figure 30A**]. Upon testing of the silicone, we found that the material had 4 times the stiffness of a real cat tongue (ex-vivo). We attached the artificial cat tongue to the newly retrofitted Elo-Rheo, then measured the associated forces during grooming of a fake nylon fur sample. For similar normal forces, we find that the cat tongue mimic can de-tangle fur faster and with less force than a standard

hairbrush [**Figure 30B**]. Another benefit of the anisotropic papillae is the ease of hair removal; we find that a swipe along the papillae direction removes nearly all the trapped fur in a matted roll **Figure 31**.

We are currently developing a new revision to the brush, where the spines are able to wick fluid from a central cavity in the hairbrush using similar principles to the cat papillae. We filed a provisional patent titled "Hairbrush inspired by cat tongue grooming mechanics" (U.S. patent application No. 62/585,651), and look to commercially develop the product. This novel brush may have applications pet medicine, where applying dermal medicine to fight pet bacterial infections can be expensive, stressful, and time-consuming. Additionally, this may provide a way to distribute dye in human hair, aid in removal of allergens from pet fur through leave-in shampoo's, and even carpet-cleaning solutions.

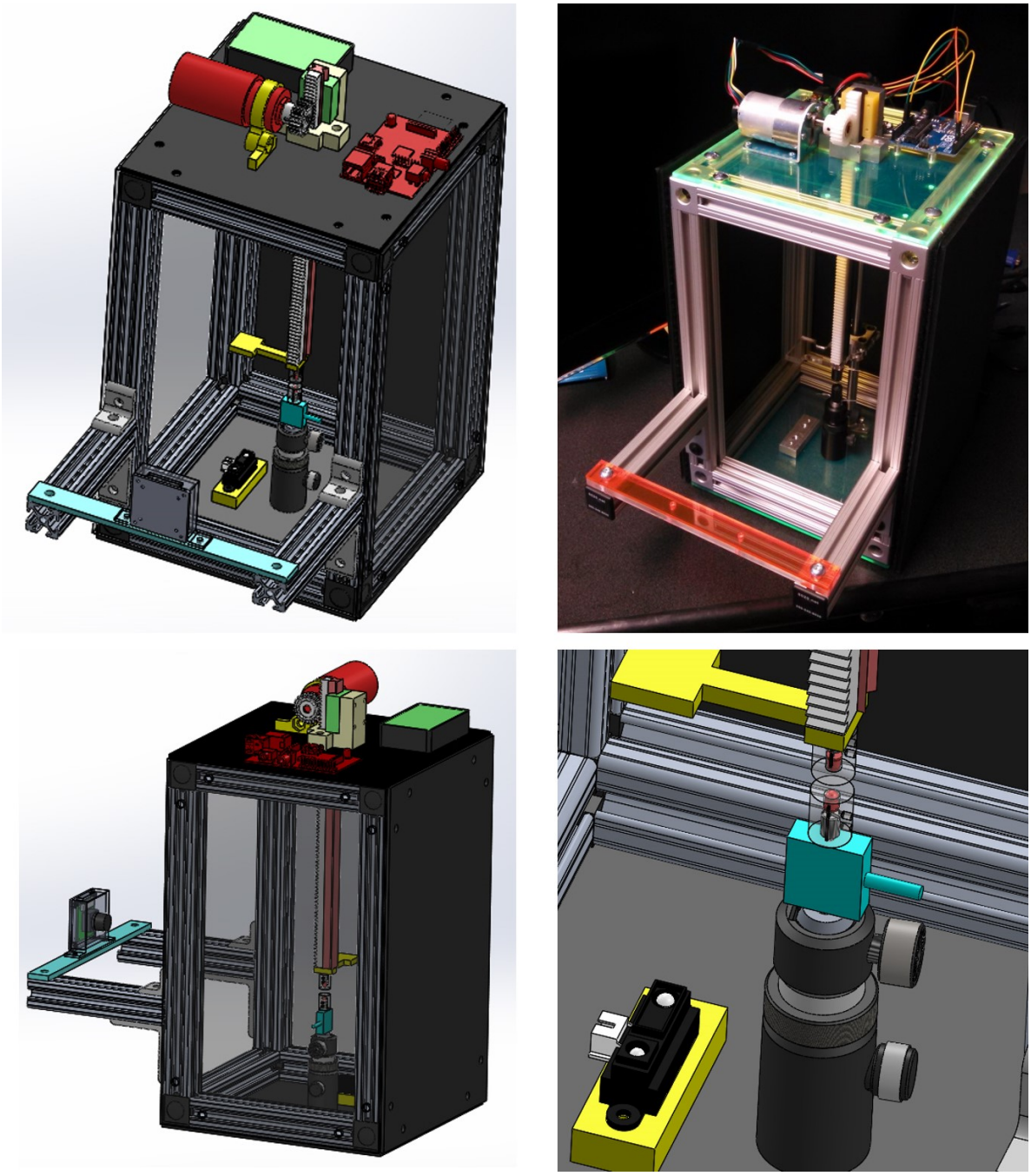

Figure 28: Elo-Rheo. (top, left) CAD model of Elo-Rheo. (top, right) Final photo of Elo-Rheo. (bottom) Alternative views of Elo-Rheo.

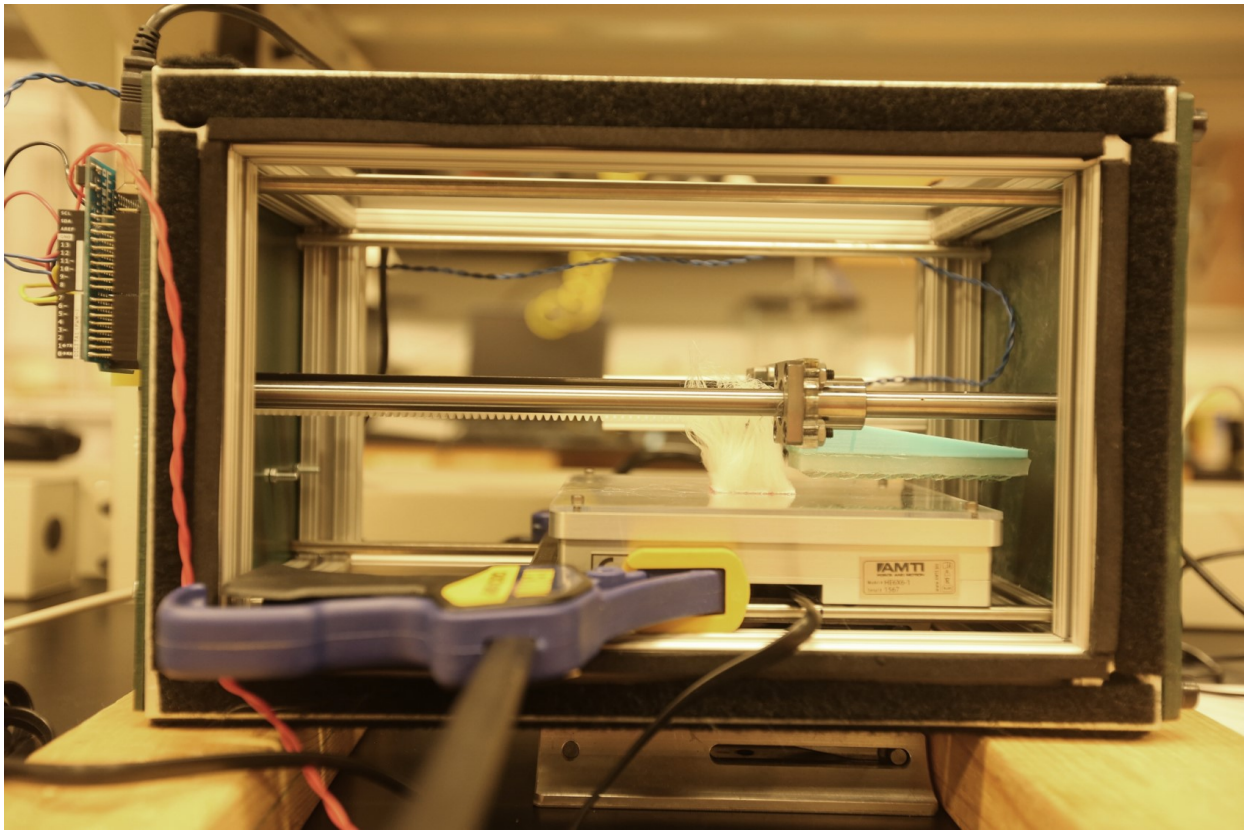

Figure 29: Elo-Rheo, retrofitted. Elo-Rheo retrofitted into a grooming machine, to test grooming forces with a real cat tongue.

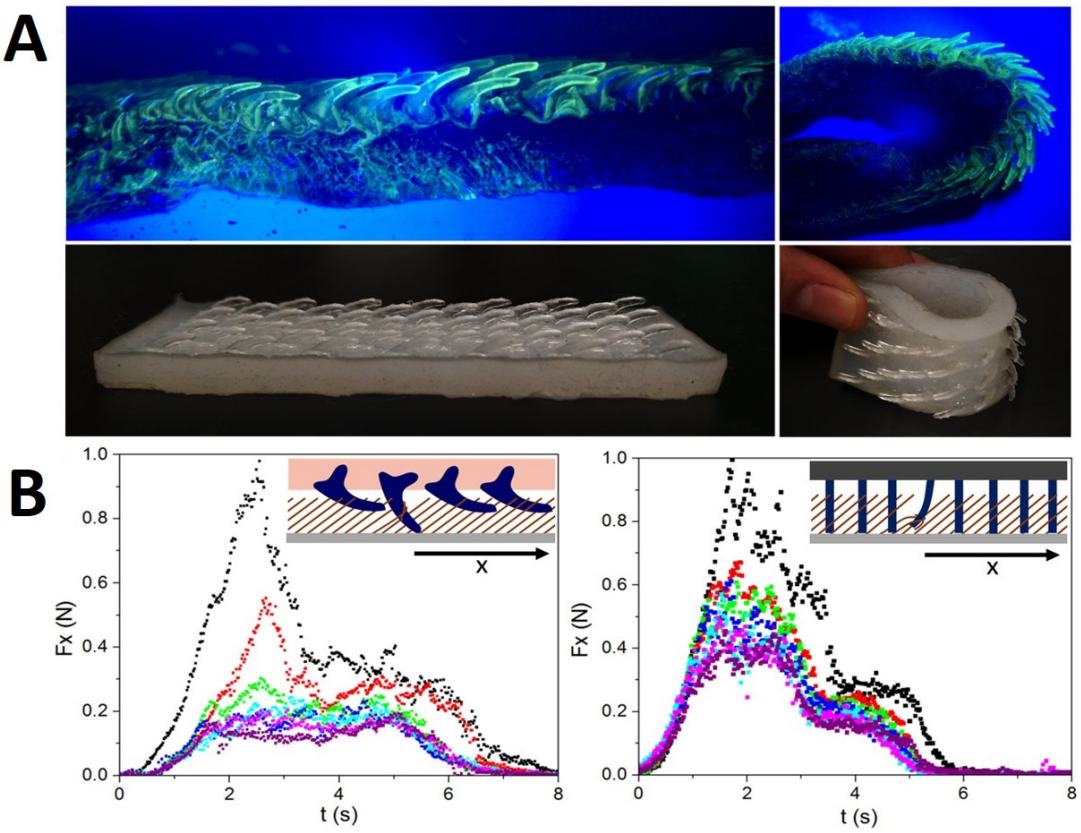

Figure 30: 3D-printed cat tongue mimic. (top) Slice of a domestic cat tongue, illuminated using UV dye and a black light. (bottom) 3D-printed mimic, displaying flexibility similar to the cat tongue.

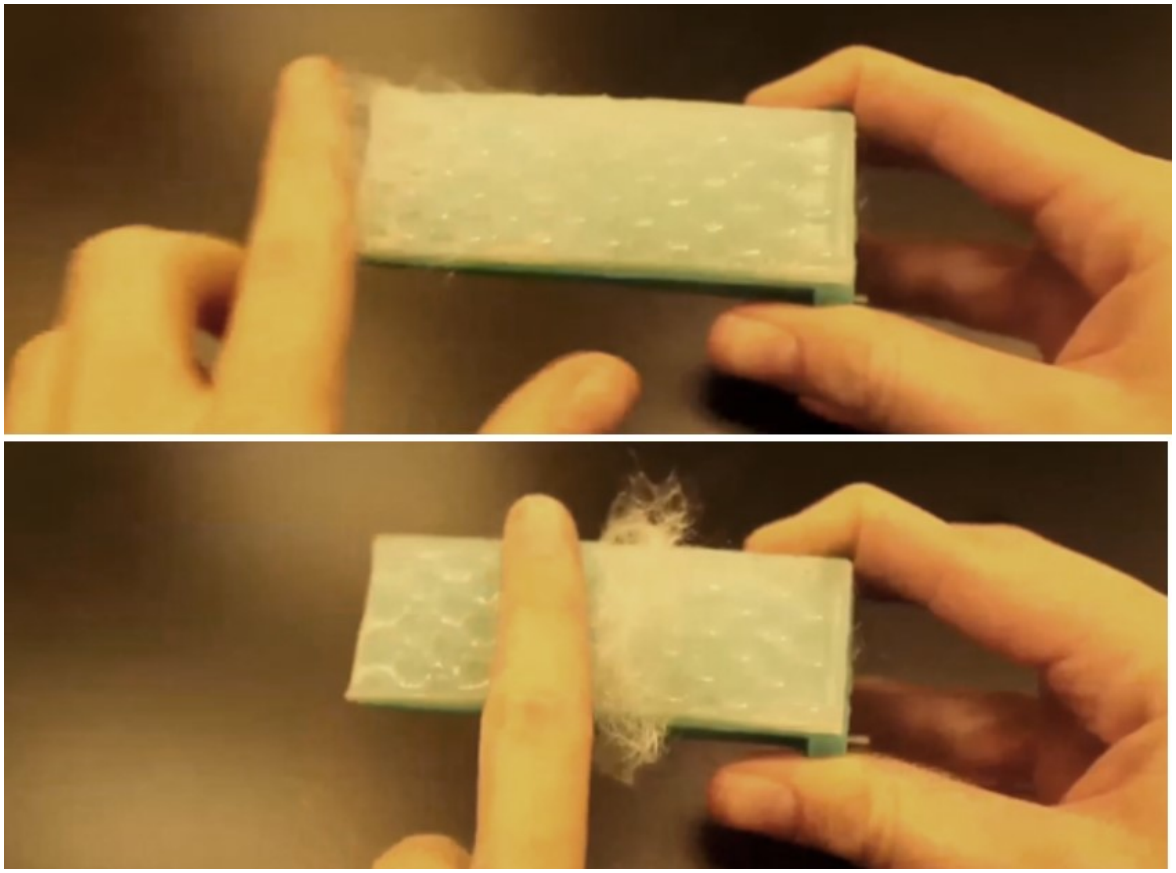

Figure 31: Anisotropic spines allow for easy removal of hair.

CHAPTER VII

CONCLUDING REMARKS

We have reported the results of a combined experimental and theoretical thesis on the role of tongues and bioadhesives for gripping, grabbing, and grooming. In chapter 3, we investigated how shear-thinning saliva and a soft, elastic tongue aids in prey capture at high tongue accelerations. We first tested the shear viscosity of frog saliva, collected from 16 frog tongues of species *Rana pipiens*. We found that the saliva is a shear-thinning non-Newtonian fluid, where viscosity changes drastically with shear rate. At low shear rates, frog saliva is 175 times more viscous than human saliva. At high shear rates, frog saliva becomes 50 times less viscous. During prey impact, a low viscosity saliva is better at penetrating rough surfaces and increasing contact area, much like paint on a wall. During retraction of prey, a high viscosity allows the insect to stick to the tongue. We model the saliva during prey capture using the theory of Stefan adhesion, where viscous fluids resist high rates of separation. We find that the frog tongue is 10 times softer than the human tongue. This extreme elasticity allows the tongue to stretch during prey capture, minimizing forces on prey which could induce separation. Viscoelastic damping within the tongue also helps reduce applied forces on insects by as much as 30% by aborbing stored elastic energy. The frog tongue could inspire novel reversible adhesives, capable of gripping onto a number of diverse surfaces.

In chapter 4, we discovered that the unique cavity morphology of the cat papillae on the tongue aids in distributing saliva deep into the feline coat. Using papillae samples taken from 6 different cat species, we find that the cavo papillae maintain near identical size and shape regardless of cat mass. Using data gathered on fur properties of numerous cat species, we find that the papillae length equals or exceeds the fur depth when compressed during grooming, allowing the cat to penetrate its fur to the hair root. Exceptions to this papillae/fur relationship include long-haired domestic breeds of cats, whose long fur does not allow full penetration of papillae. Additionally, we analyze the papillae resistance to rotation (ex-vivo) up to perpendicular to the tongue surface, and find that resistance increases exponentially. This resistance ensures that papillae reach full penetration depth during grooming, and prevents food from falling out of the mouth during eating. We model saliva distribution on the fur using Darcy's capillary model for wicking in porous media. We find that the tongue also holds saliva, and volume deposited through porous wicking corresponds to a wetted fur porosity between 0.098 and 0.3. We analyze the capacity for saliva evaporation to aid in thermoregulation, and find that deposited saliva can account for up to 40% of the needed heat release.

In chapter 5, we discuss how other biofluids aid in wetting and grip to particulate. We consider how fluid flows across small papillae on a pig tongue, and wicks up a rough deer tongue. We observe a dyed water drop impacting a dry pig tongue, and find that the wicking rate spreads with a time course of $t^{1/2}$, matching well with the 1/2 exponent predicted by the diffusion law of Bico and Quere in Eq. (5). In a separate experiment, we vertically dip a deer tongue into a vat of dyed water, and observe the fluid progression up the tongue using time-lapse videography. We find that the fluid wicks in a fractal pattern; the flow matches well with the theory that surface tension forces are being resisted by both gravitational and viscous forces. In a separate study, we analyze the role of earwax for dust collection within the inner ear. We observe the earwax within the human ear canal to create web-like surfaces between hairs. We collect earwax samples from rabbit, pig, sheep, and dog, and find that the earwax is viscoelastic, with viscosity for all animals matching the same shear-thinning curve.

In chapter 6, we present the two inventions developed during the thesis: Elo-Rheo and the cat tongue hairbrush. Elo-Rheo is an inexpensive, portable elongational rheometer built to test saliva samples in the field, with the goal of avoiding saliva degredation. The machine was retrofitted to replicate grooming kinematics between ex-vivo cat tongues and fur. To replicate the tongue of the cat, we developed a hairbrush using μCT scans of actual cat papillae embedded in a silicone substrate. The hairbrush demonstrates the anisotropic nature of the papillae, which allows for easy removal of fur post-groom. The 3D-printed cat tongue mimic shows how anisotropic, flexibly-embedded papillae aid in hair detangling and removal.

APPENDIX A

CAT TONGUE GROOMING DATA

Table 1: Kinematics

Animal		Trials	L_{groom} (mm)	v_{groom} (mm/s)	Lick frequency (1/s)	Ref.
Common name	Scientific name					
Cat	*Felis catus*	5	63 ± 20	220 ± 9.3	3.2 ± 0.6	1
Bobcat	*Lynx rufus*	8	38 ± 18	150 ± 1.2	2.1 ± 0.7	2
Cougar	*Puma concolor*	1	120	270	2.0	3
Snow leopard	*Panthera uncia*	3	53 ± 27	220 ± 19	3.3 ± 0.6	4
Tiger	*Panthera tigris*	8	190 ± 36	270 ± 20	1.5 ± 0.2	5
Lion	*Panthera leo*	4	180 ± 57	260 ± 38	2.2 ± 0.2	6
Leopard	*Panthera pardus*	5	79 ± 3	240 ± 18	3.5 ± 0.5	7
Black panther	*Panthera pardus*	2	74 ± 10	270 ± 38	4.2 ± 0.7	7

[1] In lab
[2] YouTube - Benji The Bobcat
[3] YouTube - Mexicrackah
[4] YouTube - TheSacramentoZoo
[5] YouTube - IEAS, BigCatDerek
[6] YouTube - Dougie Hamilton
[7] YouTube - Lock Head

Table 2: Tongue properties

Animal		Tongue samples	M (kg)	L_T (mm)	W_T (mm)	# Cavo papillae
Common name	Scientific name					
Cat	*Felis catus*	2	4	16.5 ± 3.5	13.0 ± 2.8	253 ± 52
Bobcat	*Lynx rufus*	4	10.5 ± 1.6	23.5 ± 3.1	21.3 ± 1.7	305 ± 43
Cougar	*Puma concolor*	1	54	38.0	33.0	483
Snow leopard	*Panthera uncia*	1	40	42.0	33.0	650
Tiger	*Panthera tigris*	4	116.3 ± 25.6	64.0 ± 11.3	54.5 ± 4.4	717 ± 277
Lion	*Panthera leo*	1	135	71.0	60.0	767

Table 3: Cavo papillae properties

Animal		$h_{papillae}$ (mm)	w_{cavity} (mm)	V_{cavity} (µL)
Common name	Scientific name			
Cat	*Felis catus*	2.1	0.30	0.014
Bobcat	*Lynx rufus*	2.3	0.30	0.009
Cougar	*Puma concolor*	2	0.30	0.035
Snow leopard	*Panthera uncia*	2.3	0.17	0.021
Tiger	*Panthera tigris*	2.3	0.22	0.082
Lion	*Panthera leo*	2.7	0.50	0.160

Table 4: Hair and fur properties

Animal		M (kg)	r_{hair} (µm)	ρ_{fur} (hairs/mm^2)	L_{hair}(mm)	Ref.
Common name	Scientific name					
Caucasian Wildcat	*Felis silvestris caucasica*	5	9.5	80	35	1, 4
Caracal	*Caracal caracal*	11.8	9.6	25	30	1, 4
Eurasian lynx	*Lynx lynx*	18	9.3	90	35	2, 4
Cheetah	*Acinonyx jubatus*	40	14.5	20	25	1, 4
Snow leopard	*Panthera uncia*	32	9.2	40	50	1, 4
Leopard	*Panthera pardus*	27	10.2	30	30	1, 4
Tiger	*Panthera tigris*	130	15.0	25	30	1, 4
Bobcat	*Lynx rufus*	8.6	7.9	90	31	2
Cougar	*Puma concolor*	54	8.9	80	35	2
American short hair	*Felis catus*	4	11.0	75	25	3, 5
Siamese	*Felis catus*	4	11.0	75	28	5
Egptian Mau	*Felis catus*	4	11.0	75	31	5
Oriental short hair	*Felis catus*	4	11.0	75	35	5
American short hair	*Felis catus*	4	11.0	75	37	5
Himalayan (Persian)	*Felis catus*	4	11.0	75	50	5
Japanese cat (native)	*Felis catus*	4	11.0	75	58	5
Persian	*Felis catus*	4	11.0	75	81	5
Chincilla (Persian)	*Felis catus*	4	11.0	75	88	5
English rex	*Felis catus*	4	8.1	75	20.4	6
German rex	*Felis catus*	4	8.5	75	20.6	6

[1] Museum of Comparative Zoology at Harvard University

[2] Promiselandranch.net

[3] On campus camples

[4] Kitchener, A. C., Van Valkenburgh, B. & Yamaguchi, N. Felid form and function. *Biology and conservation of wild felids* 83-106 (2010).

[5] Sato, H., Matsuda, H., Kubota, S. & Kawano, K. Statistical comparison of dog and cat guard hairs using numerical morphology. *Forensic science international* **158**, 94-103 (2006).

[6] Searle, A. & Jude, A. The rex type of coat in the domestic cat. *Journal of Genetics* **54**, 506-512 (1956).

APPENDIX B

SCHOLARLY ACHIEVEMENTS

Journal papers

Noel, A. C., Guo, H. Y., Mandica, M., & Hu, D. L. "Frogs use a viscoelastic tongue and non-Newtonian saliva to catch prey." *Journal of The Royal Society Interface*, 14(127), 2017.

Noel, A. C., & Hu, D. L. "The tongue as a gripper." *Journal of Experimental Biology*, 221(7), jeb176289, 2018.

Noel, A. C., & Hu, D. L. "How cats groom." *PNAS*. (In Preparation)

Conference presentations

A. Noel, D.L. Hu, How cats groom. Annual Society for Integrative and Comparative Biology, San Francisco, CA. January, 2018.

A. Noel, D.L. Hu, The mechanics of feline grooming. Society of Engineering Science Annual Meeting, Boston, MA. July, 2017.

A. Noel, D.L. Hu, 3D printed cat tongue is a self-cleaning, tangle-teasing brush. American Physical Society March Meeting, New Orleans, LA. March, 2017.

A. Noel, D.L. Hu, Sweat, spines and saliva: How to grab with soft biomaterials. The Adhesion Society 40th Annual Meeting, St. Petersburg, FL. February, 2017.

A. Noel, A. Martinez, H. Jung, T.W. Tsai, D.L. Hu, Cat tongue Velcro. Annual Society for Integrative and Comparative Biology, New Orleans, LA. January, 2017.

A. Noel, Y. Zhou, D.L. Hu, Sweating can improve grip in humans. Annual Society for Integrative and Comparative Biology, New Orleans, LA. January, 2017.

A. Noel, A. Martinez, H. Jung, T.W. Tsai, D.L. Hu, Cat tongue Velcro. American Physical Societys Division of Fluid Dynamics, Portland, OR. November, 2016.

A. Noel, D.L. Hu, The fluid mechanics of taste. Annual Society for Integrative and Comparative Biology, Portland, OR. January, 2016.

A. Noel, D.L. Hu, The fluid mechanics of taste. American Physical Societys Division of Fluid Dynamics, Boston, MA. November, 2015.

A. Noel, C. Wagner, G. McKinley, J. Mendelson, D. Hu, To catch a fly: The role of saliva adhesivity during prey capture in frog tongue projection. Annual Society for Integrative and Comparative Biology, West Palm Beach, FL. January, 2015.

A. Noel, C. Wagner, G. McKinley, J. Mendelson, D. Hu, The role of extensional viscosity in frog tongue projection. American Physical Societys Division of Fluid Dynamics, San Francisco, CA. November, 2014.

A. Noel, H. Choe, J. Ha, A. Fernandez-Nieves, D. Hu, To catch a fly: Viscosity and elasticity-based prey capture by frog tongue projection. ACS Colloid & Surface Science Symposium, Philadelphia, PA. June, 2014.

Bibliography

[1] Nishikawa, K. & Cannatella, D. Kinematics of prey capture in the tailed frog ascaphus truei (anura: Ascaphidae). *Zoological journal of the Linnean Society* **103**, 289–307 (1991).

[2] Sumbre, G., Gutfreund, Y., Fiorito, G., Flash, T. & Hochner, B. Control of octopus arm extension by a peripheral motor program. *Science* **293**, 1845–1848 (2001).

[3] Waller, A. V. X. minute structure of the papill and nerves of the tongue of the frog and toad. *Philosophical Transactions of the Royal Society of London* **139**, 139–149 (1849).

[4] Helton, K. L. & Yager, P. Interfacial instabilities affect microfluidic extraction of small molecules from non-newtonian fluids. *Lab on a Chip* **7**, 1581–1588 (2007).

[5] Erni, P., Varagnat, M., Clasen, C., Crest, J. & McKinley, G. H. Microrheometry of sub-nanolitre biopolymer samples: non-newtonian flow phenomena of carnivorous plant mucilage. *Soft Matter* **7**, 10889–10898 (2011).

[6] Kim, S., Laschi, C. & Trimmer, B. Soft robotics: a bioinspired evolution in robotics. *Trends in biotechnology* **31**, 287–294 (2013).

[7] Rus, D. & Tolley, M. T. Design, fabrication and control of soft robots. *Nature* **521**, 467 (2015).

[8] Seok, S. *et al.* Meshworm: a peristaltic soft robot with antagonistic nickel titanium coil actuators. *IEEE/ASME Transactions on mechatronics* **18**, 1485–1497 (2013).

[9] Jung, K., Koo, J. C., Lee, Y. K. & Choi, H. R. Artificial annelid robot driven by soft actuators. *Bioinspiration & biomimetics* **2**, S42 (2007).

[10] Shepherd, R. F. *et al.* Multigait soft robot. *Proceedings of the National Academy of Sciences* **108**, 20400–20403 (2011).

[11] Onal, C. D. & Rus, D. Autonomous undulatory serpentine locomotion utilizing body dynamics of a fluidic soft robot. *Bioinspiration & biomimetics* **8**, 026003 (2013).

[12] Calisti, M. *et al.* An octopus-bioinspired solution to movement and manipulation for soft robots. *Bioinspiration & biomimetics* **6**, 036002 (2011).

[13] Suzumori, K., Endo, S., Kanda, T., Kato, N. & Suzuki, H. A bending pneumatic rubber actuator realizing soft-bodied manta swimming robot. In *Robotics and Automation, 2007 IEEE International Conference on*, 4975–4980 (IEEE, 2007).

[14] Marchese, A. D., Onal, C. D. & Rus, D. Autonomous soft robotic fish capable of escape maneuvers using fluidic elastomer actuators. *Soft Robotics* **1**, 75–87 (2014).

[15] Sugiyama, Y. & Hirai, S. Crawling and jumping of deformable soft robot. In *Intelligent Robots and Systems, 2004.(IROS 2004). Proceedings. 2004 IEEE/RSJ International Conference on*, vol. 4, 3276–3281 (IEEE, 2004).

[16] Lin, H.-T., Leisk, G. G. & Trimmer, B. Goqbot: a caterpillar-inspired soft-bodied rolling robot. *Bioinspiration & biomimetics* **6**, 026007 (2011).

[17] de Groot, J. H. & van Leeuwen, J. L. Evidence for an elastic projection mechanism in the chameleon tongue. *Proceedings of the Royal Society of London-B* **271**, 761 (2004).

[18] Debray, A. Manipulators inspired by the tongue of the chameleon. *Bioinspiration & biomimetics* **6**, 026002 (2011).

[19] Hatakeyama, T. & Mochiyama, H. Shooting manipulation inspired by chameleon. *IEEE/ASME Transactions on Mechatronics* **18**, 527–535 (2013).

[20] Kim, S. *et al.* Micro artificial muscle fiber using niti spring for soft robotics. In *Intelligent Robots and Systems, 2009. IROS 2009. IEEE/RSJ International Conference on*, 2228–2234 (IEEE, 2009).

[21] Hannan, M. W. & Walker, I. D. Kinematics and the implementation of an elephant's trunk manipulator and other continuum style robots. *Journal of Field Robotics* **20**, 45–63 (2003).

[22] Laschi, C. *et al.* Soft robot arm inspired by the octopus. *Advanced Robotics* **26**, 709–727 (2012).

[23] Cheng, N. G. *et al.* Design and analysis of a robust, low-cost, highly articulated manipulator enabled by jamming of granular media. In *Robotics and Automation (ICRA), 2012 IEEE International Conference on*, 4328–4333 (IEEE, 2012).

[24] Anderson, R. H., Ho, S. Y., Redmann, K., Sanchez-Quintana, D. & Lunkenheimer, P. P. The anatomical arrangement of the myocardial cells making up the ventricular mass. *European journal of cardiothoracic surgery* **28**, 517–525 (2005).

[25] Doran, G. & Baggett, H. A structural and functional classification of mammalian tongues. *Journal of mammalogy* **52**, 427–429 (1971).

[26] Deban, S. M., O'Reilly, J. C., Dicke, U. & Van Leeuwen, J. L. Extremely high-power tongue projection in plethodontid salamanders. *Journal of Experimental Biology* **210**, 655–667 (2007).

[27] Naples, V. L. Morphology, evolution and function of feeding in the giant anteater (myrmecophaga tridactyla). *Journal of Zoology* **249**, 19–41 (1999).

[28] Nishikawa, K. C. Neuromuscular control of prey capture in frogs. *Philosophical Transactions of the Royal Society of London B: Biological Sciences* **354**, 941–954 (1999).

[29] Van Leeuwen, J. L., De Groot, J. H. & Kier, W. M. Evolutionary mechanics of protrusible tentacles and tongues. *Netherlands Journal of Zoology* **50**, 113–139 (2000).

[30] Nishikawa, K. C. & Gans, C. Mechanisms of tongue protraction and narial closure in the marine toad bufo marinus. *Journal of Experimental Biology* **199**, 2511–2529 (1996).

[31] Deban, S. M., Wake, D. B. & Roth, G. Salamander with a ballistic tongue. *Nature* **389**, 27 (1997).

[32] Kier, W. M. & Smith, K. K. Tongues, tentacles and trunks: the biomechanics of movement in muscular-hydrostats. *Zoological Journal of the Linnean Society* **83**, 307–324 (1985).

[33] Kier, W. M. The diversity of hydrostatic skeletons. *Journal of Experimental Biology* **215**, 1247–1257 (2012).

[34] Anderson, C. V., Sheridan, T. & Deban, S. M. Scaling of the ballistic tongue apparatus in chameleons. *Journal of morphology* **273**, 1214–1226 (2012).

[35] Deban, S. M. & Nishikawa, K. C. The kinematics of prey capture and the mechanism of tongue protraction in the green tree frog hyla cinerea. *Journal of Experimental Biology* **170**, 235–256 (1992).

[36] Emura, S., Okumura, T. & Chen, H. Morphology of the lingual papillae in the giraffe. *Okajimas folia anatomica Japonica* **89**, 99–103 (2013).

[37] Igado, O. O. Gross morphometric study of the eyeball and tongue of the nigerian local dog. *Italian Journal of Anatomy and Embryology* **116**, 104–110 (2011).

[38] Meijaard, E. The malayan sun bear (helarctos malayanus) on borneo, with special emphasis on its conservation status in kalimantan, indonesia. *International MOF Tropendos Kalimantan Project and the World Society of the Protection of Animal, London* (1997).

[39] Muchhala, N. Nectar bat stows huge tongue in its rib cage. *Nature* **444**, 701–702 (2006).

[40] Nishikawa, K. C. & Roth, G. The mechanism of tongue protraction during prey capture in the frog discoglossus pictus. *Journal of experimental biology* **159**, 217–234 (1991).

[41] Noel, A. C., Guo, H.-Y., Mandica, M. & Hu, D. L. Frogs use a viscoelastic tongue and non-newtonian saliva to catch prey. *Journal of The Royal Society Interface* **14**, 20160764 (2017).

[42] Pfeiffer, C., Levin, M. & Lopes, M. Ultrastructure of the horse tongue: further observations on the lingual integumentary architecture. *Anatomia, histologia, embryologia* **29**, 37–44 (2000).

[43] Reis, P. M., Jung, S., Aristoff, J. M. & Stocker, R. How cats lap: water uptake by felis catus. *Science* **330**, 1231–1234 (2010).

[44] McMahon, T. A. & Bonner, J. T. *On size and life* (Scientific American Library, 1983).

[45] Prapong, T. *et al.* Macroscopic and microscopic anatomy of pangolins tongue (manis javanica). *Kasetsart Veterinarians* **19**, 9–19 (2009).

[46] Goriely, A. & McMillen, T. Shape of a cracking whip. *Physical review letters* **88**, 244301 (2002).

[47] Yekutieli, Y. *et al.* Dynamic model of the octopus arm. i. biomechanics of the octopus reaching movement. *Journal of neurophysiology* **94**, 1443–1458 (2005).

[48] McKee, C. T., Last, J. A., Russell, P. & Murphy, C. J. Indentation versus tensile measurements of young's modulus for soft biological tissues. *Tissue Engineering Part B: Reviews* **17**, 155–164 (2011).

[49] Hashimoto, K. & Suga, S. Estimation of the muscular tensions of the human tongue by using a three-dimensional model of the tongue. *Journal of the Acoustical Society of Japan (E)* **7**, 39–46 (1986).

[50] Crompton, A. & Musinsky, C. How dogs lap: ingestion and intraoral transport in canis familiaris. *Biology letters* **7**, 882–884 (2011).

[51] Lauga, E., Pipe, C. J. & Le Rvrend, B. Sensing in the mouth: A model for filiform papillae as strain amplifiers (2016).

[52] Iwasaki, S. Evolution of the structure and function of the vertebrate tongue. *Journal of Anatomy* **201**, 1–13 (2002).

[53] Abd-Elnaeim, M. M., Zayed, A. E. & Leiser, R. Morphological characteristics of the tongue and its papillae in the donkey (equus asinus): a light and scanning electron microscopical study. *Annals of Anatomy-Anatomischer Anzeiger* **184**, 473–480 (2002).

[54] Fouda, Y. A., Sabry, D. A. & Abou-Zaid, D. F. Functional anatomical, histological and ultrastructural studies of three chameleon species: Chamaeleo chamaeleon, chamaeleo africanus, and chamaeleon vulgaris. *International Journal of Morphology* **33** (2015).

[55] Kleinteich, T. & Gorb, S. N. Frog tongue surface microstructures: functional and evolutionary patterns. *Beilstein Journal of Nanotechnology* **7**, 893–903 (2016).

[56] Kobayashi, K., Kumakura, M., Yoshimura, K., Inatomi, M. & Asami, T. Fine structure of the tongue and lingual papillae of the penguin. *Archives of histology and cytology* **61**, 37–46 (1998).

[57] Kumar, S. & Bate, L. A. Scanning electron microscopy of the tongue papillae in the pig (sus scrofa). *Microscopy research and technique* **63**, 253–258 (2004).

[58] Mascitti, V. & Osvaldo Kravetz, F. Bill morphology of south american flamingos. *The Condor* **104**, 73–83 (2002).

[59] Okada, S. & Schraufnagel, D. E. Scanning electron microscopic structure of the lingual papillae of the common opossum (didelphis marsupialis). *Microscopy and Microanalysis* **11**, 319–332 (2005).

[60] Verssimo, C. J., DAgostino, S. M., Pessoa, F. F., de Toledo, L. M. & de Miranda Santos, I. K. F. Length and density of filiform tongue papillae: differences between tick-susceptible and resistant cattle may affect tick loads. *Parasites & vectors* **8**, 594 (2015).

[61] Zweers, G., De Jong, F., Berkhoudt, H. & Berge, J. V. Filter feeding in flamingos (phoenicopterus ruber). *Condor* 297–324 (1995).

[62] Humphrey, S. P. & Williamson, R. T. A review of saliva: normal composition, flow, and function. *The Journal of prosthetic dentistry* **85**, 162–169 (2001).

[63] Carrier, W. H. The temperature of evaporation. *ASHVE Transactions* **24**, 25–50 (1918).

[64] Bush, J. W. & Hu, D. L. Walking on water: biolocomotion at the interface. *Annu. Rev. Fluid Mech.* **38**, 339–369 (2006).

[65] Bico, J., Tordeux, C. & Qur, D. Rough wetting. *EPL (Europhysics Letters)* **55**, 214 (2001).

[66] Virot, E., Ma, G., Clanet, C. & Jung, S. Physics of chewing in terrestrial mammals. *Scientific Reports* **7** (2017).

[67] Bongaerts, J., Rossetti, D. & Stokes, J. The lubricating properties of human whole saliva. *Tribology Letters* **27**, 277–287 (2007).

[68] Park, M., Chung, J., Kim, Y., Chung, S. & Kho, H. Viscosity and wettability of animal mucin solutions and human saliva. *Oral diseases* **13**, 181–186 (2007).

[69] Davis, S. The rheological properties of saliva. *Rheologica Acta* **10**, 28–35 (1971).

[70] Schiffman, H. R. *Sensation and perception: An integrated approach* (John Wiley & Sons, 1990).

[71] Kleinteich, T. & Gorb, S. N. Tongue adhesion in the horned frog ceratophrys sp. *Scientific reports* **4**, 5225 (2014).

[72] Vogel, M. J. & Steen, P. H. Capillarity-based switchable adhesion. *Proceedings of the National Academy of Sciences* **107**, 3377–3381 (2010).

[73] Autumn, K. *et al.* Adhesive force of a single gecko foot-hair. *Nature* **405**, 681–685 (2000).

[74] Peters, S. E. & Nishikawa, K. C. Dyscophus guinetti, and bufo marinus. *Journal of morphology* **242**, 107–124 (1999).

[75] Sneddon, I. N. The relation between load and penetration in the axisymmetric boussinesq problem for a punch of arbitrary profile. *International journal of engineering science* **3**, 47–57 (1965).

[76] Johnson, K., Kendall, K. & Roberts, A. Surface energy and the contact of elastic solids. *Proc. R. Soc. Lond. A* **324**, 301–313 (1971).

[77] Maugis, D. Adhesion of spheres: the jkr-dmt transition using a dugdale model. *Journal of colloid and interface science* **150**, 243–269 (1992).

[78] Grenon, J.-F. & Walker, G. The tenacity of the limpet, patella vulgata l.: an experimental approach. *Journal of experimental marine biology and ecology* **54**, 277–308 (1981).

[79] Stefan, J. Versuche ber die scheinbare adhsion. *Annalen der Physik* **230**, 316–318 (1875).

[80] Dienes, G. & Klemm, H. Theory and application of the parallel plate plastometer. *Journal of Applied Physics* **17**, 458–471 (1946).

[81] Noel, A. C. & Hu, D. L. How cats groom (2018).

[82] Alexander, R., Bennett, M. & Ker, R. Mechanical properties and function of the paw pads of some mammals. *Journal of Zoology* **209**, 405–419 (1986).

[83] Jusufi, A., Zeng, Y., Full, R. J. & Dudley, R. Aerial righting reflexes in flightless animals. *Integrative and comparative biology* **51**, 937–943 (2011).

[84] Russell, R. A. Using tactile whiskers to measure surface contours. In *Robotics and Automation, 1992. Proceedings., 1992 IEEE International Conference on*, 1295–1299 (IEEE, 1992).

[85] Heffner, R. S. & Heffner, H. E. Hearing range of the domestic cat. *Hearing research* **19**, 85–88 (1985).

[86] Beaver, B. V. *Feline Behavior-E-Book* (Elsevier Health Sciences, 2003).

[87] Hsu, M.-H., Hsu, T.-C. & Wu, W.-J. Distribution of cat fleas (siphonaptera: Pulicidae) on the cat. *Journal of medical entomology* **39**, 685–688 (2002).

[88] Amador, G. J. & Hu, D. L. Cleanliness is next to godliness: mechanisms for staying clean. *Journal of Experimental Biology* **218**, 3164–3174 (2015).

[89] Gebremedhin, K. G. & Wu, B. A model of evaporative cooling of wet skin surface and fur layer. *Journal of Thermal Biology* **26**, 537–545 (2001).

[90] Miller, W. H., Griffin, C. E., Campbell, K. L. & Muller, G. H. *Muller and Kirk's Small Animal Dermatology7: Muller and Kirk's Small Animal Dermatology* (Elsevier Health Sciences, 2013).

[91] Boshel, J., Wilborn, W. & Singh, B. Filiform papillae of cat tongue. *Cells Tissues Organs* **114**, 97–105 (1982).

[92] Iwasaki, S.-i. Surface structure and keratinization of the mucosal epithelium of the domestic cat tongue. *Journal of the Mammalogical Society of Japan* **15**, 1–13 (1990).

[93] Ojima, K. Quantitative and distributive study of the fungiform papillae in the cat tongue in microvascular cast specimens. *Annals of Anatomy-Anatomischer Anzeiger* **180**, 409–414 (1998).

[94] Prakash, M., Qur, D. & Bush, J. W. Surface tension transport of prey by feeding shorebirds: the capillary ratchet. *science* **320**, 931–934 (2008).

[95] Hu, D. L., Chan, B. & Bush, J. W. The hydrodynamics of water strider locomotion. *Nature* **424**, 663 (2003).

[96] Koh, J.-S. *et al.* Jumping on water: Surface tensiondominated jumping of water striders and robotic insects. *Science* **349**, 517–521 (2015).

[97] Gart, S., Socha, J. J., Vlachos, P. P. & Jung, S. Dogs lap using acceleration-driven open pumping. *Proceedings of the National Academy of Sciences* **112**, 15798–15802 (2015).

[98] Noel, A. C. & Hu, D. L. The tongue as a gripper. *Journal of Experimental Biology* **221**, jeb176289 (2018).

[99] Boyer, G., Laquieze, L., Le Bot, A., Laquize, S. & Zahouani, H. Dynamic indentation on human skin in vivo: ageing effects. *Skin Research and Technology* **15**, 55–67 (2009).

[100] Cheever, E. The convolution integral (2015). URL `http://lpsa.swarthmore.edu/convolution/convolution.html`.

[101] Searle, A. & Jude, A. The rex type of coat in the domestic cat. *Journal of Genetics* **54**, 506–512 (1956).

[102] Kitchener, A. C., Van Valkenburgh, B. & Yamaguchi, N. Felid form and function. *Biology and conservation of wild felids* 83–106 (2010).

[103] Sato, H., Matsuda, H., Kubota, S. & Kawano, K. Statistical comparison of dog and cat guard hairs using numerical morphology. *Forensic science international* **158**, 94–103 (2006).

[104] Engler, A. J., Richert, L., Wong, J. Y., Picart, C. & Discher, D. E. Surface probe measurements of the elasticity of sectioned tissue, thin gels and polyelectrolyte multilayer films: correlations between substrate stiffness and cell adhesion. *Surface Science* **570**, 142–154 (2004).

[105] Farren, L., Shayler, S. & Ennos, A. The fracture properties and mechanical design of human fingernails. *Journal of Experimental Biology* **207**, 735–741 (2004).

[106] Harding, J. & Sneddon, I. The elastic stresses produced by the indentation of the plane surface of a semi-infinite elastic solid by a rigid punch. In *Mathematical Proceedings of the Cambridge Philosophical Society*, vol. 41, 16–26 (Cambridge University Press, 1945).

[107] Saxena, T., Gilbert, J. L. & Hasenwinkel, J. M. A versatile mesoindentation system to evaluate the micromechanical properties of soft, hydrated substrates on a cellular scale. *Journal of Biomedical Materials Research Part A* **90**, 1206–1217 (2009).

[108] DiSabato-Mordarski, T. & Kleinberg, I. Measurement and comparison of the residual saliva on various oral mucosal and dentition surfaces in humans. *Archives of oral biology* **41**, 655–665 (1996).

[109] Yasuda, K., Armstrong, R. & Cohen, R. Shear flow properties of concentrated solutions of linear and star branched polystyrenes. *Rheologica Acta* **20**, 163–178 (1981).

[110] Lai, S. K., Wang, Y.-Y., Wirtz, D. & Hanes, J. Micro-and macrorheology of mucus. *Advanced drug delivery reviews* **61**, 86–100 (2009).

[111] Hammerman, D. L. The frog tongue: I. general development and histogenesis of filiform papillae and mucous glands in rana catesbeiana. *Acta Zoologica* **50**, 11–23 (1969).

[112] Cai, S. & Bhushan, B. Meniscus and viscous forces during normal separation of liquid-mediated contacts. *Nanotechnology* **18**, 465704 (2007).

[113] Barnes, W. J. P., Goodwyn, P. J. P., Nokhbatolfoghahai, M. & Gorb, S. N. Elastic modulus of tree frog adhesive toe pads. *Journal of Comparative Physiology A* **197**, 969 (2011).

[114] Nigg, B. M. & Liu, W. The effect of muscle stiffness and damping on simulated impact force peaks during running. *Journal of biomechanics* **32**, 849–856 (1999).

[115] Washburn, E. W. The dynamics of capillary flow. *Physical review* **17**, 273 (1921).

[116] Chang, H.-C. & Wang, L.-C. A simple proof of thue's theorem on circle packing. *arXiv preprint arXiv:1009.4322* (2010).

[117] Masoodi, R., Pillai, K. M. & Varanasi, P. P. Darcy's lawbased models for liquid absorption in polymer wicks. *AIChE journal* **53**, 2769–2782 (2007).

[118] Masoodi, R. & Pillai, K. M. A general formula for capillary suction-pressure in porous media. *Journal of Porous Media* **15** (2012).

[119] Lekakou, C. & Bader, M. Mathematical modelling of macro-and micro-infiltration in resin transfer moulding (rtm). *Composites Part A: Applied Science and Manufacturing* **29**, 29–37 (1998).

[120] Py, C., Bastien, R., Bico, J., Roman, B. & Boudaoud, A. 3d aggregation of wet fibers. *EPL (Europhysics Letters)* **77**, 44005 (2007).

[121] Fenner, W. R. *Quick reference to veterinary medicine* (1991).

[122] Kimmel, E., Arkin, H., Broday, D. & Berman, A. A model of evaporative cooling in a wetted hide. *Journal of agricultural engineering research* **49**, 227–241 (1991).

[123] Hart, B. Feline behavior: The role of grooming activity. *Feline practice* (1976).

[124] Earle, K. & Smith, P. Digestible energy requirements of adult cats at maintenance. *The Journal of nutrition* **121**, S45–S46 (1991).

[125] White, C. R. & Seymour, R. S. Mammalian basal metabolic rate is proportional to body mass2/3. *Proceedings of the National Academy of Sciences* **100**, 4046–4049 (2003).

[126] Watanabe, S., Izawa, M., Kato, A., Ropert-Coudert, Y. & Naito, Y. A new technique for monitoring the detailed behaviour of terrestrial animals: a case study with the domestic cat. *Applied Animal Behaviour Science* **94**, 117–131 (2005).

[127] TORII, M. Maximal sweating rate in humans. *Journal of human ergology* **24**, 137–152 (1995).

[128] OBrien, S. J. *et al.* State of cat genomics. *Trends in genetics* **24**, 268–279 (2008).

[129] Lloyd, A. T. Cats from history and history from cats. *Endeavour* **11**, 112–115 (1987).

[130] Hainsworth, F. Saliva spreading, activity, and body temperature regulation in the rat. *American Journal of Physiology-Legacy Content* **212**, 1288–1292 (1967).

[131] Dawson, T. J., Robertshaw, D. & Taylor, C. R. Sweating in the kangaroo: a cooling mechanism during exercise, but not in the heat. *American Journal of Physiology-Legacy Content* **227**, 494–498 (1974).

[132] Avner, D. B., Perzanowski, M. S., Platts-Mills, T. A. & Woodfolk, J. A. Evaluation of different techniques for washing cats: quantitation of allergen removed from the cat and the effect on airborne fel d 1. *Journal of allergy and clinical immunology* **100**, 307–312 (1997).

[133] Carayol, N. *et al.* Fel d 1 production in the cat skin varies according to anatomical sites. *Allergy* **55**, 570–573 (2000).

[134] Charpin, C. *et al.* Fel d i allergen distribution in cat fur and skin. *Journal of allergy and clinical immunology* **88**, 77–82 (1991).

[135] Zhu, D. *et al.* A chimeric human-cat fusion protein blocks cat-induced allergy. *Nature medicine* **11**, 446 (2005).

[136] Roeser, R. J. & Ballachanda, B. B. Physiology, pathophysiology, and anthropology epidemiology of human earcanal secretions. *Journal-American Academy of Audiology* **8**, 391–400 (1997).

[137] Feig, M. A., Hammer, E., Vlker, U. & Jehmlich, N. In-depth proteomic analysis of the human cerumena potential novel diagnostically relevant biofluid. *Journal of proteomics* **83**, 119–129 (2013).

[138] Alberti, P. Epithelial migration on the tympanic membrane. *The Journal of Laryngology and Otology* **78**, 808–830 (1964).

[139] Bhat, P. P. *et al.* Formation of beads-on-a-string structures during break-up of viscoelastic filaments. *Nature Physics* **6**, 625–631 (2010).

[140] Al-Sadi, S. & Hasso, A. Comparative study of the auricle and external acoustic meatus of the cattle and buffalo. *Iraqi Journal of Veterinary Sciences* **26**, 65–72 (2012).

[141] Gurr, A., Kevenhrster, K., Stark, T., Pearson, M. & Dazert, S. The common pig: a possible model for teaching ear surgery. *European Archives of Oto-Rhino-Laryngology* **267**, 213–217 (2010).

[142] HaiJin, Y. *et al.* Microdissection of miniature pig ear. *Journal of Otology* **8**, 91–96 (2013).

[143] Huang, H., Little, C. J. & McNeil, P. E. Histological changes in the external ear canal of dogs with otitis externa. *Veterinary dermatology* **20**, 422–428 (2009).

[144] Saunders, J. C., Kaltenbach, J. A. & Relkin, E. M. The structural and functional development of the outer and middle ear. *Development of auditory and vestibular systems* 3–25 (1983).

[145] Schnabl, J. *et al.* Sheep as a large animal model for middle and inner ear implantable hearing devices: a feasibility study in cadavers. *Otology and Neurotology* **33**, 481–489 (2012).

[146] Sommerauer, S., Snyder, A., Breuer, J. & Schusser, G. F. A technique for examining the external ear canal in standing sedated horses. *Journal of Equine Veterinary Science* **33**, 1124–1130 (2013).

[147] Di Giusto, B., Grosbois, V., Fargeas, E., Marshall, D. J. & Gaume, L. Contribution of pitcher fragrance and fluid viscosity to high prey diversity in a nepenthes carnivorous plant from borneo. *Journal of Biosciences* **33**, 121 (2008).

[148] Sahni, V., Blackledge, T. A. & Dhinojwala, A. Viscoelastic solids explain spider web stickiness. *Nature Communications* **1**, 19 (2010).

[149] Katija, K. & Dabiri, J. O. In situ field measurements of aquatic animalfluid interactions using a selfcontained underwater velocimetry apparatus (scuva). *Limnology and Oceanography: Methods* **6**, 162–171 (2008).